TUDelft Delft
University of
Technology

Challenge the future

DESIGN OF TRAVEL LIMITS FOR BISTABLE VIBRATION ENERGY HARVESTING

M.Sc. Thesis

In partial fulfillment of the requirements for the degree of
Master of Science in Mechanical Engineering.
at the Department of High Tech Engineering,
Delft University of Technology, Delft, The Netherlands
to be defended on Thursday, March 11th, 2021 at 13:00.

by

Kylian van Puffelen

born in Zuid-Beijerland, The Netherlands

This thesis was approved by the thesis committee:

Dr.ir. R.A.J. van Ostayen	MSD,PME,3ME,TU Delft	Chairman
Ir. T.W.A. Blad	MSD,PME,3ME,TU Delft	Daily supervisor
Prof.dr. P.G. Steeneken	DMN,PME,3ME,TU Delft	Independent committee member

An electronic version of this thesis is available at
`http://repository.tudelft.nl/`.

Preface

The curiosity and affinity for technical components began in the early days of my life. This started with Lego and Meccano, where different components could be combined in order to create the constructions I had in my mind. My parents also helped me realising of how the human being is capable of creating something on their own out of raw materials instead of just buying finished product at the store. This creativity brought in by my parents helped me by realising my increasing interest for mechanical designs.

The decision for studying mechanical engineering was not only of the affinity for the technique, but also because of the other engineer in our family, my granddad. He was chief of the research department at the business of KONI B.V., which manufactured shock absorbers for many applications like cars and bridges. His career, and possibilities in life encouraged me to study mechanical engineering.

During the study mechanical engineering I realised my interest for mechanical designs, capable of capturing kinetic energy from ambient resources and their conversion into electrical energy. This topic is almost analogue to the technique used in shock absorbers, however applied on smaller scales. The first energy harvesting design was constructed during my bachelor final project, where a small generator was optimized in order to enlarge thee power output generation. The specialisation direction of mechatronic system design (MSD) enlarged my vision of the utilisation of compliant mechanical designs for energy harvesting. The possibility of the integration of compliant structures for energy harvesting from environments like for example human motion encouraged me to elaborate my research direction in the field of vibration energy harvesting.

I am grateful for having the opportunity of fulfilling my academic life in Delft. And I hope that this work will contribute to the integration of vibration energy harvesting for wearable low power electronics within the near future.

Please be entertained and inspired by reading my thesis!

K. van Puffelen
Delft, March 2021

Genius, is 1% talent and 99% hard work
Albert Einstein

Summary

Energy harvesting from renewable energy sources has become more popular in the last decades than ever before. New energy sources consisting of human input vibrations are hopeful alternatives for powering wearable low power electronics. These sensors currently rely on the lifetime of the battery and come along with high maintenance costs in case of a replacement. Many designs found within literature are based on the working principles of linear resonant energy harvesters, consisting of high output generation when they are exited on their resonance frequency. However, if the vibration energy harvester is not accurately tuned to the input signal of the real world, poor output performance can be expected.

Bistability, consisting of a unique double well potential energy curve is an interesting alternative. The oscillation between the two potential wells contribute to higher output performance in comparison with resonant configurations. However, these potential wells are segregated by an energy barrier and the motion between the two wells will not always occur during excitation. A solution is found to reduce the energy barrier by means of mechanical end-stops.

A mechanical model based upon beam theory is created in ANSYS and their stiffness characteristics are used as an input parameter for the dynamical model. To confirm this model a prototype is constructed and investigated. A mechanical analysis is carried out using a quasistatic force-deflection measurement and the dynamical analysis is performed on a linear air bearing stage, consisting of a maximum stroke of half a meter being able to reproduce low frequency input excitations.

It could be observed that participation of the desired trajectory between the two potential wells is enhanced and occur at lower input accelerations, as the oscillators motion is confined by means of hard mechanical end-stops. Therefore, the integration of mechanical end-stops as a design parameter for bistable energy harvesters can be considered as a viable solution to capture the kinetic energy induced by human input motion with the use of bistable mechanisms.

Contents

1

Vibration Energy Harvesting

In this chapter, the reader is introduced to the world of energy harvesting. The effect of replacing batteries with vibration energy harvesters, able of converting ambient vibration energy into electrical energy will be explained by typical applications and their significance. The topic of vibration energy harvesting will be elaborated with commonly used energy transducers and their basic working principles. At the end of the chapter the thesis outline will be presented.

1.1   Introduction towards Energy Harvesting

Since the industrial revolution, energy has been one of the greatest demands in our society. As fossil fuels are running scarce, renewable energy sources have received great attention. In our current society many advantages have been made to integrate energy harvesting principles for ambient resources. Examples are solar panels, hydroelectric power plants and wind turbines, which uses the earth's natural resources such as sunlight, fluid and aerodynamic flows to capture ambient energy and convert them into the electrical energy. These principles are used on large scales and are therefore great competitors for pollutable alternatives like charcoal and nuclear power plants. Although these renewable energy sources are able to supply large amount of energy, they are incapable of continuously charging low power wearable electronics. However, the same conversion principles can be applied on smaller scales. An example of small scale energy harvester based on the classical energy conversion principle is a wind powered high way light, which uses the ambient aerodynamics of the wind to rotate the turbine and provide our transportation network with enough light to ensure our safety during night time. Another commonly used energy harvester application is the wristwatch. The energy in wristwatches can be supplied on different ways, the most commonly used method is the usage of a simple battery, however it comes along with confined energy capacity and needs to be replaced in case of an empty battery. Some more advanced principles are radio controlled and solar energy. One of the most interesting conversion principles is the energy conversion induced by human motion, where the kinetic energy is captured and directly used for powering a low power electronic device embodied by for example a wristwatch. This energy conversion principle is not new, however due to the high demand for batteries in low power electronics an interesting research direction in terms of ecological and environmental challenges will happen within the near future.

(a)   (b)   (c)
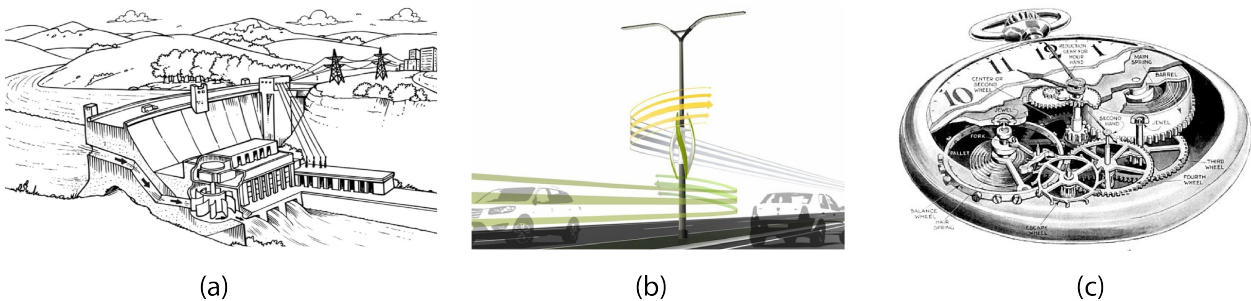
Figure 1.1: Commonly used energy harvester mechanisms, sorted by scale: (a) Hydro electric power plant (b) Wind turbine (c) Kinetic watch [[Tur; DRC; 3]]

1.2   Application and significance

For decades people are convinced that our future will be autonomous. In an autonomous world, it is of importance that the whole system is monitored and in case of an emergency, action could be taken at an early stage. Accurate sensing equipment is required in order to fully rely on autonomous systems, increasing the level of difficulty as well as the costs. Examples of systems involving low power electronics are sensors for health monitoring of a bridge or the track and trace tag within buses for updating the department schedule at the bus station. These low power electronics are currently powered with the use of batteries, which are subjected to a certain lifetime and needs to be replaced when the battery is empty, involving expensive maintenance costs. In these systems, energy harvesting from ambient resources could be a great solution. Reducing the societal demand for batteries with the use of energy harvesting of ambient resources, is almost if you remove the most important foundation of a house of cards, in other words it is a multi-purpose solution for our vision of getting the world greener.

The expensive maintenance cost of battery powered electronics depends on their location. The position of these sensors in autonomous systems are positioned on remote locations and the cost of an industrial battery cannot compete with the costs of the extra involved safety measures taken by the service mechanic in case of a replacement. Think for example of a sensor, able of sensing the health status of the concrete components of a bridge. These sensors are mostly located underneath the bridge and several meters above the ground. Therefore it is highly desirable to utilise sensors for these application instead of periodic manual inspection. Moreover, the sensing capability of the sensor is more accurate and gives a better representation of the condition of the bridge. However, when the energy confined by the battery is depleted overtime it should be replaced and we cannot escape from the safety measures to cope with the hazardous working conditions. Moreover, these sensors on remote locations are often protected by a sealing for environmental influences like water wind or dirt and the location of the battery is mostly not easy to access. This requires sophisticated dismantling procedures and again increases the cost. Therefore, it is often chosen to replace the sensors in total, but comes along with unnecessary waste.

Recent development within the fields of vibration energy harvesting received an increased potential to power low power electronics within the near future. Vibration energy powered devices reduces the demand for batteries and favours the aspect of large availability throughout the whole world. Moreover, an increase in accuracy can be expected. Battery powered sensors have a limit design space for the data transmission rate, because it should be designed to satisfy the specified lifetime of the sensor. This limitation on the data transmission rate can be disconnected when the power supply is provided by vibration energy and therefore increases the accuracy of the sensing equipment of autonomous systems.

1.2.1   Ecological & environmental challenges

As long as the world population grows, the demand for batteries grows with it. The demand for batteries in our daily life is too high to distance ourselves from it, leaving us with a concerning increase of ecological and environmental challenges for the years to come.

One of the greatest environmental challenge we face today is the earths global warming. In the climate agreement of Paris, it is stated that each country should contribute to legislate these rules in order to lower the earth's global warming. The carbon dioxide footprint reduction is one of the most important feature to tackle in order to reach this goal. Batteries as we use today are still manufactured using pollutable methods and induces a large contribution of the production of carbon dioxide. The materials used for the production of batteries rely on the limited availability of earths raw materials. Therefore, the use of batteries is a short term solution for powering low power electronics, however the depletion of natural resources and limited knowledge on how to process their waste is an urgent call for alternative powering possibilities.

1.3 Vibration energy harvesting

The term vibration indicates the appearance of movements within structure or mechanisms and are mostly considered to be unwanted, because the vibration affects the accuracy and usability. Many designs have taken the appearance of unwanted vibrations into accounts and are mostly damped out by the material characteristics itself or by the construction of an external damper like for example shock absorbers in cars to increase the driving comfort. The goal is to capture the unwanted movements and remove them out of the structure by means of dissipation in for example energy forms like heat. Vibration energy harvesting is the addition of an extra step in this process and introduces the ability of utilising this dissipated energy for powering electric devices. This captured energy can be stored and introduces an interesting alternative power source in comparison to the confined energy capacity of the battery. Vibration energy is because of their availability and long lasting characteristics an interesting power source for sensors in autonomous systems.
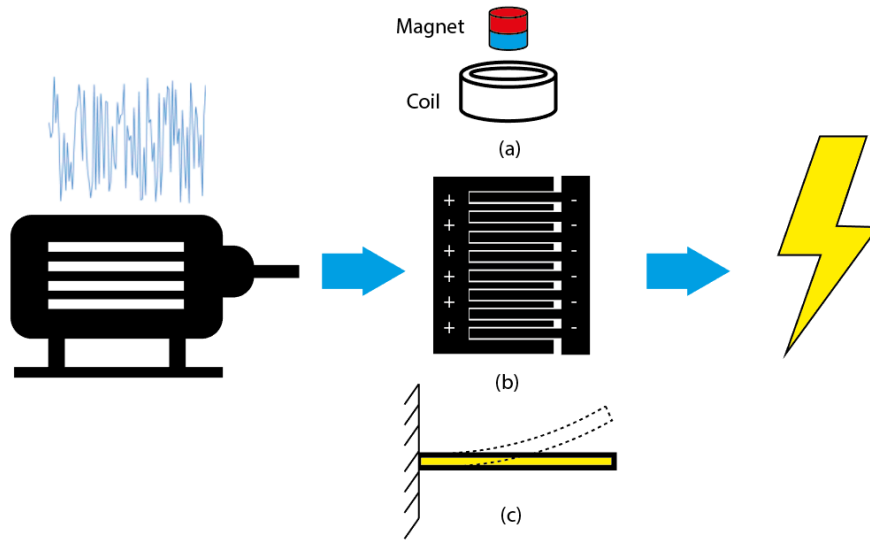
The principle of vibration energy conversion has two functions, it captures the unwanted induced vibrations and converts them into useful electrical power. This transduction is done by means of an energy transducer. Commonly used energy transduction mechanisms for vibration energy harvesting are electromagnetic, electrostatic and piezoelectric transduction. This process is schematically shown in figure 1.2, where the motor shows the origin of the induced kinetic energy and an schematic overview shows the embodiment of the used conversion principles in vibration energy harvesters.

The first energy conversion principle in vibration energy harvesters is the principle of electromagnetism. This configuration is shown in figure 1.2(a), where a magnet flows through a coil and induces an electro-magnetic force by means of change in magnetic flux. The generated output power depends on the flux and larger output power can be expected as the velocity of the magnet is increased.

The second transduction principle is the conversion by means of electrostatics, shown in figure 1.2(b). In comparison with the other conversion principles, it received great attention to be used for energy harvesters on small scale. This principle consist of perfect scaling possibilities and are able to power MEMS devices. This mechanisms consist of two electrodes, one is fixed while the

other is allowed to move. When the device is subjected to a vibrations the unconstrained electrode moves and induces a change in capacitance. This sudden change in capacitance is the transduction of vibration energy into electricity and induces more voltage as the change in capacitance between the two electrodes is increased.

The third principle is piezoelectricity shown in figure 1.2(c) and depends on the piezoelectric effect, where a voltage is induced by means of mechanical stresses within the structure. This principle is highly appreciated in vibration energy harvesting designs, since they generate large amount of output power. However, the usability in small scale energy harvesters is limited due to their stiff and brittle characteristics.

Figure 1.2: The vibration energy conversion principle, with three types of transducers. (a) Electromagnetic (b) Electrostatic (c) Piezoelectric

1.4 Thesis outline

Throughout this thesis, the conversion of ambient vibration energy into electrical energy is the main focus. This thesis document is a design phase structured thesis, formed by state of the art design strategy architectures synthesised into a new a design principle for energy harvesting from human motion.

In the second chapter of this thesis, the literature paper is presented. In this paper a review is made of the state of the art end-stop design principles in resonant energy harvesting designs. The end-stops imposes a limitation on the generated amplitude and at the collision many frequencies are excited where an increase in frequency bandwidth can be expected. This nonlinear effect induced by the end-stops results in interesting phenomenon for energy harvesting on small scales. To

encourage and investigate their usability a literature survey is conducted. In this survey five design parameters are identified and reviewed by their trade-offs in power output and reliability.

In the third chapter the main focus of this thesis is outlined, starting with the working principles of the energy harvester design in general. Shortcoming of state of the art resonant designs are highlighted and compliant mechanisms are proposed to be a better solution for capturing the ambient kinetic energy. The integration of compliant bistable structures suffers from the requirement of relatively high input force in low frequency environments. To address this limitation a design is proposed, where the principle of bi-stability is combined with hard characteristics of mechanical end-stops. Furthermore, the methodology approach and model are presented.

In the forth chapter of this thesis, the main work is presented in the form of a research paper. In this paper the end-stops are integrated in a bistable structure and their influence on the generator output is investigated. The model of the bistable structure showed earlier oscillation in the desired trajectory as it was more constrained by the end-stops. Moreover, a prototype was constructed and used to experimentally validate the simulated outcomes..

In the fifth chapter the hypothesis and the observations from the simulation and experimental work are reviewed by means of the critical attitude of the author. Conclusions are made and recommendations for future work are given. Furthermore, a reflection on the thesis process is given with successful and unsuccessful achievements

The following appendices are added to give more information on how this thesis was constructed. The information contained by these appendices consist of a more elaborative character and did not all accommodated directly to the main conclusions of this thesis. Appendix A describes the design process, where the process of a morphological scheme was used to find several concepts and the final design was determined with using the selection process based on the Pugh method. Appendix B describes the construction of the prototype and gives an overview of al the required components. In Appendix C the mechanical analysis of the bistable structure is elaborated, where the construction of the model in ANSYS is explained and followed by a sensitivity analysis indicating the weak spots of the energy harvesting design. This mechanical model is used in the dynamical model described in Appendix D.4.2, followed by experimental observations. To show and validate the correctness of the experiments, test protocols are included in Appendix E. The technical drawings of the components of the prototype are reported in Appendix F, which might be used in combination with the test protocols for the reproduction or continuation of this thesis. Finally Appendix G describes the contact mechanics model made in ANSYS, which were intended to be used in combination with the model of the bistable oscillator to predict the contact characteristics of the end-stop.

2

Review on the dynamic behaviour of energy harvesters utilising mechanical end stops

K.VAN PUFFELEN & T.W.A. BLAD & R.A.J. VAN OSTAYEN

Vibration energy is a promising source for, for instance, powering wireless sensors, due to its inexhaustible behaviour. Resonant harvesters are too sensitive with respect to varieties within the energy spectrum. However, mechanical end-stops increase the bandwidth, allowing harvesters to collect energy over a larger frequency region. This literature survey reviews the design variables accompanying the end-stop configuration, instead of introducing new end-stop classifications. A general model incorporating stopper configuration, stopper stiffness characteristics, stopper location, stopper distance, stopper shape is presented. Each design variable is accompanied by the trade-offs in performance and reliability.

2

2.1 Introduction

Energy harvesting with renewable energy sources has become more popular in the last decade than ever before, due to the high demand and increasing need for large amount of energy. Vibration energy can be used as a power source for wireless sensors, because of its inexhaustible behaviour [40]. The challenge with vibration energy harvesting is to create a design which can generate enough power for low frequency applications. Most designs are based upon resonant harvester designs with a high quality factor, furthermore simulated and tested upon optimal input signal, however small differences within practice will result in poor performance of the harvester [11]. A lot of research has been done to increase the bandwidth around the resonance frequency to enhance the performance [53]. Most of these methods come along with an increase in components and respectively the volume. The average output energy of the harvester can be managed with the use of mechanical end-stops, without increasing its overall volume, because of their implementation in the original design space [30]. End-stops limit the excitation amplitude, which enhances the ability of miniaturization and decreases the potential of introducing hazardous loads onto the system [17]. Besides, the utilization of end-stops is independent of the kind of transducer [41]. The impact behaviour of the seismic mass with the end-stops introduces nonlinearity to the system while it increases the bandwidth, allowing the system to collect energy over a larger frequency region. Bandwidth enlargement is paramount for real-world vibration sources, which has a large variety within their energy spectrum and increases the opportunity for end-stop architectures to outperform the linear counterpart based on resonance.

The physics of an end-stop can be described with the use of a spring-dashpot model [11]; however, visualisation in real-world applications, end-stops will not always have the distinct forms of a spring and dashpot, in fact there a many possible end-stop configurations. Haroun et al. [26] utilises conventional springs as end-stops. Liu et al. [32] omits the physical existence of a spring and utilises a cantilever beam to act as a mechanical end-stop. Nonlinearity can be introduced in multiple ways, for instance with magnets. Magnets create a nonlinear stiffness and a bandwidth increase; as they reduce the force coming from the seismic mass, they act as a force-limiter rather than a amplitude-limiter. Though combinations exist within literature, Tornciasa et al. [44] uses a rubber bumper in combination with the repulsive force coming from magnets, in which combination of both elements influences the bandwidth enlargement.

In literature many attempts have been made to classify systems which utilise end-stops as a part of their dynamics. Soliman et al. [41] is one of the first to investigate the influence of the stopper configuration on one or two sides of a generating beam. In the work of Soliman et al. [42] a design procedure for wideband micro generators is developed, in which the stiffness and velocity at impact are expressed as the dominant factors of the performance of a wideband generator with end-stops. Halim et al. [24] uses the terminology of rigid and flexible for their end-stops and examined the difference within their architecture. Based upon these classifications, Zhou et al. [51] elaborated this research with material selection denoted as either hard, medium or soft, without further explanation on the distinction between the classes. Blad et al. [9] compared single degree of freedom generators with end-stops, regarding their stiffness characteristics.

Although, many efforts have been made to classify systems utilizing end-stops as a part of their dynamics, to date, no single classification distinguishes the differences between end-stops, soft and hard stops.

In this paper, a literature review is done based on the design variables accompanying a harvester model utilizing the end-stops architecture as a part of its dynamics. The goal of this literature review is to give a comprehensive overview of the design variables, which cause effects in the dynamic behaviour; influencing the ability of the energy harvester to collect more energy.

Section 2.2 will describe the existing kinds of end-stop classification. Section 2.3 describes the importance and effects on the dynamic behaviour of each variable, followed by section 2.4 in which the total set of design variables will be reviewed and trade-offs will be revealed. Finally, section 4.5 will give the reader some general remarks, which should kept in mind when building a wide-band harvester design based on the end-stop architecture.

2.2   Existing classifications

In literature there are many descriptions of end-stops to be found, which all imply specific properties of an end-stop. This section discusses the existing kinds of classifications.

Soliman et al. [41] investigated the end-stop architecture, in which a one-sided configuration with end-stop was expanded to a two-sided configuration by placing another end-stop on the other side of the oscillator. Halim et al. [24] uses the cantilever beam architecture and introduces the terminology of two kinds of stoppers, *Rigid stopper* and *Flexible stopper*. Differences occurs at the place of impact, which can be seen in figure 2.1. The rate of change of their stiffness characteristics is the main contributing factor for the distinction between the two classes, which determines the amount of travel beyond their stopper distance (d_1,d_2) in figure 2.1.
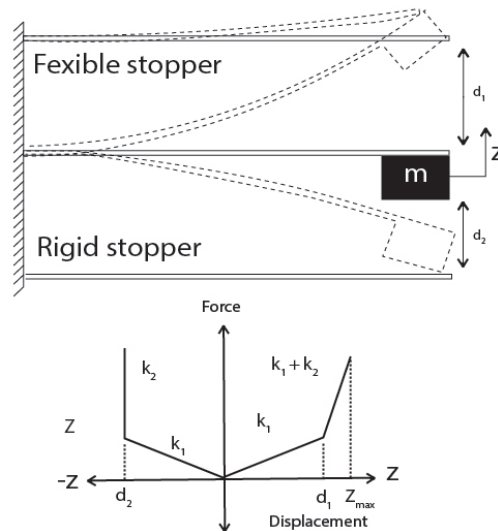
Figure 2.1: Graphical interpretation of rigid and flexible stopper configurations, in addition the force-deflection curve for clarification of the differences within the stiffness characteristics. Adapted from [24].

Based on the previous works, Zhou et al. [51] elaborated this classification with types and

2

material selection. Four stopper types, *fixed single-sided*, *fixed double-sided*, *followed single-sided* and *followed double-sided* were used and the different effects of the types on bandwidth broadening were investigated. The most promising stopper type is elaborated with material and spring selection. The effect of rigid materials (plastic, aluminium, and steel) were compared with the effect of soft materials (rubber and foam). Although plastic is relatively softer than steel, they are placed in the same rigid materials group. Blad et al. [9] is one of the first to make a general comparison based on the dynamic behaviour of generators utilizing end-stops. The classes can be seen in figure 2.2, in which comparisons between the generator types are confined to single degree of freedom generators utilising no or either soft or hard stops. This work introduces the motion ratio
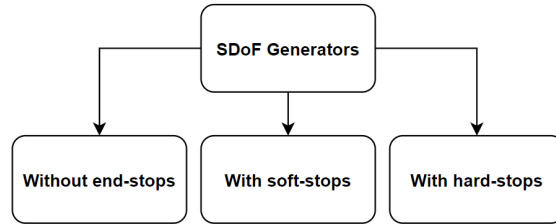
Figure 2.2: Classification of different types of end-stops within the work of Blad et al. [9].

λ, defined as the ratio of the generator travel dimension and the amplitude of the driving motion, and uses it as a measure to compare end-stop generators with respect to their peak efficiency and normalised bandwidth. Gradual and rapid stiffening effects are the distinct properties of the two classes, which again stresses the dependency of the stiffness characteristics on their dynamic behaviour. Limitations arise at the boundaries between soft and hard stops, which again do not have a clear interpretation.

In short, no single classification can cover all the possibilities within the end-stop generator architecture; therefore a comprehensive overview of the design variables will give a better view on how to implement end-stops in wide band generators.

2.3   Design variables

Figure 2.3 shows the graphical interpretation of a wide band generator with end-stops, from which the design variables can be identified. The design variables, which cause effects in the power output performance will be explained in this section step by step.

$$
\begin{cases}
M\ddot{x} + (C+C_1)\dot{x} + (K+K_1)x = F(x), x > d_1. & \text{(2.1a)} \\
M\ddot{x} + C\dot{x} + Kx = F(x), x < d. & \text{(2.1b)} \\
M\ddot{x} + (C+C_2)\dot{x} + (K+K_2)x = F(x), x > d_2. & \text{(2.1c)}
\end{cases}
$$
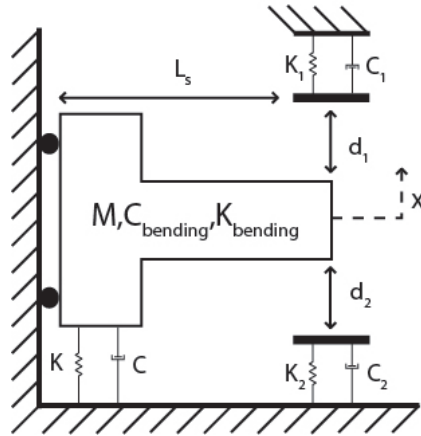
Figure 2.3: **A comprehensive overview of the important design variables accompanying the end-stop architecture.**

2.3.1 Stopper configuration: Single or double sided

Energy harvester designs with end-stops utilise the single-sided or double-sided configuration, depending on the desired system characteristics. Since the two configurations are too distinct in terms of performance, each configuration is explained in a separate subsection.

2.3.1.1 Single-sided

Resonant harvesters can mathematically be described with equation (4.1), where the mass M, damping C and stiffness K characteristics are determined by the oscillator without impacting the end-stops. Exceeding the level of excitation ($x > d_1$), such that it couples with the single-sided end-stop, expands the equation of motion with (2.1a), transforming the system into a non-linear system. The effect of nonlinearity can be seen in the performance output where the bandwidth increases around the resonance frequency, increasing the region for harvesters to collect sufficient energy.

The work of Soliman et al. [42] stresses the importance of the stiffness and velocity at the place of impact, for the bandwidth enlargement.Tuning the mechanical damping of the end-stop, such that it effectively increases the bandwidth, is often too complex, because it depends on the type of stopper; however, the stiffness can actively be tuned. The rate of change and impact behaviour are the main contributing factors for the generation of nonlinearity, which increases as the coupling lasts longer or due to the abrupt change in stiffness upon impact. The single-sided end-stop configuration limits the oscillator motion in one direction, while the system is allowed to move uninterruptedly in the opposite direction. Larger amplitude generation towards the opposite direction, induces larger impact velocities at the end-stop. Blystad et al. [11] investigated the effect of higher impact velocities, where power output is measured with increasing acceleration. It can be seen that the power output still increases after impact, although at a slower rate than before. This can be explained by the increase in acceleration, allowing the seismic mass to have larger amplitude towards one side. This increases the velocity at impact with the end-stop, inducing larger power output. The same author suggest that the double-sided end-stops also show increase in power output, when the acceleration is increased; however, at a slower rate than with the single-sided configuration,

2

due to the extra amplitude limitation of the seismic mass. This behaviour can be verified with the experimental work of Zhou et al.[51].

2.3.1.2   Double-sided

Double-sided end-stops will limit the motion amplitude on both sides [31]. The addition of a second stopper, expands the equations of motion for single-sided end-stops (2.1a) and (4.1) with equation (4.2), which changes the dynamics, by introducing periodic impacts on two stoppers during each cycle. This increases the amount of coupled motion, resulting in increased nonlinearity in the system and bandwidths, compared to single-sided end-stops. However, the peak output voltage decreases. Upon examining the bandwidth enlargement, while modifying the stiffness ratio between the system and stopper ($\rho = \sqrt{\frac{K_2}{K_1}}$) with the use of various stopper locations, different results can be obtained regarding the behaviour between single-sided and double-sided end-stops. Both configurations reach a maximum bandwidth at a certain stiffness ratio, which is called the saturation bandwidth. The double-sided end-stop configuration reaches the saturation bandwidth much earlier than the single-sided configuration [42]. The amount of contact with the stopper is responsible for this behaviour, as longer contact induces larger nonlinearity. The rate of saturation is defined by the trade-off between output power and bandwidth enlargement. The difference in saturation is an important aspect in the design of a wideband generator. The stiffness ratio namely depends on the bandwidth enlargement, allowing single-sided end-stops to have larger stiffness characteristics than the double-sided end-stops, before reaching the saturation bandwidth.

2.3.2   Stopper stiffness characteristics

2.3.2.1   Stopper stiffness model

Periodical contact increases the system bandwidth around the natural frequency, due to non-linear behaviour. The increase in coupling with the end-stop can be done with the addition of a second stopper, or due to modifying the stiffness characteristics. Softer end-stoppers increases the travel beyond the stopper distance, increasing larger coupling and bandwidth. All the end-stop characteristics can be considered non-linear, requiring numerical solvers. Narimani et al. [39] is one of the first to introduce the principle of piecewise linear modelling on energy harvesters. Piecewise linear systems have fixed stiffness values for the system and stopper, which do not change during their travel within the end-stops as can be seen in figure 2.4(a). Because of this behaviour systems can be solved analytically using the equations of motion (2.1). Zhao et al. [50] uses the cantilever beam configuration, in which two cantilevers collide with each other, where the stiffest one acts as the stopper. Each beam has its own stiffness, allowing the system to be modelled as a piecewise linear system [10; 31; 15; 50].

Whereas previous classifications lack the ability of giving a clear interpretation of either hard or soft end-stops, piecewise linear modelling introduces a way for comparing systems based upon the stiffness ratio of the system and end-stop. However, the limitations arise when end-stops are used with continuous nonlinear stiffness characteristics (figure 2.4(b)) like rubber [44; 17]. Their stiffness changes along their travel within the stopper, limiting the usability of the simplified piecewise linear model. The clear distinction between these kinds of end-stops can be seen within their
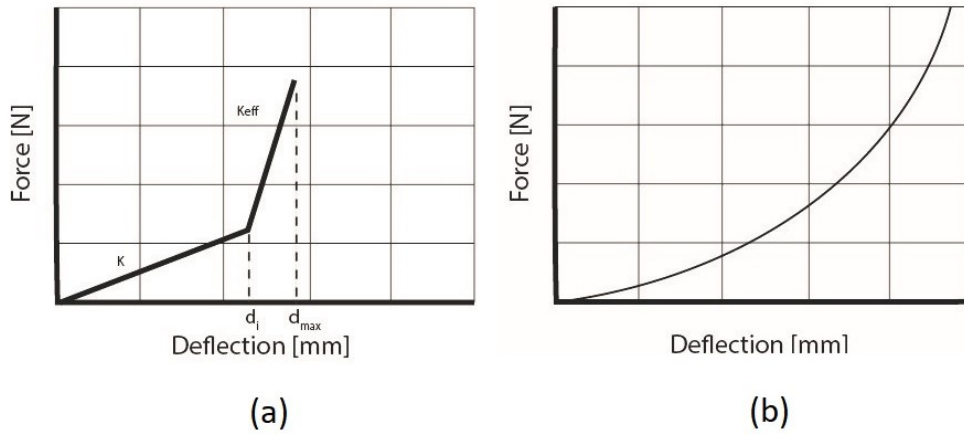
Figure 2.4: Force-deflection characteristics of a (a) piecewise linear system and (b) continuous nonlinear system.

force-deflection curves (figure 4). The main difference is the abrupt change in stiffness from K to $K_{(eff)} = (K + K_{stopper})$, for piecewise linear systems.

2.3.2.2   Energy loss

The amount of nonlinearity can also be controlled by the energy losses during collision. Energy losses are often not incorporated within simulations, this results in the theoretical overestimation in power performances of the energy harvesters. Ashraf et al. [6] introduces a method to incorporate energy losses in the analytical model, which gives a better prediction of the voltage throughout the whole frequency range, than simulations in which the energy losses are omitted. Impact changes the inertial velocity of the seismic mass, depending on the amount of the dissipated energy. The dissipated energy is converted into heat, and depends on the elasticity of the stopper material. A physical simplification of the material elasticity can be described with the use of the coefficient of restitution (COR) (2.2), which describes the change in kinetic energy (KE) before and after the impact. The restitution coefficient is not a material property, but rather depends on more such as the shape of the end-stop[7].

$$COR = \sqrt{\frac{KE_{after}}{KE_{before}}} = \frac{V_2}{V_1} \tag{2.2}$$

$$COR = \begin{cases} e = 0 & (2.3a) \\ 0 < e < 1 & (2.3b) \\ e = 1 & (2.3c) \end{cases}$$

Perfect elasticity can be described with a coefficient of restitution of one (2.3c), where the velocity before (V_1), is the same as the velocity after (V_2). Inelastic restitution coefficients are described with a COR of zero, where all the energy is dissipated in the material of impact (2.3a) and the velocity after impact is zero. Both of these values are ideal cases, real-world application of the restitution coefficient will be somewhere between these values (2.3b). Although the restitution coefficient is a

physical simplification, only few works in literature specify their method of measuring the change in velocity before and after impact. Edwards et al. [17] uses a cantilever beam configuration to impact on a high density rubber end-stop. The COR was measured using a drop test, where laser sensors tracked the displacement of the dropped mass. This method had the imperfection of lacking the ability to measure the coupled motion time. Measuring the coupled motion time is required for examining the effect of more nonlinear behaviour on the bandwidth enlargement. Ashraf et al. [6] uses the phase-space diagram, as a method to measure both contact time and the coefficient of restitution. The velocity was obtained using the recorded open loop voltage, while information on the displacement was provided by numerical integration of the velocity. Converting this into a phase-space diagram gives a clear visual interpretation of how the system interacts with the end-stop. Since the stopper distances are known, the travel beyond this point can be assigned to coupled motion with the end-stop. The phase-space diagram can be used to identify the velocity before and after impact, from which the COR can be calculated. The time required for the seismic mass to change velocity can be seen as the impact time, and can be obtained from the steep change in the velocity profile. Limitations with the restitution coefficient arise when the system is not exited on the same frequency input throughout the whole operation. The coefficient of restitution is not constant, but is dependent on the incoming velocity, which changes in the vibrational environment [22]. Blystad et al. [12] studied the influence of stopper stiffness. The dependency of the stopper stiffness on the coefficient of restitution can be clearly seen in their simulations, where stiffer stoppers result in lower restitution coefficients. Summarising, the coefficient of restitution cannot be a fixed value over the total vibration spectrum, and larger energy losses can be identified with stoppers utilising relatively hard characteristics, resulting in lower energy output with an increase in bandwidth.

2.3.3   Stopper location

The location of the amplitude stopper (L_s) is a significant parameter for energy harvesters with cantilever beam configurations. When no end-stops are used, the full length of the cantilever is allowed to have free uninterrupted motion with the same system characteristics. The stiffness of a cantilever is defined by (2.4), where the effective length is the design variable which can be controlled by the mechanical end-stops to increase the stiffness. However, the system characteristics change when the oscillator impacts the mechanical end-stops. The effective length of the cantilever is reduced, due to the new placement of clamping with the end-stop (figure 2.5), which increases the effective stiffness of the system after impact. Soliman et al. [41] was one of the first to investigate the influence of the stopper location on the dynamic behaviour of the system. The fraction of the stiffness after impact with the stiffness before impact was used as a measure to compare the energy harvester on the bandwidth enlargement. Larger bandwidths can be expected when larger stiffness ratios are obtained.

$$K = \frac{3EI}{L^3} \tag{2.4}$$

Smaller bandwidths can be seen when the stiffness ratio is reduced, allowing the seismic mass to travel further beyond the stopper distance, increasing the moment arm and rotary inertia of the seismic mass, while increasing the generated power output. A design procedure based on this design variable is examined in the work of Soliman et al. [42], where the dynamics of the harvester based

upon different stopper locations are investigated and optimized for the input vibration.
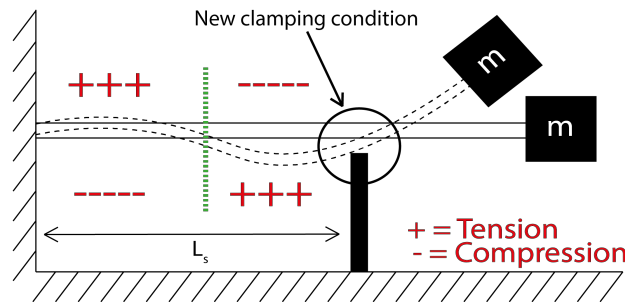
Figure 2.5: Schematic differences within the stress regimes after impact. Adapted from [34].

The impact behaviour of the oscillator with the end-stops will induce different stress regimes throughout the cantilever as shown in figure 2.5. Tension and compression are the two different stress regimes induced by impact with the stopper. The amount of stress in compression and tension can be controlled with the use of end-stops, as can be seen in the work of Mak et al. [34], who investigated the influence of stopper location with respect to the output voltage and stress reduction in the beam. The stress reduction is denoted as the fraction of the maximum bending stress when impacting the end-stop at the place of clamping, with the maximum bending stress when no amplitude limit is used. Significant differences can be seen when the stopper is placed closer to the roots; the tip of the cantilever is allowed to have a larger amplitude, inducing larger stresses at the place of clamping in favour of the energy transducer. However reduces the reliability. Therefore increasing the stopper location reduces the amount of stress at the place of clamping making it more robust against fatigue of the beam structure, at the expense of the voltage output.

2.3.4   Stopper gap distance

Increasing the stopper distance (d_1,d_2) allows the system to have a larger region in which it behaves uninterruptedly, which accentuates the importance of the stopper distance on the performance of the energy harvester.

Blystad et al. [11] investigated the theoretical differences in the dynamic behaviour of larger and smaller stopper distances, with respect to the initial stopper distance, called the nominal case. Increasing the stopper distance results in larger output power at the expense of bandwidth enlargement. Decreasing the stopper distance will however result in lower output power with an increase in bandwidth. Figure 2.6 schematically shows the differences within the performance when changing the stopper distances. Experimental verification of the effect of the stopper distance on the dynamic behaviour can be seen in the work of Dhakar et al. [15] and Soliman et al. [42], where again larger stopper distances result in narrower bandwidth and increase in power output, and where a smaller stopper distance behaves in the opposite fashion.

With the use of double-sided end-stops, different design strategies can be implemented: equal and unequal stopper distances. Liu et al. [31] investigated this design variable for different stopper gap distances ($d_1 \leq d_2$), where a cantilever beam is used to act as the top stopper, and the bottom stopper is configured to be the metal casing of the harvester. When the system is vibrated at a
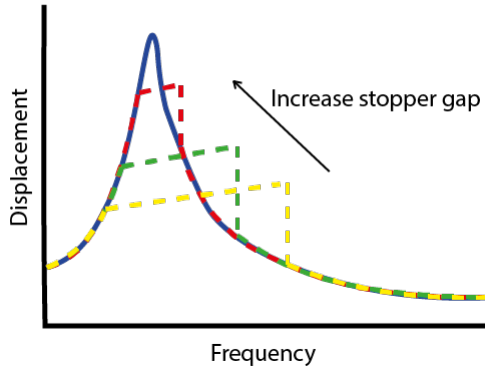
Figure 2.6: Performance differences when changing the stopper gap distance. It should be noted that no other physics are taken into account rather than the stopper gap distance.

certain level of excitation, the system will interact only with the top stopper, while making no use of the bottom stopper. Increasing the level of excitation will include the metal casing within their dynamics and will act as an additional stopper.

The bottom stopper is stiffer than the top-stopper, because of the extra function of overload prevention. Differences of the stopper stiffness can be seen in the dynamical response of the system shown in figure 2.7. When impacting the bottom stopper larger energy losses can be expected, which decreases the slope of the output power, while increasing the bandwidth, introducing stages in the output performance. A parametric study is investigated with different top stopper distances. Decreasing the top stopper distance will result in slower increase of the first stage, but it will increase the bandwidth. Increasing the top stopper distance towards the gap distance of the bottom stopper, a smaller bandwidth increase accompanied with steeper increase of output voltage can be identified.
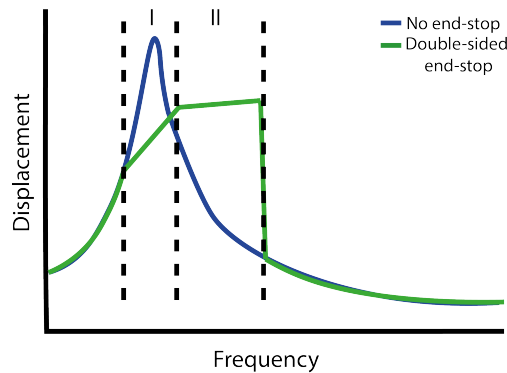
Figure 2.7: Difference in performance with unequal stopper distances, stage I is the performance with the top stopper, stage II is the performance including the bottom stopper.

Gu et al. [23] stresses the importance of the stopper distance larger than zero in single-sided configurations, zero gap distance opposes the ability of energy harvester to respond to low frequency excitations.

The stopper distance also has an effect on the stresses induced at the place of clamping. This

effect can be seen in the work of Mak et al. [34]. The voltage increase, when increasing the stopper distance, is proportional to the decrease in stress reduction, which can be explained by the larger allowable amplitudes with larger stopper gap distances, inducing larger strain at the place of clamping. Stress reduction can be achieved with smaller stopper distances, where the amplitude is more limited and lower levels of strain occurs at the place of clamping.

2.3.5   Stopper shape

Most designs within literature omit the design principle of the end-stop shape, which causes significant influences on the dynamic behaviour of the system. End-stops can be used either internal or external as can be seen in figure 2.8. Internal end-stops, shown in figure 2.8(a), can be assigned to motion limitations coming from the seismic mass, whereas the external implementation of the end-stop is on the casing of the harvester. Li et al. [30] investigated the influence of the internal end-stop configuration, utilising the wasted space above the generator beam without increasing the overall volume. The end-stop was given a curved shape such that it follows the mode shape of the beam, reducing the possibility of excessive loads in the structure of the system. Introducing internal motion limits on the generator beam increases the proof mass whereas it decreases the fundamental frequency making it a tempting design principle for low frequency applications. Besides, addition of mass increases the amount of strain at the place of clamping, generating more voltage than their conventional counterpart.

External shape optimization can be found within the works of Liu et al. [33] and Yuan et al. [49]. Liu et al. introduces non-linearity onto the system with the use of continuously changing their stiffness due to smooth transition of the effective length of the generating beam. The end-stop consist of a curved shape, which continuously limits the amplitude of the beam even further when larger excitation levels occurs (figure 2.8(b)). Yuan et al. elaborated this work with a novel stiffness-merging end-stop. One of the greatest advantage of this design principle, is the ability of designing the desired stiffness characteristic for each system.

The stopper shape have also influence on the stresses within the harvesters. Limiting the amplitude with an end-stop will prevent the system from excessive loads, however impact with the end-stop induces different stress regimes (figure 2.5). Wang et al. [46] investigated the shock reliability of the cantilever architecture. Care should be taken that in this work no use is made of the dynamical advantage of the impact with the end-stop, however the failure mechanisms discussed can have the same form in end-stop configurations. The high stress regimes can be identified at the place of clamping and at the place where the seismic mass is bonded onto the cantilever. Impacting the end-stop will induce large amounts of stres that might go beyond the maximum bending stress, resulting in failure of the oscillator. An important observation within this research is the dependency of the shock reliability on the fundamental frequency. Four types of piezoelectric energy harvesters are tested, each with different resonant frequency. The critical shock magnitude, in terms of acceleration is measured for each type. Decreasing the fundamental frequency resulted in earlier failure of the piezoelectric material, which can be explained by the larger allowable amplitude of the seismic mass, resulting in more impacts with the end-stops. This once again stresses the importance of the stiffness of the cantilever, because the fundamental frequency is dependent on the geometry and material property. The original design of the end-stop (figure 2.9(a)) changes the cantilever into a S shaped curve, in which different stress regimes start to appear. The stress

regimes are responsible for the failure within the system and can be reduced with the proposed shape optimisation of the end-stop. A stepped cavity is suggested to improve the shock reliability, where two impacts with the end-stop reduces the inertial force of the seismic mass, resulting in a more continuous shape of the cantilever at impact, as can be seen in figure 2.9(b).   Shape of the
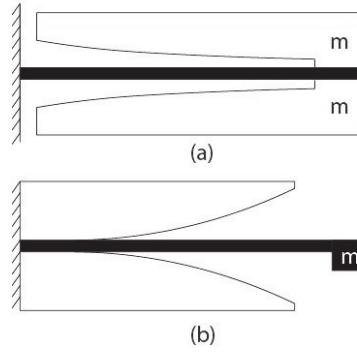
Figure 2.8: End-stop shape design principles, (a) internal (b) external.   Adapted from [30],[33].
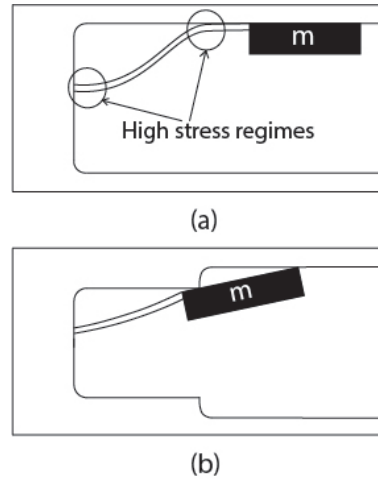
Figure 2.9: End-stop shape design principles for shock reliability, (a) Original design (b) stepped cavity, Adapted from [46].

end-stop, with perfect fit of the mode shape of the beam will prevent the system from overloads. The shape optimization of the end-stop is for this reason an important design variable with respect to the durability and the robustness of systems against shocks within the unpredictable vibration energy source spectrum.

2.4   Discussion

Design variable	Advantage	Disadvantage
Stopper configuration:		
• Single-sided	• Larger amplitude than II • Larger impact velocity than II • Larger voltage output than II • Larger power increase after impact than II	• Slow bandwidth saturation • Smaller bandwidth enlargement than II • Fatigue problems at an earlier stage than II
• Double-sided	• Rapid bandwidth saturation • Larger bandwidth enlargement than I • Longer coupling with end-stop than I	• Lower amplitudes than I • Lower impact velocity than I • Lower voltage output than I • Lower power increase after impact than I • Fatigue problem at high level of excitation

Design variable	Property
• Stopper stiffness characteristics	• Tuning of coupled motion • Regulation of energy loss • Regulation of the stress
• Stopper location	• Only for cantilever beam architectures • Active stiffness tuning • Determines the travel beyond the stopper distance • Regulation of the stress • Adjustable during operation
• Stopper gap distance	• Large gap distance result in small bandwidth enlargement • Small gap distance result in large bandwidth enlargement • Too large gap distance results in resonant behaviour • Design strategy unequal stopper distance, only applicable in II • Regulation of the stress • Adjustable during operation
• Stopper shape	• Internal end-stop decreases the fundamental frequency • Design element for the desired stiffness characteristic • Regulation of the stress

Table 2.1: The advantage and disadvantages of the design variable stopper configuration I for single-sided and II for double-sided end-stops. Followed by an overview of the main properties of the other design variables.

The energy harvester utilising end-stops is too distinct to be captured within one classification. Table 2.1 shows the main advantages and disadvantages of the design variable stopper configuration, followed by an overview of the other design variables. The most remarkable trade-off is between the voltage output and bandwidth enlargement. The overall utilisation of end-stops is to prevent the system from excessive travel and subsequently the overload, however the positive side-effect is bandwidth enlargement, which depends also on the test condition. Most designs in literature are subject to frequency sweeps as a measure of performance, but the up or down sweep depends on the type of nonlinearity in the system. End-stops increases the effective stiffness at impact, resulting in hardening type of nonlinearity, favouring the frequency up sweep to increase the bandwidth. Frequency down-sweeps results, however in the same bandwidths as with the linear resonant design with a significant decrease in output voltage [41]. Although up-sweeps are used as a measure to compare the performance of energy harvesters, real world vibration energy source characteristics omit the existence of these sweeps, resulting in different output than expected.

The first design variable, stopper configuration depends on the desired output voltage and bandwidth of the application. Single-sided end-stops induce larger impact velocities in favour of the output voltage, however decreases the bandwidth with respect to the double-sided configuration. The double-sided configuration decreases the voltage output whereas it increases the bandwidth, making it an interesting design parameter, depending on the nature of the vibration source. The same trade-off can be found within the use of the stopper stiffness characteristics, harder materials dissipate relatively more energy in the end-stop what results in a decrease in generated output power, however induces larger non-linearity due to harder impact with an increase in bandwidth. The active tuning comes from the design variables stopper location and stopper gap distance, which can be done during operation. The stopper location can be changed using for example a slider. Increasing the stopper location, increases the amount of periodical impacts, while it enlarges the bandwidth. Using different stopper locations results in somewhat the same behaviour as with single or double-sided end-stops. Decreasing the stopper distance results in larger bandwidth with decrease in output voltage, due to earlier limitation of the amplitude, increasing the stopper location, however results in smaller bandwidth increase in advantage of the voltage output.

The impact behaviour during collision with the end-stop induces nonlinearity and increases the bandwidth, while decreasing the voltage output. Optimization of this trade-off seems to be the possibility of building the best wide-band generator, withstanding all the challenges in the energy vibration source characteristics. However, the collision with the end-stop has besides the positive side-effect of bandwidth enlargement also a negative side-effect, namely: fatigue in the structure of the oscillator. The initial idea of end-stops was to reduce the amount of stress at the place of clamping, however impact of the seismic mass with the end-stop introduces new critical regions with high stresses. The stopper location can actively tune this region as can be seen in figure 2.5, but increasing the level of excitation results in larger amplitudes beyond the stopper, again increasing the stresses in these regions. The stopper shape is the most promising design variable for the fatigue regulation. Internal and external use of the end-stop can be used to regulate the excessive travel beyond the stopper, and the stress regimes at impact, due to for example a curvature of the end-stop. The fundamental mode shape of the oscillator at impact determines the curvature of the end-stop, which can also be of use in designing the desired stiffness characteristics.

Some of the works within literature suggests that, bandwidth enlargement due to the impact with the end-stop is one of the main consequence of larger coupling with the end-stop, however

no-one specify the coupling time. The work of Ashraf et al. shows an example of how to measure the coupling time. Verification of these claims within literature can be used as an inspiration for future literature research, while optimisation and reduction of the failure mechanisms in cantilever configurations will be left as a topic for future experimental research.

2.5   Conclusion

Many designs in literature are based on the resonant behaviour, which have large power output at a specific frequency, however small differences in practice results in significant drop in power. Utilising end-stops in the energy harvester design, enlarges the bandwidth near the resonant frequency, increasing the potential of outperforming the linear resonant designs. In this paper, a comprehensive literature review is done based on the design variables accompanying the end-stop model. The following design variables are identified: stopper configuration, stopper stiffness characteristics, stopper location, stopper gap distance, stopper shape, which are elaborated with their main properties in table 2.1. The stopper configuration of single-sided and double-sided end-stops, depends on the trade-off between power output and bandwidth enlargement. The single-sided configuration generates more power at the cost of smaller bandwidth enlargement than with the double-sided configuration. The introduction of modelling end-stop energy harvesters as piecewise linear systems, makes it possible to solve systems analytically. Piecewise linear systems also introduce a method of comparing systems based on the stiffness ratio, while at the same time giving an relative interpretation of how soft or hard end-stops are. Energy losses can be regulated with the stopper stiffness, but also depends on the trade-off between power and bandwidth of the application. The stopper location design variable is only applicable in cantilever beam configurations, which can tune the power and the bandwidth enlargement due to the active stiffness tuning, besides it regulates the amount of stress due to the place of the amplitude limit. Expanding this design variable with various stopper gap distances, gives rise to somewhat the same behaviour making it an interesting design variable for systems in which the stopper location cannot be adjusted. The stopper shape is one of the most interesting design variable, which should be taken into account when building an energy harvester design with end-stops. Shape optimization of the end-stop increases the potential of bandwidth enlargement, accompanied with prevention of overload conditions, whereas it increases the power at the same time. All with all, implementations of these design principles depends on the source characteristics and the desired application characteristics. The design variables discussed in this paper will give the designer a better understanding of how varieties in end-stops behave in the output performance of energy harvesters.

3

Vibration energy harvester analysis, design and manufacturing process

In this chapter the process of bistable vibration energy harvesting is explained. Starting with an introduction, where the working principles of the general concept of energy harvesting is explained. Followed by the identification of challenges on small scales and accompanied by the relevance and problem formulation of state of the art bistable mechanisms. Furthermore, the integration of the new design concept is demonstrated and followed by the mechanical and dynamical analysis.

3.1 Introduction to vibration energy harvesting design

Vibration energy harvesting is a promising energy conversion principle to cope with the ecological and economical challenges we face today. The demand for energy increases and the general concerns about their environmental impact does not weight up against the easy accessibility of the cheap conventional products we use today. Therefore, increasing the interest in alternatives like vibration energy harvesting might change vision of the society and hopefully increases the awareness, that the changes we make today are not only for ourselves but for the generations to come.

A promising new interesting field of application is the energy harvesting from human input motion. Think for example on the powering possibilities of the vibrations induced by the arms or legs during walking. These vibrations could be used for example for human health care related applications, like a diabetes monitors or pacemakers. The human body consist of many moving parts, where each body is excited with different behaviour. The movement of the arm is different in comparison with the motion induced by the wrist to power for example a wristwatch. In the medical world the motion of the heart have received great attention to be controlled by a pacemaker able of generating its own power by means of vibration energy harvesting. This device depends on the motion of the heart and can supply the pacemaker with enough power to regain a normal heart rithm. This is a continuous process, where the costs can be reduced and makes surgery unnecessary. For energy harvesting it is of importance to be acknowledged with the signal profiles occurring at the location of the device. The motion induced by human input motion consist mostly of low frequency contents ($f = < 5Hz$) and comes along with an energy varying spectrum. Besides, the combination of varying low frequency content and large amplitudes results in different acceleration profiles. To emphasize this varying content, a schematic overview is made and can be seen in figure 3.1. Table 3.1 demonstrates the variation of experimental obtained acceleration data for typical energy harvesting locations, measured under different conditions.
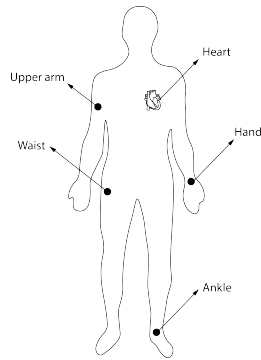
Location	Acceleration [g]	Condition	Reference
Ankle	1.38	Walking	[19], [47]
Ankle	3.61	Running	[47]
Waist	0.8-1.5	Walking	[37],[43]
Upper arm	6.12	Running	[20]
Hand	1.45	Shaking	[18]
Heart	0.1	At rest	[16]

Table 3.1: Comparison of induced acceleration profiles under different excitation conditions within the human body

From this overview it can be seen, that on each location of the human body unique acceleration profiles can occur, which differs greatly with the profiles induced on different lotions or at another condition. This overview indicates the complexity of the process of mechanism design for capturing possibility of the induced kinetic energy by human motion.

3.2   Working principles of energy harvesters

In beginning of this thesis the art of transforming vibration energy into electrical energy is introduced. Where in addition briefly three commonly used transducers are explained by their difference in working principles. This section explains the total general concept of vibration energy harvesting, where a component is added to the well known theory of vibration damping. This component is the representation of the connection between the mechanical and electrical domain. Furthermore, the topic of mechanism design and model are explained.

Figure 3.2 shows the total diagram of a vibration energy harvester. This diagram starts with a block consisting of the vibration source, indicating that each environment has unique characteristics and should be analysed prior to the mechanism design in order to optimize the power output of the energy harvester. As soon as the characteristics of the vibration source are recognized it is connected with an extra block, called the receiver This block is the main focus of this report, and represents the capture mechanism of the energy flow induced by the kinetic energy of the vibrations within the structure of which the energy is extracted. Vibration energy harvesting is the art of recycling unwanted vibrations and mostly consist of a continuous process, this makes it mostly unnecessary to add an block for energy storage. However, the continuous character forces the system to convert the captured energy directly into electrical energy by means of a transducer. Although the generated electrical energy depends on the transducer, the losses within the receiver contributes also to this generated output. The losses are defined by the part of the incoming vibration energy, which were not captured by the receiver. Therefore it is highly necessary to be acquainted with the environmental vibration spectra in order to harvest the kinetic energy in the most efficient way.

Even though this diagram shows the general concept of vibration energy harvesting from ambient resources, it is too basic to be familiar with their properties and challenges. Therefore, the receiver and transducer are explained in more detail in the following subsections.
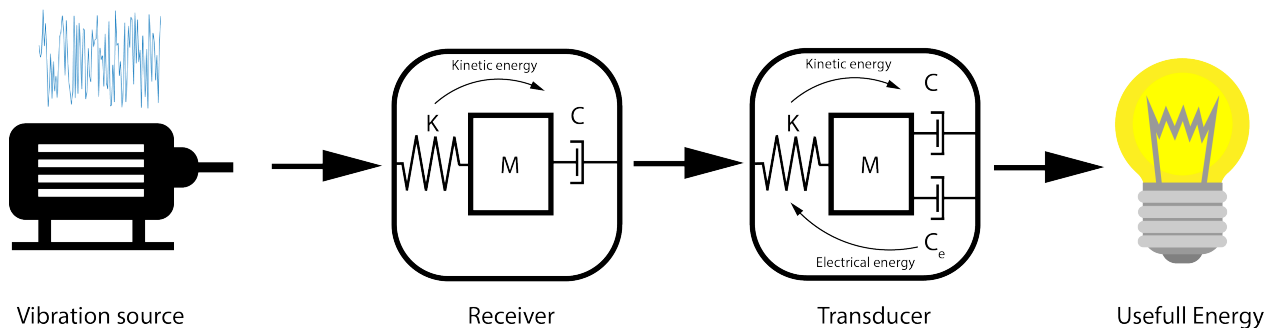
Figure 3.2: Schematic overview of the working principle of an vibration energy harvester

3.3   Linear energy receivers

Conventional energy harvesting designs found within literature are constructed as a linear resonant energy harvester. This design principle consist of large amplitude amplification in case the harvester is excited on a specific frequency and denoted as the resonance frequency. The performance of the harvester is at its greatest when it is exited on this frequency and is mostly capable of providing the device with enough energy. The working principle of a typical resonant energy harvester design is shown in figure 3.3. The simplicity of the mechanics of a cantilever beam in combination with a known mass at the tip of the cantilever, makes it not a complex process to design a harvester for a specific frequency (3.2).
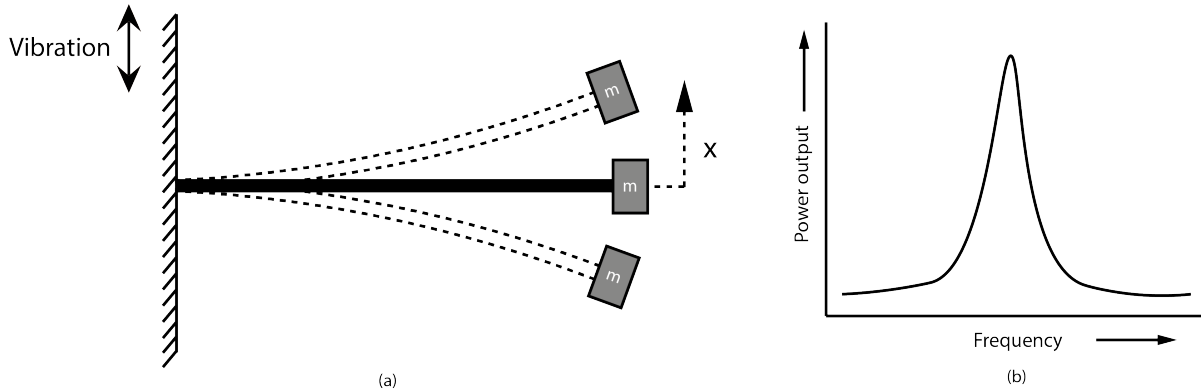
Figure 3.3: **The behaviour of a linear cantilever design, (a) working principle cantilever design (b) output performance**

$$k = \frac{3EI}{L^3} \tag{3.1}$$

$$f = \sqrt{\frac{k}{m}} \tag{3.2}$$

The stiffness of the cantilever beam can be calculated with equation 3.1, where EI represents the flexural rigidity and L the length of the beam. It is this simplicity and their alleviated manufacturing complexity, that makes the principle of resonance in energy harvesters an attractive design element. Moreover, the dynamical behaviour of these systems are mostly modelled as a single degree-of-freedom model. The construction of this model is analogue to the to the configuration of an physical damper and spring in parallel. A representation of this model can be seen in figure 3.4 and their corresponding equation of motion can be described with equation (3.3).

$$m\ddot{x} + c\dot{x} + kx = F(x) \tag{3.3}$$

In this equation the relative motion of the cantilever with respect to the environment is represented with x, where x $\dot{x}$ and $\ddot{x}$ represents respectively the displacement, velocity and acceleration of the proof mass. The stiffness and mass are defined by k and m and term c represents the linear viscous damping.
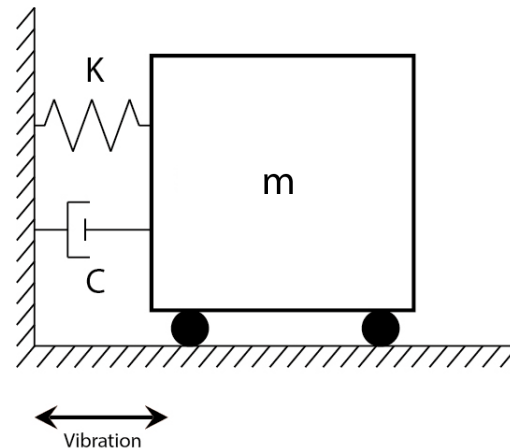
Figure 3.4: Graphical interpretation of the linear vibration energy harvester

Validation of this model is mostly performed with an electromagnetic shaker, capable of representing a sinusoidal frequency or decreasing input signal. The introduction already explained the large output performance of linear resonance energy harvesters on their resonance frequency. A schematic representation of typical experimental outcomes of such devices can be observed in figure 3.3(b). In this figure the resonance frequency can easily be identified by the rapid increase of measured output displayed on the y-axis. However, the frequency bandwidth over which sufficient power can be generated is relatively small and affects the reliability of the output performance in energy varying spectra like human input motion. Although these systems can be simulated and tested with high accuracy, small mistune with the real world signal results in poor output performance. Therefore, a single resonant energy harvester is mostly not used for industrial applications. However, there are design possibilities to use this configuration and are able to cope with the small bandwidth. For example the use of an array resonant energy harvesters, where each configuration consist of a different resonant frequency. This increases the reliability in energy varying spectrum, since the responsibility of power generation is altered with an other beam in case the input excitation is changed. Although this configuration is able to generate energy over a larger bandwidth in comparison with the original configuration, nevertheless is it not a not a favourable design for powering small scale electronics. The reason is the conflict between the increase in components and the interest in miniaturization of small scale electronics.

3.4 Challenges on small scale energy conversion

To make energy harvesting an appropriate competitor for batteries, a lot of research should be done in terms of reliability and performance. The limitation of small electronic devices depends mostly on the size of a battery, which is confined to guarantee the lifetime of the battery. Therefore, it is highly appreciated that vibration energy harvesters enlarges the possibility of the device in total, without imposing a limitation on the size. Although energy harvesters are capable of miniaturizing it is not a general property and each design comes along with challenges.
Many works found within literature maximizes their power output, when it is excited on their reso-

nance frequency. However, this design principle can be quite challenging in case the vibration amplitude is larger than the maximum allowable amplitude of the harvester. Figure 3.5 schematically shows the working principle of resonators on small scale, where the input vibration is indicated with Y_0 denoted as the amplitude, Ω the angular frequency and Z_{max} the maximum proof mass displacement. From this figure it becomes clear that challenges introduces themselves in case $Y_0 > Z_{max}$.
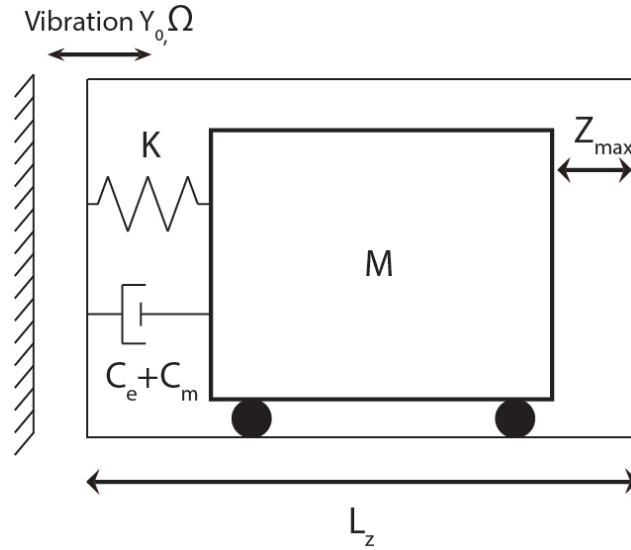
Figure 3.5: Working principle of a resonator on small scale

In the work of Blad et al. [9] a dimensionless design parameter was introduced, called the motion ratio (3.4). This design variable is the fraction of the generator dimension (L_z) over twice the input amplitude (Y_0).

$$\lambda = \frac{L_z}{2Y_0} \tag{3.4}$$

From this design parameter it can be obtained that the system is not able to respond with resonant behaviour, when the twice the input amplitude is larger than the generator dimension, resulting in collisions with the end positions of the energy harvester.

However, there are possibilities where resonant energy harvesters could be used when it is subjected to vibrations with larger input amplitudes than the oscillator dimensions. This method is based on the level of damping within the system, where the damping is used to oppose the ability of large amplitude magnification of the proof mass. The level of damping occur in either the mechanical or electrical domain, however the tuning possibility of the mechanical damping is limited and depends on the design. Electrical damping is a more viable option, since this can be tuned from the electrical domain and depends not on the geometry of the system. Moreover, electrical tuning can be done actively and increases the possibility to control the systems amplitude with respect to the variations within the energy spectra. The method of electrical damping is investigated by the work of Geisler

et al [21], however it was experienced that much larger input excitations resulted in no physical achievable damping coefficients to confine the proof mass within the two end-stops of the generator. Therefore, small scale environments makes the use of the favourable large amplification of resonant devices no feasible design element for energy harvesters on small scale. Nevertheless, this limitation, doesn't oppose the usability a linear design on small scales. Moreover, the combination of the linear configuration with the rapid increase in stiffness and damping induces at the collision with the end-stops results in nonlinear behaviour and is able to outperform the linear counterpart in energy varying spectra.

3.5   Nonlinear energy receiver

The main drawback of linear energy harvesters is the small bandwidth, resulting in low power output when the system is exited slightly off resonance. Although the system is simulated and tested under optimal conditions, the system might have a high potential of being unreliable within the unpredictable and varying behaviour of the vibration energy spectrum. In order to increase the reliability within the real world vibration energy spectrum, the bandwidth needs to be increased. This increase can be done with the use of nonlinear harvesters.

Durability is another important aspect for small scale vibration energy harvesters. In order to outperform sensors powered with batteries the durability of energy harvesters should be increased. This means that the lifetime harvester should be much longer than the lifetime of a battery. This requirement increases the level of difficulty and requires advanced manufacturing processes. The increase in complexity of nonlinear energy harvesters comes along with an increase in components, which is in contrast with the requirement for a maintenance free design. However, there are design possibilities to reduce the amount components and still posses nonlinear behaviour. Without losing grip on the main focus of this thesis and being too elaborative with respect to design possibilities for existing nonlinear energy harvesters, it is decided to only describe the nonlinear parts within the energy harvester of this research. The nonlinear parts are embodied by the motion limitations of end-stops and by the bistable suspension, which received great attention to be used within low frequency environments.

3.5.1   End-stops

The first components to contribute to nonlinear characteristics are the sudden changes in stiffness and damping when the proof mass collide with the end-stops. The name end-stops already implies the location of these systems, which are defined as the limitation of the oscillator amplitude. When the system is excited with larger input motion like on small scale, the proof mass will collide with the end-stops. The nonlinear phenomenon to occur at the impact is the rapid change in stiffness and damping, where the system in total is excited with many frequencies and results in a larger frequency bandwidth in comparison with the linear resonant configuration without end-stops. However, the end-stops limits the proof mass motion an as a consequence decreases the generated power output.

The main motivation for using end-stops instead of the other mechanisms is the compatibility within the original design, without increasing the overall volume. Using end-stops would require less advanced manufacturing processes and decreases the level of difficulty, since the design itself is not different than the linear configuration. These reasons enhances the potential of miniaturizing and increases the reliability as well the durability. Moreover, end-stops can be used to reduce the stresses within linear cantilever configurations. The end-stops reduces the amplitude motion and the consequentially limit the occurrence of high stresses due to bending at the place of clamping. Furthermore, this additional design element doesn't depend on the type of transducer. Figure 3.6 shows the working principle of the end-stop in a linear cantilever configuration accompanied with their typical experimental outcome.
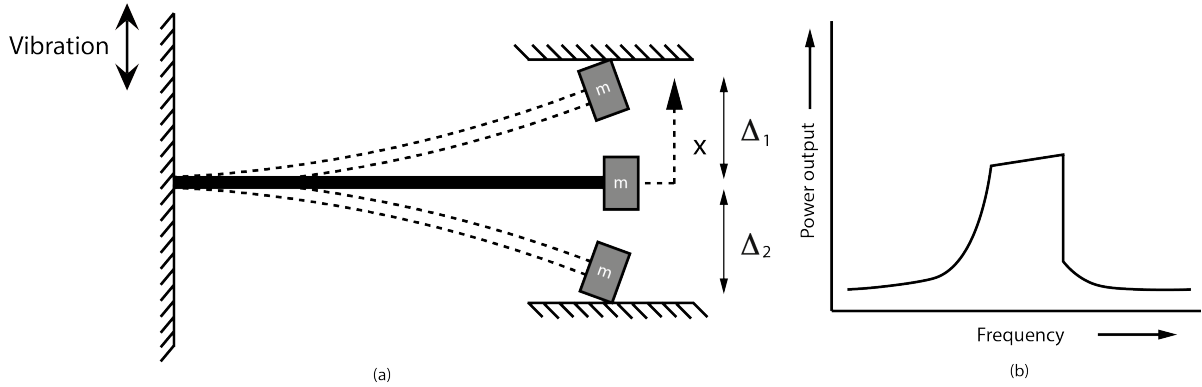
Figure 3.6: The behaviour of a linear cantilever design with end-stops, (a) end-stop working principle (b) output performance

These systems comes again along with also a relatively simple modelling method. The corresponding equation of motion is expanded with an additional force (3.5), represented by the end-stop force F^{stop} and expressed with (3.6).

$$m\ddot{x} + c\dot{x} + kx + F^{stop} = F(x) \tag{3.5}$$

$$F^{stop}(x) = \begin{cases} K_s(x - \Delta_1) + C_s\dot{x}, & \text{if } x \geq \Delta_1 \\ 0, & \text{if } \Delta_2 \leq x \leq \Delta_1 \\ K_s(x + \Delta_1) + C_s\dot{x}, & \text{if } x \leq \Delta_2 \end{cases} \tag{3.6}$$

In this equation the terms in the eom (3.5) are the same as for the linear cantilever configuration. However, the difference upon impact of the proof mass and end-stops ($x \geq \Delta_i$), increases the damping and stiffness characteristics of the system. In equation (3.6) the extra damping is represented by C_s and the stiffness by k_s.

3.5.2 Bistable mechanisms

Another mechanism to incorporate nonlinearity within the system is the method of bistability. The difference of bistable mechanisms with respect to linear systems can be obtained within the potential graph 3.7(a).
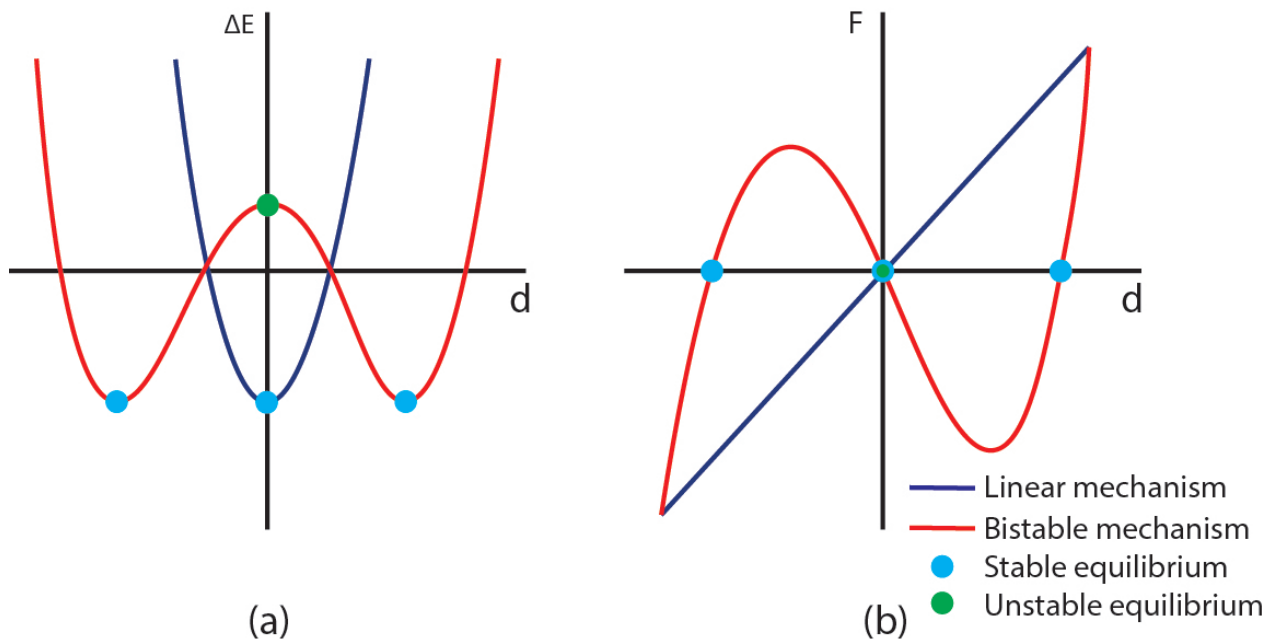
Figure 3.7: Graphical interpretation between linear monostable and bistable mechanisms. Figure (a) shows the graphical behaviour of how the energy potential is distributed, figure (b) gives the force (F) deflection (d) curve

The potential graph can be used as a measure of how much energy is needed to move a certain structure. Since linear mechanisms have one stable equilibria, which is often the position of the oscillator at rest, the potential graph will show only one "well". Obtaining the same behaviour of the oscillation in bistable mechanisms, it can be obtained that bistable structures have 2 stable equilibria as well as two wells in the potential graph. Besides the existence of the stable equilibria, the bistable structure has also an unstable equilibria creating a potential barrier between the two wells. The introduction of negative stiffness in bistable structures is responsible for the potential barrier, which will be less when the amount of negative stiffness is decreased. The force deflection curve of the linear and bistable structures can be observed in 3.7(b). When the displacement of the linear mechanism is increased, no change in stiffness can be expected. Increasing the displacement of the bistable structure, such that it overcomes the potential barrier the system will deflect to the other stable equilibrium point. Between these points the negative stiffness part can be observed, in which no force is needed for actuation. This can be clearly understood with a ball positioned on a steep mountain. When the ball is positioned on top of the mountain, it is unable to rest and will start to roll down to one of the valleys on either sides of the mountain. The same phenomenon occurs when the systems energy is high enough to overcome the potential barrier, it will never reach the unstable equilibria. When the energy of the input vibration is larger than the energy of the potential barrier, the system will deflect to the other potential well. Therefore three unique trajectories can be observed and schematically shown in figure 3.8.

The first trajectory is called intrawell motion(I), where the oscillation is confined in one well and exhibits the same characteristics as monostable oscillators. The second trajectory is called chaotic interwell motion (II). In this trajectory the energy is not high enough to oscillate between the two
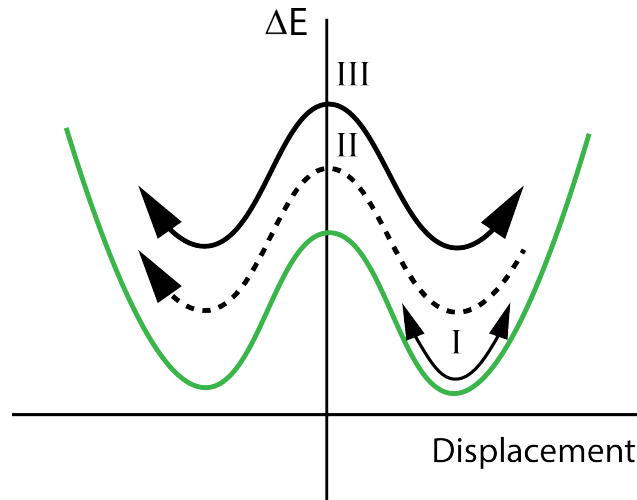
Figure 3.8: Distinct trajectories within bistable mechanisms, Intrawell (I), Chaotic interwell (II), Periodic interwell (III)

potential wells with periodical motion, however jumps can be observed. In this trajectory the system accumulates energy as it is confined in one well and used to overcome the barrier. After the jump all the energy is dissipated by the damping characteristics in the second well and a new energy accumulation is required for the jump. This behaviour results in chaotic jumping behaviour and the occurrence of the jump depends on the varying input spectrum. The periodic oscillation between the two potential wells is called interwell motion, and their large amplitude generation makes this the most desirable trajectory. Moreover, the dynamic response can be related to the motion ratio. It is explained that linear resonant energy harvesters require large motion ratios ($\lambda > 1$), while the dynamic response of bistable mechanism shows great responses in the reverse direction and on low motion ratios ($\lambda < 1$). Therefore is bistability greatly desired in low frequency excitations like human input motion.

Three commonly used bistable configurations can be found within literature and shown in figure 3.9.
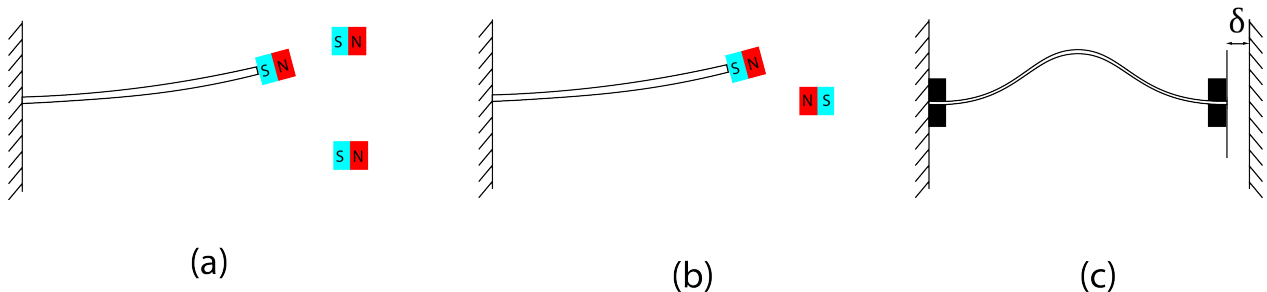
Figure 3.9: Bistable mechanism configurations, a) Magnetic attractive bistability, b) Magnetic repulsive bistability, c) Mechanical bistability

The first two types depends on the attractive or repulsive force of magnets. However this is mostly

not a design solution for small scale electronics, since their magnetic force can interfere with the electrical circuit and the brittle characteristics of magnets limits the scaling possibility. The third configuration is more desirable and mostly configured as a beam, which is clamped on both sides. In this design preload is applied by means of an axial force, whereafter the system buckles and bifurcate to the first buckling mode. The stresses induced by the oscillation between the two potential wells have received great interest to be converted into electrical energy by means of strain dependent energy transducers.

The mechanical behaviour of bistable structures mostly consist of a numerical model, but the dynamical behaviour can be described by the same single degree-of-freedom model equation of the linear resonant energy harvester (3.3). However, in bistable structures the stiffness depends on the amplitude of the oscillator and changes locally. This varying parameter is the reason for the non-linearity within the system and can be calculated from the mechanical analysis and is mostly used as an input parameter for the dynamical simulation $k(x)$.

3.6 Energy transducer

The energy captured by the energy receiver is converted into electrical energy, represented by the transducer block of the schematic overview of the working principle of an energy harvester, figure 3.2. This transduction of energy between the mechanical and electrical domain can be done with three types of transducers, electromagnetic, electro static and piezoelectric. The type of transducer depends mostly on the geometry and type of mechanism. The first energy transducer, which is mostly used since their simplicity is the electromagnetic transducer. This conversion mechanism depends on the Faraday's law of induction, which combines a magnetic field with an electrical circuit to induce an electromotive force. The embodiment of such systems in energy harvesters consist of a moving magnet through a coil, where the generated elecro mangetic force can be described by formula (3.7). In this equation, the N is defined as the number of windings of the coil and $\frac{\Delta\phi}{\Delta t}$ the change in magnetic flux. Therefore, high velocities are required to increase the power output and are therefore well suited for linear resonant energy harvesters.

$$\mathscr{E} = -N\frac{\Delta\phi}{\Delta t} \tag{3.7}$$

The electro static transducer depends on the difference in charge between two electrostatic charged objects. One electrode is fixed, while the other charged electrode is allowed to move parallel to the fixed plate and induce a potential difference. The induced potential difference depends on the capacitance between the plates which is defined by equation (3.8), in which d is defined as the separation distance, A the area of the electrodes and ε_0 the relative permittivity of the operation medium of the environment. The capacitance in combination with the transfer of charge between the plates defines the induced potential difference and can be calculated according to equation (3.9). This configuration is due to their high potential of miniaturization mostly used in MEMS energy harvesters.

$$C = \frac{\varepsilon_0 A}{d} \tag{3.8}$$

$$V = \frac{Q}{C} \tag{3.9}$$

Piezoelectric transducers depend on the amount of change in stress and are therefore mostly often used in combination with bistable configurations. A piezoelectric beam consist of two electrodes, which are separated by a separation layer to prevent short circuit conditions. The induced voltage depends on the condition of the stresses within the beam, due to deflection one electrode is forced to have compressive stress while the other is subjected to compressive stress. The change of potential induced by the difference in stresses within each piezo layer depends the generated output power. This principle can be used in three different configurations, namely: in compression, flexural and in shear. The flexural configuration is mostly used in energy harvesters, which are often configured as a cantilever beams. This energy transduction principle can be described with the govern equations of (3.10) and (3.11) and is orientated in 3D. The mechanical part of these equations are described by the quantities of S and T, and defines respectively the strain and stress components of the beam. The electrical part is defined by the electric field components E and described by the distribution of the the electric field components D. The piezoelectric charge components and their corresponding relativity are described by d and ε.

$$S = s^E T + d^t E \tag{3.10}$$

$$D = dT + \varepsilon^T E \tag{3.11}$$

3.7   Problem formulation

The usability of bistable structures for vibration energy harvesting have received great attention to powering low power electronics. Their ease of manufacturability and their capability to capture kinetic energy induced by low frequency vibrations, makes it an interesting alternative for linear resonant energy harvesters. The desired oscillation of interwell induces large amplitude oscillations and are capable of capturing ambient induced kinetic energy when the input amplitude is much larger than the output amplitude of the oscillator ($\lambda < 1$). However, the potential energy barrier between the potential wells and the energy varying spectra do not guarantee that the motion of the energy harvester only consist of periodical large amplitude amplitude interwell oscillation. Therefore, utilising bistable structures in energy varying spectra consist of the following problem:

"Small scale bistable vibration energy harvesters require high accelerations in order to move between the potential wells".

Vibration energy harvesters are dependent on the oscillator amplitude, and the bistable structure generate the largest power output when the system can move between the two potential wells. This work combines the ability of capturing low frequency vibrations by means of bistability with the hard and rigid stiffness characteristics of end-stops. The height of the potential energy barrier and locations of the stable equilibria depends on the amount of axial preload, however the mechanical end-stops disconnects this dependency and introduces a new design parameter for tuning the height

of the potential energy barrier. Therefore, the mechanical end-stops can be used to lower the potential energy barrier and enhances the oscillation within the large amplitude trajectory of interwell. This theoretical statement can be observed in figure 3.10, where the initial energy barrier $\Delta E_{bistable}$ is reduced to $\Delta E_{end-stop}$ in case the oscillator motion is constrained by the end-stops, however this dynamical advantage comes along with an decrease in generated amplitude.
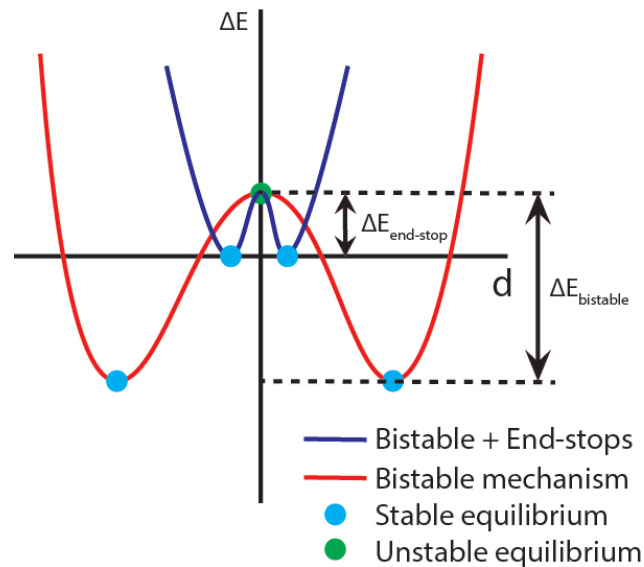
Figure 3.10

The research objective of this work is:

"Investigate the influence of end-stops in bistable structures with respect to their performance under low frequency excitation"

To achieve this objective, the main question to be answered is:

"How is the bistable mechanism affected by the utilisation of end-stops?"

Before tackling the main question stated above, a research in the direction of the additional nonlinearity induced by the end-stops will be addressed first. In this study the following question will be answered:

Literature study:

"What effect does the design variables in end-stop configurations have on the performance of the vibration energy harvester?"

3.8   Methodology approach

Figure 3.11 shows schematically the working principle and the potential energy characteristics of our proposed design. The bistability in this design is introduced by the combination of a parallel guidance flexure and a post buckled beam. The parallel guidance flexure is responsible for the positive stiffness and the buckling flexure introduces negative stiffness, resulting in bistable behaviour when a preload is applied. The reason for the utilisation of the parallel guidance mechanism is to ensure that the trajectory of the proof mass is only confined to be in straight motion, without introducing unwanted rotations. Moreover, the stiffness of the parallel guidance flexure can be analytically calculated and therefore used as a design element to reduce the negative stiffness of the buckled flexure in order to have excitation characteristics, which can be tested with experimental lab setups. However, this design principle can also be used to flatten out the potential energy barrier. This principle is called static balancing, where zero stiffness is obtained when the negative stiffness is cancelled out with positive stiffness. However, from literature it became clear that snap-through behaviour between the two potential wells is the responsible nonlinear motion which increases the power output [54; 14]. Therefore, it is only used for stiffness compensation.
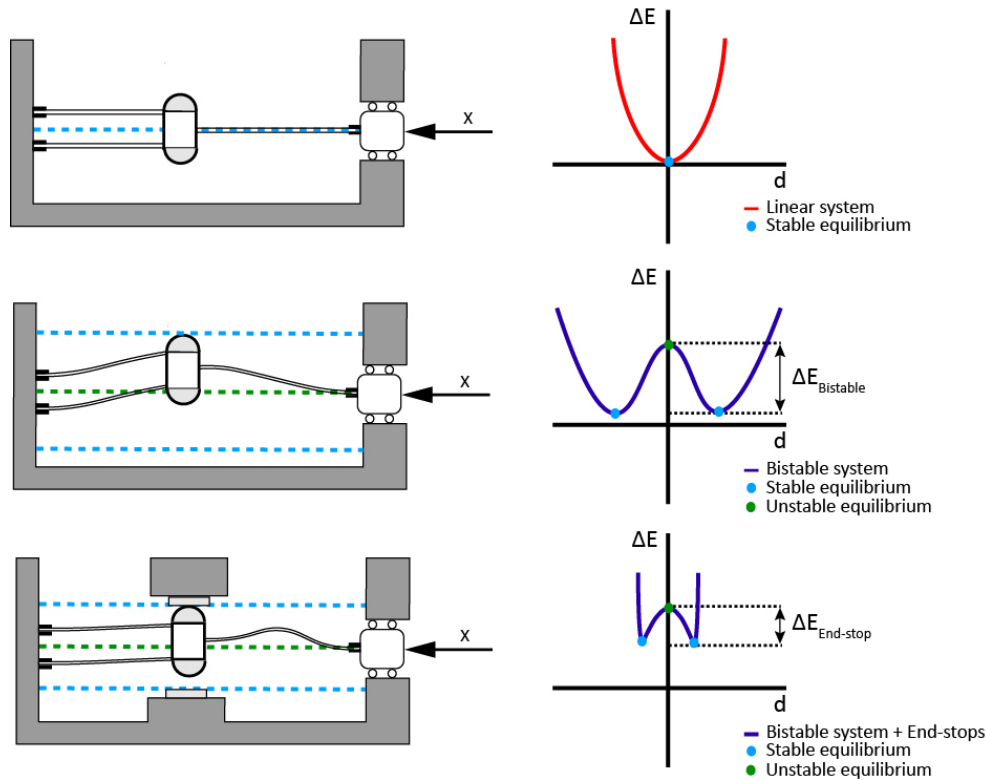
Figure 3.11: schematic overview of the proposed mechanism

The first figure of 3.11 shows the behaviour of our design in the unloaded configuration, represented by a single well. As soon as the preload surpasses the critical buckling load, the system start to bifurcate and induces the bi-stability to our system and a double well potential energy characteristics are created. The last picture shows schematically the integration of the end-stops in the bistable system. The energy characteristics are the same as with the unconstrained bistable configuration, however the end-stops forces the stable equilibria to be shifted to a different location on the potential graph and reduces the energy barrier between the equilibria positions. Therefore, it is highly assumable that this system require less acceleration to change its trajectory from intrawell to interwell oscillations. Because of the hard characteristics of the end-stops, it is also expected that the intrawell participation will be less significant than in the unconstrained configuration. Although this dynamical advantage is very desired for low frequency energy harvesters, it comes with a major drawback and that is the reduction in amplitude. And because the transducer depends on the generated amplitude a reduction in power output can be expected.

3.8.1 Prototype

A rendered overview of the constructed prototype can be observed in 3.12, where the locations of the end-stops and components of the bistable suspension are indicated. In this design the captured energy is transduced to the electrical domain with the use of a strain dependent piezoelectric transducer. This transducer is called PVDF foil and consist in comparison with piezo ceramic transducers of a more flexible segregation layer and are therefore more capable of measuring the dynamical behaviour in systems with high stress locations.
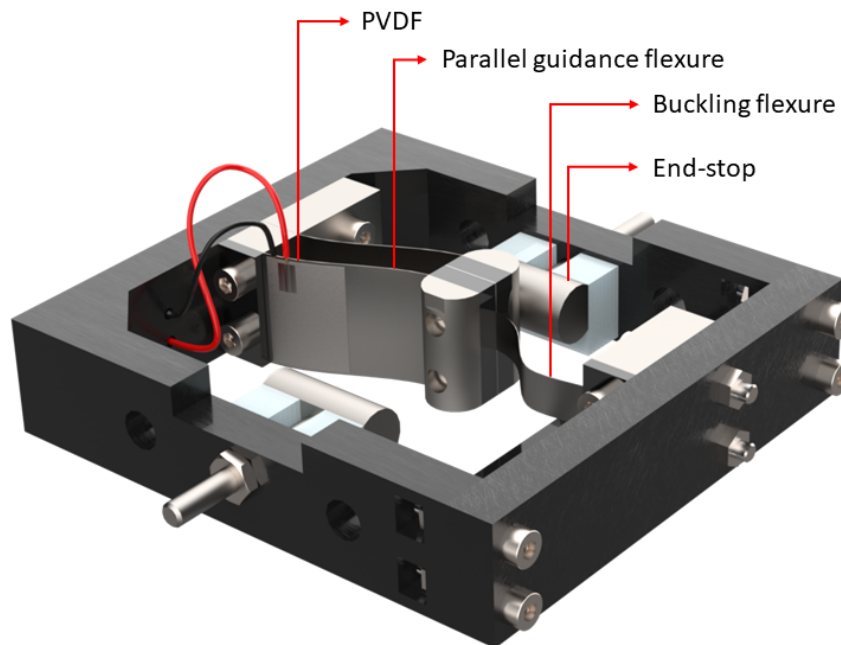
Figure 3.12: 3D render of the bistable vibration energy harvester design

3.8.2   The model

The model is constructed in two parts, first the mechanical analysis is performed and used in the second part, the dynamical analysis to calculate the stiffness of the bistable structure on each location during excitation.

The mechanical model is constructed in ANSYS mechanical APDL and a graphical interpretation of the model can be seen in figure 3.13. Figure 3.13(a) indicates the locations of the keypoints in the monostable configuration. Where the keypoints 2, 3 & 4, 8 correspond to the parallel guidance flexures and 1, 5, 6 the buckling flexure. The proof mass is constructed out of two parts and indicated with keypoints 2, 4 & 3, 1. After all the keypoints are connected with their corresponding lines a mesh is added to each line to give the line a 3D interpretation and material properties. After the geometry was constructed the axial degree-of-freedom located on keypoint 6 of the buckling flexure were deleted and a preload was applied, shown in figure 3.13(b). To help the numerical solver to let the flexure to bifurcate to the first buckling mode a small negligible parasitic force is applied onto keypoint 5. The point of actuation is indicated with *Measurement point*, where also the reaction forces were recorded to calculate the force-deflection characteristics of bistable mechanism and shown in figure 3.13(c).
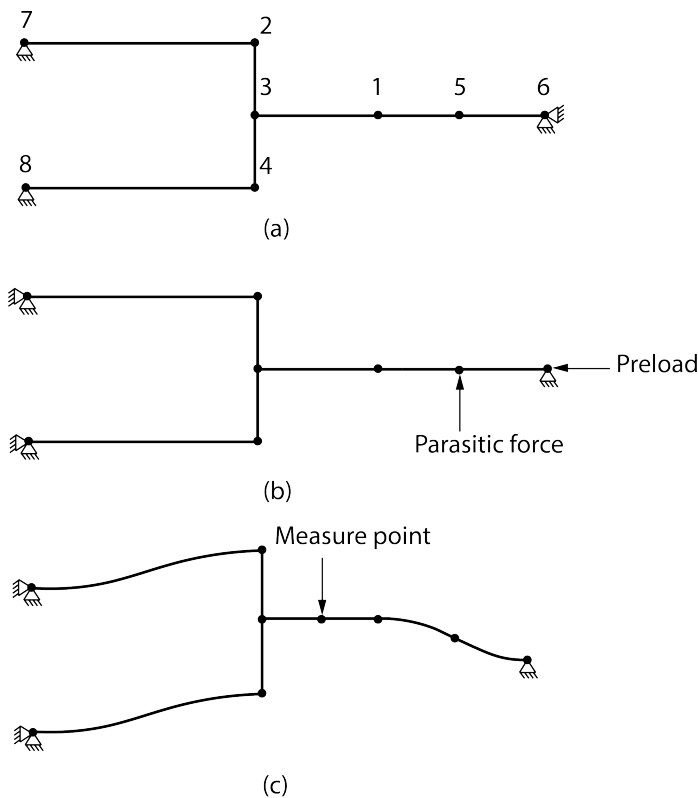
Figure 3.13: Schematic overview of the construction of the mechanical analysis model in ANSYS. a) Monostable configuration with indicated keypoints, b) Boundary conditions and loads, c) Buckled configuration with indicated measurement point

Finally the simulated mechanical force-deflection characteristics of the bistable vibration energy harvester can be observed in figure 3.14.
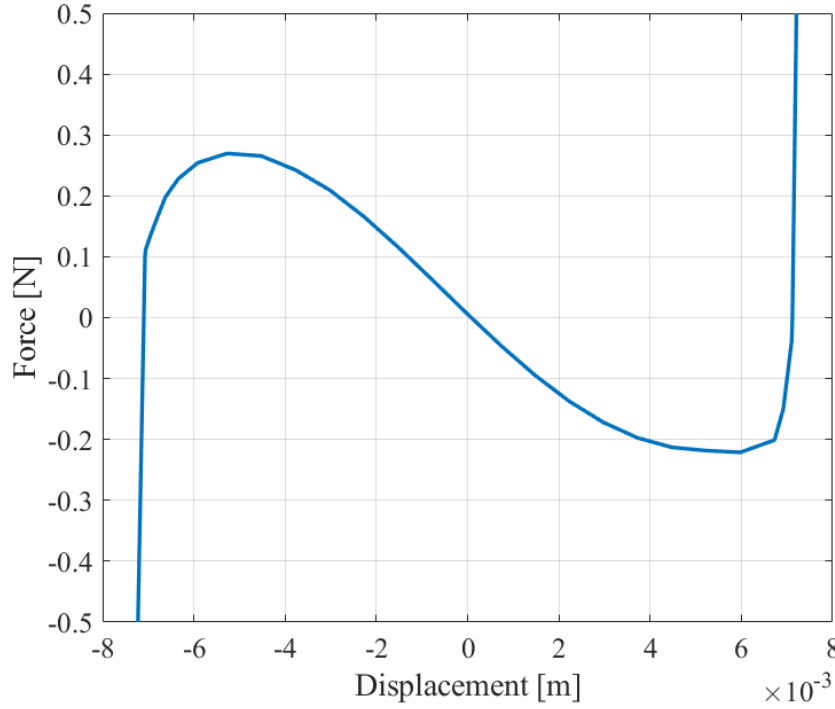
Figure 3.14: Force-deflection characteristics of the unconstrained bistable vibration energy harvester

The dynamical model is constructed in MATLAB and is analogue to the lumped-parameter single degree-of-freedom model described in sub section 3.5.1, however expanded with a varying stiffness parameter $k(x)$, which is calculated in the mechanical analysis. The equations of motion were described with equation (3.12), where the nonlinear force of the end-stops are expressed by the expression of (3.13). In this expression, the end-stop stiffness is defined as the contact stiffness and identified with a Hertz contact analysis. However, the damping characteristics are more difficult to be measured and therefore a simplified model is used to approximate the damping behaviour at the impact. This model is called the coefficient of restitution model, and defines the loss in kinetic energy in case of an collision. This parameter can be calculated with the relation of (3.14), where V_1 is denoted as the incoming velocity and V_2 the outcoming velocity.

$$m\ddot{x} + c\dot{x} + k(x)x + F^{stop} = F(x) \tag{3.12}$$

$$F^{stop}(x) = \begin{cases} K_s(x - \Delta_1) + C_s\dot{x}, & \text{if } x \geq \Delta_1 \\ 0, & \text{if } \Delta_2 \leq x \leq \Delta_1 \\ K_s(x + \Delta_1) + C_s\dot{x}, & \text{if } x \leq \Delta_2 \end{cases} \tag{3.13}$$

$$CoR = \frac{V_2}{V_1} \tag{3.14}$$

Finally, the dynamical response of the synthesis of end-stops in bistable mechanisms can be observed from the results shown in figure 3.15. In this figure, the dynamical response to variations in accelerations and stopper distances can be seen for two different frequencies. The simulated data is the absolute displacement and RMS velocity, which is for each combination calculated for the last 20% of a time signal of 10 seconds. It is said that dynamical oscillations of bistable structures are well observable in environments, where the motion ratio is below 1 ($\lambda < 1$) and less observable in case the vibrations are much larger than the output displacement of the oscillator amplitude ($\lambda > 1$). This theory can be verified with the results from this model, where the maximum peak output performance of the system exited at $f = 3Hz$ were found to be under the condition of $\lambda = 0.036$ and for $f = 15Hz$ $\lambda = 0.57$.
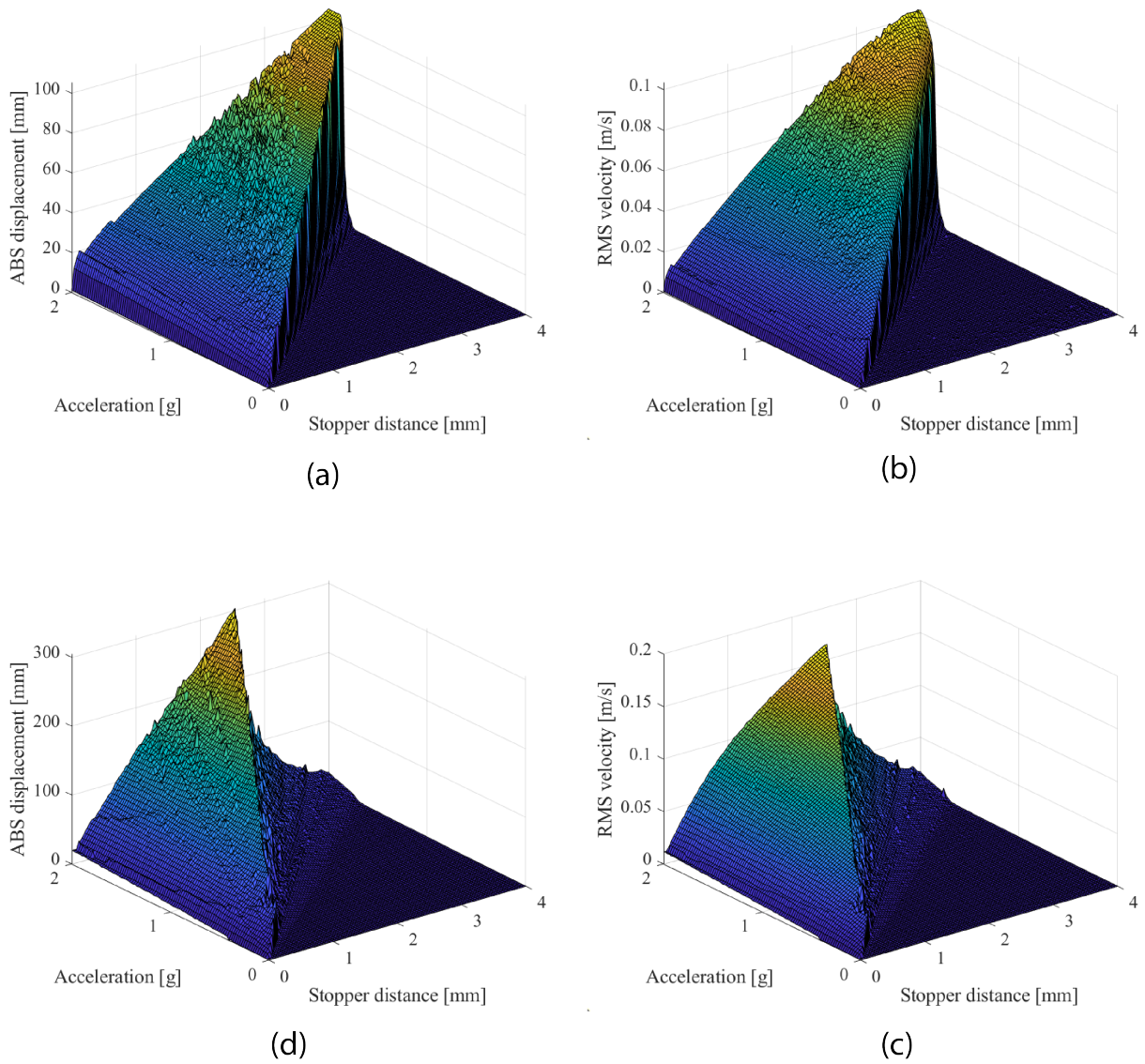
Figure 3.15: Dynamical results of the model for variations in acceleration and stopper distance for two sinusoidal excitations a & b 3Hz, c & d 15Hz

The main conclusion to be observed from this graph is a decrease in required acceleration to oscillate with large displacement output, and therefore satisfies the hypothesis. However, the expected decrease in amplitude is also observable. Validation of this model will be done in the following chapter, where the process is described in the form of a paper. Detailed information of the manufacturing process, mechanical and dynamical analysis, experimental protocols and dimensions of the harvester design can be found within the Appendix, respectively B, C, D.4.2, E, F.

3

3

4

Using travel limits to tune buckled bistable oscillators for low-frequency vibration energy harvesting

K.ᴠᴀɴ Pᴜғғᴇʟᴇɴ & T.W.A. Bʟᴀᴅ & R.A.J. ᴠᴀɴ Oꜱᴛᴀʏᴇɴ

Vibration energy is a promising source for powering wireless sensors, for example in human input environments with large excitation vibrations. These environments suffer from unpredictable vibration spectra and their low-frequency and large amplitude characteristics offer great possibilities for mechanisms with double well potential energy characteristics. The output power generation of bistable energy harvesters depends on the oscillation in the large amplitude trajectory between the two potential wells. However requires enough force to overcome the potential energy barrier. This work aims to improve the occurrence of interwell oscillation by lowering the potential energy barrier between the two potential wells by the influence of hard mechanical travel limits. The point of interest in this work is the acceleration at which trajectory of intra and interwell alter themselves and identified as the bifurcation point. An energy harvesting prototype was developed based on bistability induced by the positive stiffness of a parallel guidance mechanism and negative stiffness of an axial loaded buckling beam. A model is made and the influence of the hard characteristics of the mechanical travel limits in the bistable architecture is experimentally tested with an acceleration sweep. This combination resulted in a decrease in required force for the oscillation in the desired large amplitude trajectory by constraining the oscillator motion with travel limits. Moreover, the results from the numerical bistable model in combination the mechanical characteristics of the travel limits at the impact, proves to be in good agreement with the experimentally obtained results.

4.1   Introduction

Over the years, advanced manufacturing processes have made it possible for new fields of applications to be monitored fully autonomous. These systems require sophisticated sensing equipment, and are mostly located at hard to reach locations. One of these new fields of applications is the healthcare industry for stimulating and monitoring the health status of the human body, examples are hearing aids, pace makers or wearable diabetes monitors [5; 45]. In these fields of application, systems reliability is paramount and depends mostly on the sensors sensing and transmission rate [29]. Although this data rate is considered to be a design element of the sensor, it consist of a small design space in order to guarantee the battery's lifetime. Besides this limitation on the reliability, the replacement of the industrial grade battery due to the confined energy capacity is the main cause of the high involved maintenance costs. Therefore, replacing batteries with renewable energy sources like vibration energy, converting ambient energy into useful electrical power, could be a promising solution for these problems.

Monostable energy harvesters are mostly designed to work as resonant harvesters, resulting in high output performance on a specific frequency [48; 52]. However, if the vibration energy harvester (VEH) is not accurately tuned to the input signal of the real world, poor output performance can be expected [11]. Non-linear energy harvesters, incorporating an extra stiffness term in their equations of motion prove to be more robust against uncertainties in the varying real world energy spectrum [28]. Examples of these systems are Duffing and impact driven energy oscillators [35; 49].

A recently new investigated mechanism for energy harvesting is the use of mechanical bistability. Bistability in energy harvesters is greatly desired because, the possibility of monolithic design and reduction in required components results in less wear and comes along with a potential of alleviated manufacturing complexity. Bistability exhibits non-linearities by the difference in potential energy characteristics, compared with monostable structures. Figure 4.1(a) schematically indicates how the oscillation trajectories of monostable structures are confined to be located in one well. As bistability is introduced, the potential energy characteristics are transformed from single to double well resulting in two stable equilibria, which are segregated by a potential energy barrier 4.1(b). When bistable structures are ambient vibrated, three unique oscillating trajectories could be observed[25]. When the system is excited, the first motion to occur is intrawell motion (figure 4.1(a) I), which confines its trajectories in one of the two potential wells. When the level of excitation is increased, an accumulation of potential energy causes the system to oscillate itself in the second well, however the accumulated energy is consumed by the jump over the energy barrier and a new energy accumulation is required to repeat this motion. While the energy harvester shows this aperiodic motion, it is called chaotic motion (figure 4.1(b) (II)). The mechanism exhibit periodic interwell motion (4.1(b) III), in case the trajectories show steady state oscillations between the two potential wells. The energy capture mechanism in these systems is the transition between the stable positions, where the ambient energy is transformed into strain energy. The captured strain energy is favourable to be extracted by strain dependent energy transducers based on the conversion principle of piezoelectricity.

However, in bistability, when not designed properly, large amount of input energy is used to overcome the potential barrier, resulting in the requirement of high accelerations [54]. This introduces challenges in low-frequency environments, for example with human input motion.
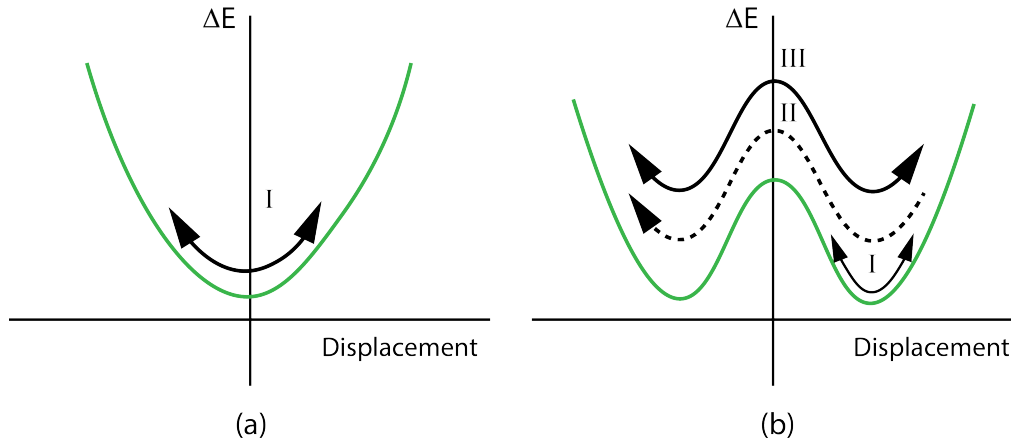
Figure 4.1: Potential energy curve of monostable (a) and bistable mechanisms (b), showing the unique oscillation trajectories, I intrawell motion, II chaotic motion, III periodic interwell motion.

In the work of Masana et al. [36], the principle of the mechanical clamped-clamped post buckled flexible beam was compared with its monostable configuration. The energy transduction in this work was done by transforming the strain energy of the beam in electrical energy with the use of a piezo ceramic energy transducer. The system was exited under harmonic excitation and a significant rise in power output could be observed comparing to its monostable unbuckled design. To show the robustness of bistable mechanisms in energy varying environments Cottone et al. performed an experimental investigation on how these mechanisms behave under random base excitations [14]. Surprisingly, the bistable energy harvester achieved up to an order of magnitude more electrical power when compared to it monostable configuration. A design principle to overcome the need for high accelerations is the use of magnets. In the work of Zhu et al. [54] a midpoint magnetic force is used to enhance the dynamical performance and increases the output performance compared with the original unbuckled design. This design resulted in an increase in output performance by triggering the second buckling mode, called the 'S' shape and more snap through behaviour could be observed. Besides the increase in power performance of these systems, it also shows the wide applicability throughout large bandwidth regions.

However, state of the art energy harvesting designs based on bistability shows great potentials to be used in low-frequency environments, the system requires relatively high input accelerations to overcome the potential barrier and oscillate in the desired interwell trajectory. The goal of this research is to lower the required input acceleration by means of relocating the stable equilibria in the mechanical domain with travel limits. These travel limits disconnect the dependency of the locations of the stable equilibria on the amount of preload and introduces a new design parameter. This new design parameter is able to tune the amount of amplitude without changing the stiffness characteristics of the bistable mechanism between the two stable equilibria.

Section 4.2 describes the working principles of the energy harvester design, followed by a mechanical and dynamical analysis. In section 4.3 the simulated and experimentally tested results are

4
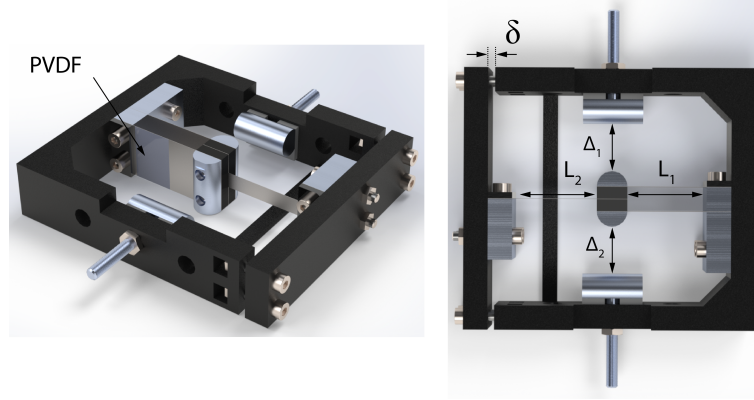
Figure 4.2: The energy harvester design with indicated parameters.

compared. Section 4.4 is used to discuss the main results found, followed by section 4.5, describing the most significant conclusions and recommendations.

4.2 Method

4.2.1 Mechanical design

The vibration energy harvester design can be seen in figure 4.2. The suspension of this design consist of two parts, a parallel guidance mechanism in combination with a buckling flexure. The parallel guidance mechanism is constructed with two parallel orientated flexures and separated at a uniform displacement. The mechanism is on both ends constrained, however one end is allowed move in the direction perpendicular to the orientation of the parallel guidance flexures. This unconstrained degree-of-freedom allows the proof mass to travel with straight motion in the forcing direction. Moreover, the mechanical behaviour of the parallel guidance flexure can be used as a design element to compensate for the large amount of negative stiffness induced the buckling flexure.

Mechanical bistability is introduced by the transformation of the buckling beam in its post buckled state by means of preload. The required load to bifurcate a buckling beam to the first buckling mode is called the first critical buckling load. The configuration of the first buckling mode corresponds to the mode with the lowest amount of internal energy after surpassing the first critical buckling load. The configuration of the second critical buckling mode of a single buckled beam is configured as a "S" shape. Even though this configuration is unstable it will not occur in the design of the energy harvester, where bistability is introduced by the combination of a parallel guidance flexure and a buckling flexure. The reason is the rotation constraint of the proof mass imposed by the parallel guidance flexure.

In order to move between the stable equilibria depends on the required force to overcome the potential energy barrier. The mechanism looses stability as it acquired enough force, this will result in an attractive force to the other stable equilibria induced by the negative stiffness of the post buckled beam. This attractive force is called snap-through and their non-linearity improves the ability of bistable energy harvesters to outperform their performance in comparison with linear energy harvesters [27]. In this work, the force required for actuation is influenced by mechanical travel

limits. Figure 4.3 schematically shows the integration of the travel limits and their corresponding difference in potential energy barrier. Figure 4.3(a) shows the unbuckled configuration, of which the pretension does not surpass the first critical buckling load and behaves as a monostable oscillator. Increasing the pretension beyond the first buckling load will result in the configuration of figure 4.3(b), showing two stable equilibria segregated by a relatively high potential energy barrier $\Delta E_{Bistable}$. The configuration of the travel limits in bistable mechanisms can be seen in figure 4.3(c), which are placed at a certain location from the origin of the range of motion imposing a limitation on the travel of the mechanisms proof mass. From the corresponding potential energy curve, it can be seen that the required potential energy (ΔE_{Limit}) is reduced and enhances the ability of snap-through motion for lower input acceleration signals.
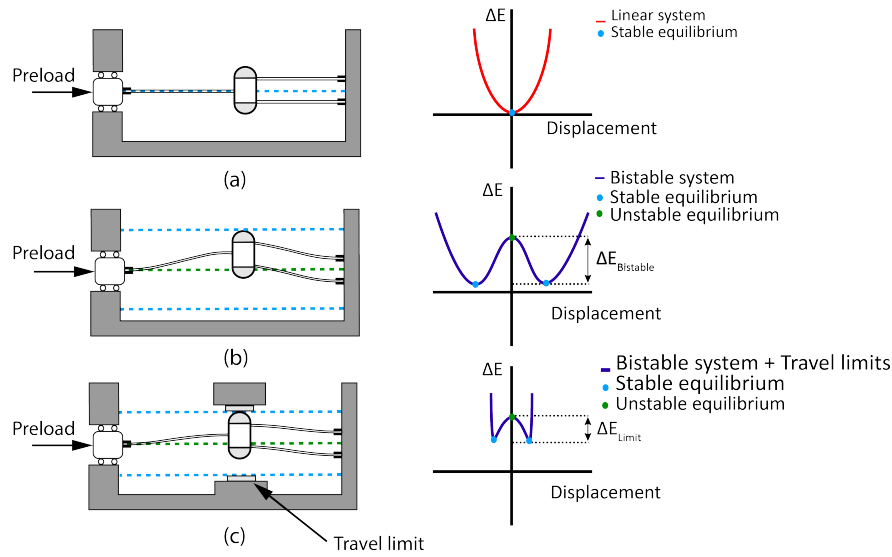
Figure 4.3: Schematic working principle bistable energy harvesting mechanism in combination with their potential energy characteristics, a.) Monostable structure, b.) Unconstrained bistable structure, c.) Constrained bistable structure.

4.2.2 Fabrication

The flexural beams in this design are made from 0.1mm thick spring steel with the properties: (E_f = 190 GPa, v_f = 0.34 ρ_f = 7.89 kg/m^3) and are manufactured using a micro laser cutting machine. The proof mass is made of a stack of steel shims, clamped by two cylindrical shaped aluminum components, in order to give the system its required mass. An important design aspect in bistable designs are its clamping conditions. Slight differences in alignment tightening torque and material stiffness, result in different behaviour. In the simulation, all degrees of freedom at the ends of the beams are fixed, therefore a aluminum milled block with much higher stiffness than the flexure's were used to mimic the same behaviour of having perfect clamping conditions as is done in the simulation. The mechanical travel limits are created using hard elements, represented by cylindrical shaped aluminum travel limits with the following properties: (E_s = 69 GPa, v_s = 0.34 ρ_s = 2.70 kg/m^3). Both cylinders of the proof mass and travel limits have corresponding

Parameter		Value	Parameter		Value
Unloaded parallel guide length	L1	26 mm	Length proof mass	L	18.3 mm
Unloaded buckling beam length	L2	27.7 mm	Proof mass width	w_3	10 mm
Parallel guide width	w_1	20 mm	Proof mass height	h	20 mm
Buckling beam width	w_2	6.8 mm	Travel limit stiffness	K_s	7.45e3 kN/m
Axial displacement	δ	2.7 mm	CoR		0.36
Proof mass mass	m	0.0152 kg	Damping coefficient	ζ	0.023

Table 4.1: Vibration energy harvester design parameters

dimensions for the radius (5mm) and length (20mm). Since the proof mass consist of the same shape, however orientated perpendicular to the travel limits, a Hertz point contact could be created. The point contact is greatly desired and limits the amount of energy lost during impact, since heat generation induced by friction at impact depends on the contact area. The frame was 3D printed in PLA at 100% infill, in order to give the system its maximum rigidity and hinder the influence of its flexibility during dynamical experiments. The bistability in this design is introduced by a predefined axial displacement (δ), transforming the buckling beam to bifurcate to the first buckling mode. The variable defining the locations of the new stable equilibria is the space between the travel limit and the proof mass, indicated in figure 4.2 with Δ. The variation of this parameter is done with the use of 0.5mm thick spacers, made from the same material as the flexures. These spacers were placed between the frame and the backside of the travel limit and squeezed with the use of a screw thread.

The energy transduction is done with a stain dependent 28μm thick Silver inked piezoelectric foil (PVDF) (TE 1-1004346-0). The PVDF transducer depends on the same governing equations as piezo ceramic transducers, however instead of using a ceramic segregation layer a more flexible material is used. Because of this flexible behaviour, PVDF foils are desirable to capture the dynamical behaviour of bistable structures. However they suffer from less power generation than the piezo ceramic energy transducers. The optimal position for the energy collection is near the clamping conditions, since these locations contribute the highest stresses in the system. Because of the occurrence of high stresses in these locations, piezo ceramic energy transducers are mostly not a feasible energy transduction mechanism for bistable mechanisms [13]. Furthermore, the parameters used for this prototype are summarized in table 4.1.

4.2.3 Mechanical analysis

4.2.3.1 Simulation

In order to understand the systems dynamical performance, the principles of its mechanical behaviour should be obtained first. This mechanical analysis was performed by a finite element (FEM) analysis in ANSYS Mechanical APDL. The model was built out of BEAM188 elements
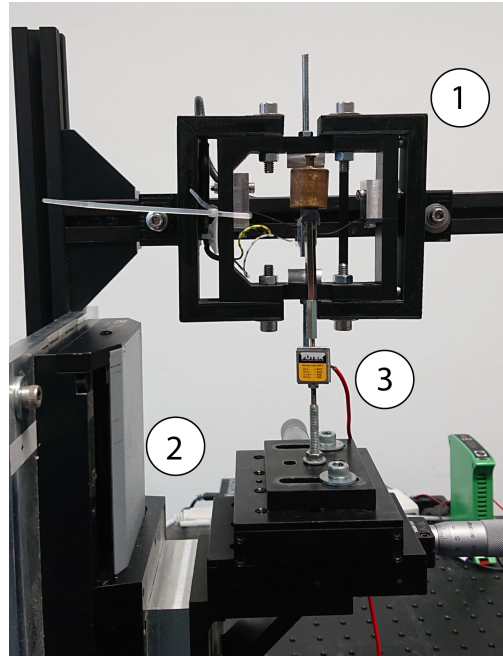
Figure 4.4: Force-deflection setup with indicated components: 1) Energy harvester mechanism; 2) Linear stage; 3) Force sensor.

based upon the Timoshenko's beam theory. To model the bistability, both ends of the structure were constrained and the in plane longitudinal degree of freedom of the buckling beam were relieved. A small force was applied to the middle of the buckling beam, to help the system to bifurcate to the first buckling mode when an axial load displacement (δ) was applied. A displacement was applied onto the middle of the proof mass and the reaction forces were recorded to simulate the quasistatic force-deflection characteristics of the design.

4.2.3.2 Experiment

Validation of this simulation was performed by a quasi-static analysis experiment of the energy harvester. The experimental setup can be seen in figure 4.4, in which the energy harvester (1) is experimentally tested using a PI M505 linear motion stage (2) and a 250g calibrated Futek LSB200 force sensor (3). The point of actuation in the simulation was located at the centre of the proof mass, however in reality this could not be achieved due to the obstruction of its frame. The proof mass is extended with a bracket to mimic the same actuation point as in the simulation. To ensure the contact between the force sensor and the system, an additional mass of $50gr$ is used and the experiment is performed vertically. This contact definition allows lateral movements imposed by the imperfections of the prototype, without introducing extra moments or forces onto the system.

4.2.4 Dynamical analysis

4.2.4.1 Simulation

The dynamical model of the bistable system is described using a lumped-parameter single-degree-of freedom model. Without the interaction of the travel limits, the system can be described using the mass-spring-damper model, represented by equation:

$$M\ddot{x} + C\dot{x} + F^{mechanism}(x) + F^{Limit}(x) = F(x) \tag{4.1}$$

In this equations x, $\dot{x}$ and $\ddot{x}$ represent the oscillator motion, velocity and acceleration relative to its base excitations. The mass (M) of the system is defined by the weight of the proof mass and the damping (C) is observed during a logarithmic decrement measurement, where the system at rest is excited with an plucking based motion. The nonlinear force of the bistable oscillator suspension is defined as $F^{mechanism}$ and is calculated locally from the force-deflection simulation. The locations of the stable equilibria of the unconstrained configuration are defined by the amount of pretension, however the utilisation of mechanical travel limits results in a extra nonlinear force in the equation of motion $F^{Limit}(x)$. This force is defined as the parameter, responsible for the new locations of the stable equilibria, when the motion is constrained by the mechanical travel limits as can be observed from figure 4.3(b) and 4.3(c). When the stable equilibria are shifted, the stiffness and damping of the system increases significantly due to the rigid characteristics of the travel limits. This force can be described by a piecewise linear model, represented by the expression of (4.2) [41].

$$F^{Stop}(x) = \begin{cases} K_s(x - \Delta_1) + C_s\dot{x}, & \text{if } x \geq \Delta_1 \\ 0, & \text{if } \Delta_2 \leq x \leq \Delta_1 \\ K_s(x + \Delta_1) + C_s\dot{x}, & \text{if } x \leq \Delta_2 \end{cases} \tag{4.2}$$

Where (K_s) and (C_s) are denoted as the stiffness and damping coefficients of the system in case the oscillator motion is larger than the travel limit displacement (Δ_i). The contact stiffness (K_s) was observed from a Hertz point contact analysis, since the area induced by the collision of the two perpendicular orientated cylinders is a contact point. In addition to the change in stiffness an increase in damping is present when the proof mass collide with the travel limits. When periodical impact occur, a fraction of the captured energy will be dissipated by the travel limit damper and converted in to heat by means of friction. The travel limit damping (C_s) is simplified using a coefficient of restitution model (CoR), which represents the amount of kinetic energy which is lost during impact. The CoR is defined as the ratio of the out coming velocity over the incoming velocity. The prototype was excited with an sinusoidal input excitation and the bouncing behaviour of the proof mass after the collision with the travel limit were measured with a laser sensor.

Finally, the dynamical model was simulated using an ODE solver in MATLAB, utilising the event function to stop the integration at point of impact after which the integration continues for new initial conditions. The new initial conditions are constructed by the travel limit location and a reduction for the incoming velocity with the coefficient of restitution. The parameter of interest is the acceleration from which the system transforms its trajectory from intra to interwell oscillation. This parameter is denoted as the bifurcation point, and found by the excitation of the system with an acceleration sweep. Moreover a surface plot was constructed for varieties in stopper distance
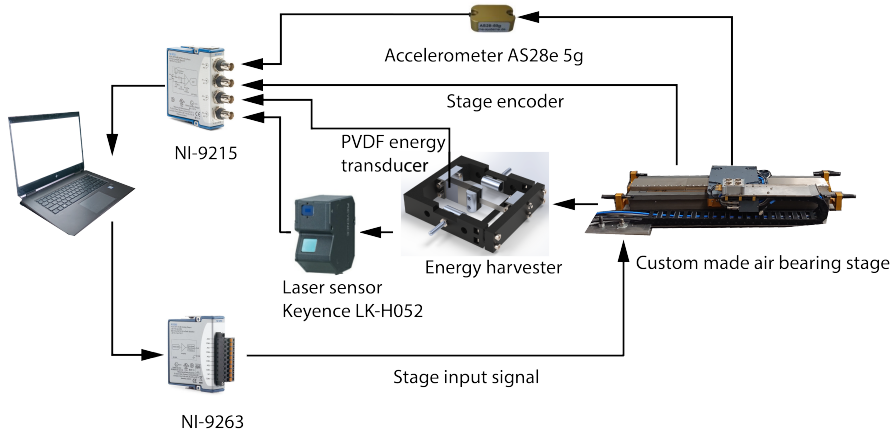
Figure 4.5: Simplified experimental overview of the dynamical setup.

and acceleration, where for each combination the absolute displacement and RMS velocity were calculated. These results were calculated over the last 20% of a time series of 10 seconds to ensure steady state oscillations.

4.2.4.2 Experiment

The validation of the dynamical simulation with the experimental data is done with an acceleration sweep consisting of a duration of 300 seconds. A schematic overview of the test equipment can be observed in figure 4.5 The VEH was tested on custom made linear air bearing stage, with a range of motion of 500mm, being able to test VEHS on low frequency input signals. The acceleration of the stage was checked by an external acceleration sensor, to validate the stage input output relation. Besides, the trajectory of the base is measured using a encoder inside the air bearing stage to validate if the movement of the air bearing stage is analogue to the input excitation signal. The voltage, due to strain energy, was measured by placing a 1 MΩ resistance in series with the terminals of the piezoelectric transducer. By placing the laser sensor on top of the base, relative motion between the proof mass trajectories and base excitations could be measured. In this experiment simultaneous recording of input signals and output signal for the controller of the linear air bearing stage were delivered by a National Instrument DAQ chassis consisting of a NI-9215 and NI-9263 voltage input/output module. The determination of the bifurcation parameter was done with a linear increasing acceleration signal under fixed frequency condition.

4.3   Results

4.3.1   Mechanical characterization

Figure 4.6 shows the simulated and experimental mechanical characterization of the bistable energy harvester. It can be seen that the stiffness and the locations in the stable equilibria showing small differences compared with the simulation. Besides, the negative stiffness slope shows similar characterization as in the simulation.

4
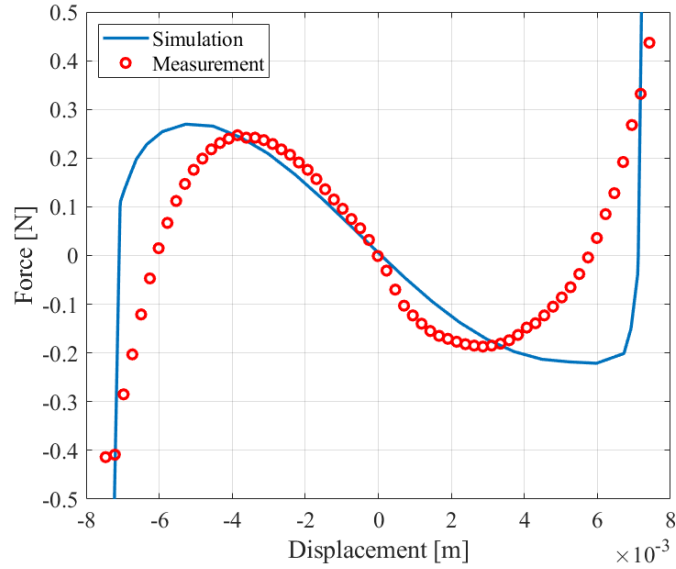
Figure 4.6: Simulated and experimentally tested bistable force deflection behaviour.

(a)   (b)
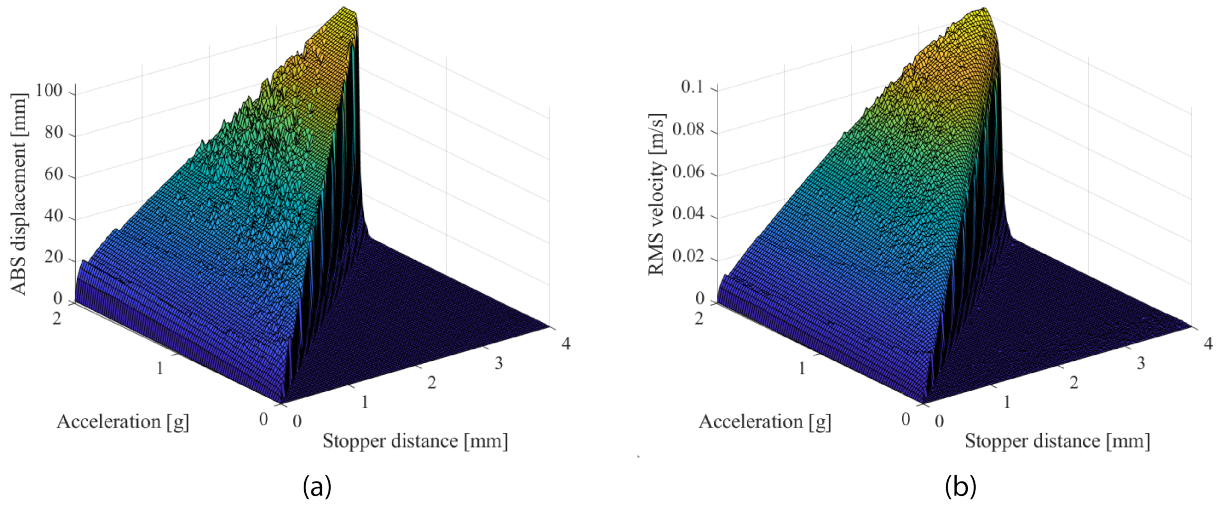
Figure 4.7: Surf plot of the absolute displacement (a) and RMS velocity (b) corresponding to an excitation of 3Hz for different accelerations and stopper distances.

4.3.2   Dynamical characterization

The absolute travel distance and the RMS velocity of the oscillator proof mass is plotted in figure 4.7 for an excitation input motion of $3Hz$. In this plot solutions were found for varieties in acceleration profiles and different travel limit locations. From these plots it can be observed that the largest output performance is obtained by the combination of the largest stopper displacement and highest
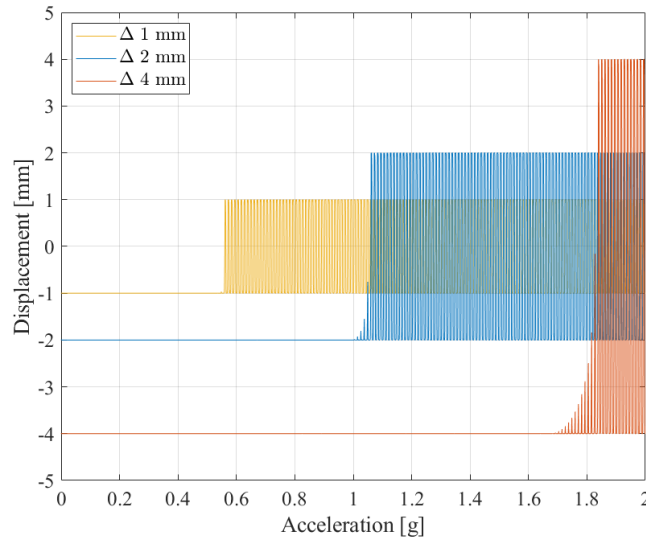
Figure 4.8: Simulated dynamical response of an acceleration sweep for three different stopper distances (Δ)**.**

acceleration. However, lower travel limit locations tend to oscillate at lower input acceleration profiles. Showing an decrease in bifurcation point as the travel limits are placed closer to the origin of the range of motion.

Figure 4.8 shows the results depicted from the dynamical simulation for three different travel limit locations. The dynamical input signal correspond to the same linear increasing acceleration input signal as in the measurement. From this simulation, the same decline in bifurcation point could be observed as the stopper corresponds to lower displacements with respect to the origin. However, a decrease in amplitude can be observed. Furthermore, it can be seen that an energy build up consisting of intrawell oscillation is more present at larger travel limit displacements.

Figure 4.9 shows the dynamical performance of the simulated model and the experimental measurement. The results plotted in figure 4.9(a) shows the relative displacement response of the oscillator and the corresponding velocity profile can be observed from figure 4.9(b). From these results it can be seen that the experiment and model yield to the same bifurcation point as is observed from the measurement. However, minor difference can be observed in the rebounce shown in the section view of 4.9(a) and emphasized with an section view of the velocity profile shown in figure 4.9(b). Furthermore an increase in velocity profile can be seen as the acceleration is increased.

4.3.3 Voltage output

The generated voltage output from the piezoelectric transducer can be observed in figure 4.10 for two stopper locations and the unconstrained configuration. It can be observed that the maximum output voltage is dedicated to the configuration with the largest travel limit displacement as the input acceleration signal was increased.

4

(a)

(b)
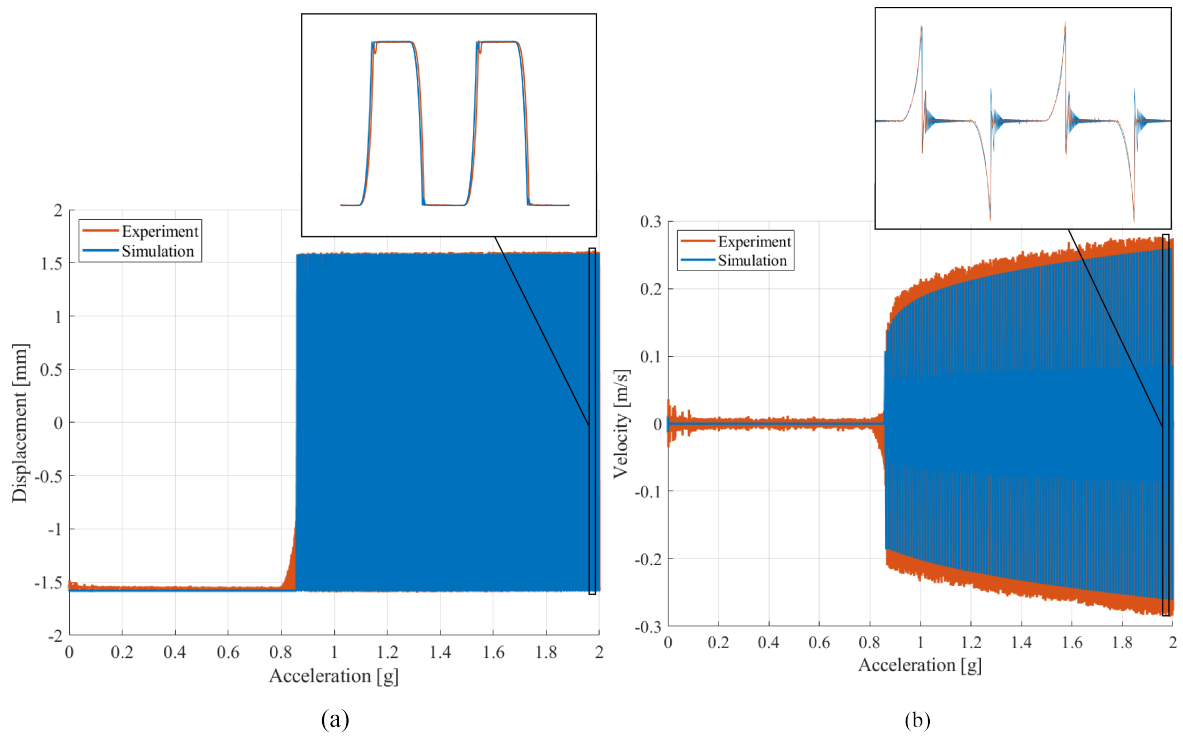
Figure 4.9: **Experimental validation of simulated dynamical response of an acceleration sweep. a) displacement response; b corresponding velocity response.**
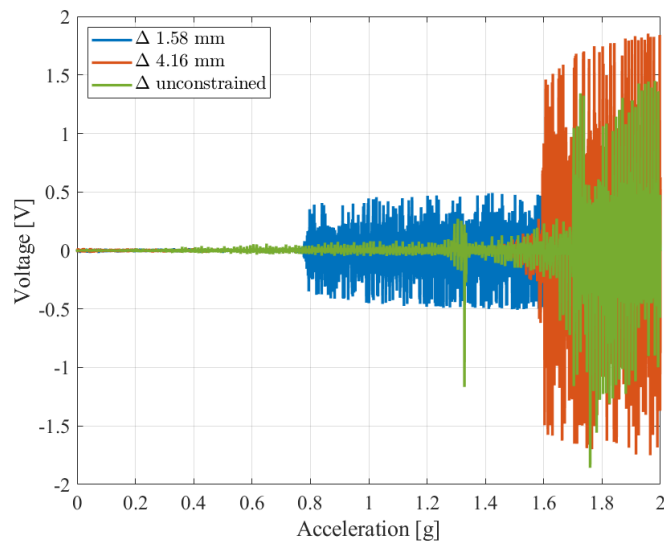
Figure 4.10: Voltage output generated by the piezoelectric foil on the parallel guidance mechanism, shown for two travel limit locations and the unconstrained configuration.

4.4   Discussion

4.4.1   Results

In this work an extra design parameter is added to the principle of bistability. The design parameter is embodied by mechanical travel limits and their influence on the dynamical response to low-frequency environments is investigated. A mechanical analysis is done by the construction of a FEM model in ANSYS to investigate the force-deflection characteristics. The corresponding prototype is created and subjected to experiments. The experimental mechanical analysis shown in figure 4.6 shows that the mechanics of bistability are well captured by the model when the quasistaic force-deflection is performed within the negative stiffness part. However, the difference start to occur when the nonlinear part is introduced, where the stiffness alternate from negative to positive characteristics. It was observed that the stable equilibria do not correspond to the same locations as were calculated by the mechanical model. Furthermore, difference in stiffness could be observed near the stable equilibria of the prototype. The responsible parameter for the locations of the stable equilibria is denoted by the pretension. However, the applied pretension is not the reason for the difference since δ was guaranteed by a spacer. Therefore, it is assumable that the not perfectly satisfying the clamping conditions and small misalignment of the parallel flexures and buckling flexure causes a difference in location and stiffness in the stable equilibria. Furthermore, the frame was built out of a more compliant material than the the clamping components and could contribute to the less stiffness characteristics of the prototype in comparison with the simulation.

Figure 4.7 confirms the research objective, where earlier oscillations can be observed for lower input accelerations in case the oscillator motion is more constrained. Moreover, the results depicted from the simulation in figure 4.8 shows less dominant participation of the intrawell trajectory as the locations of the end-stops enter the linear negative stiffness region of the force-deflection curve. This is because the stifness slope only consist of a linear envelope, resulting directly in steady state interwell oscillation as the harvester is excited beyond the bifurcation point. Although the potential energy barrier is reduced upon the utilisation of travel limits, the negative consequence of the constrained motion is the decrease in amplitude. This explains the lower travelled distance of the oscillator shown in figure 4.7(a) at smaller travel limit locations and decrease in RMS velocity in 4.7(b). Therefore, utilising travel limits as a measure to reduce the potential energy barrier comes along with a trade-off in reduction of the bifurcation point and power output.

4.4.2   Model validation

In figure 4.9 the calculated results from the model are compared with the experimentally measured results. In this figure the displacement and velocity of the dynamical behaviour are shown with a section view of their intermediate performance. The simulated and experimentally tested results contain almost the same bifurcation point, however small dynamical differences could be observed at the impact. The rebounce of the experiment in the positive direction is approximately 8% higher than calculated from the model, whereas scrutiny of the rebounce in the negative direction showed more error compared with the model. However, in both results the rebounce happen only one time

after which all the kinetic energy is absorbed by the travel limit damper. The corresponding velocity profile after impact can be seen in the section view of figure 4.9(b), from which it could be observed that the velocity in the positive direction is well captured by the model but difference could be seen in the velocity profile after impact with the travel limit in the negative direction. This difference implies a inaccuracy of the coefficient of restitution model and larger damping characteristics are observed in the travel limit located in the negative direction. This can be explained by asymmetrical behaviour of the prototype due to small difference in alignment of the parallel guidance and buckling flexure, which are not taken into account in the model. Furthermore, the velocity ring down after impact is more dominant observable in the model than in the experiment. This difference can be explained by the travel limit model, which is represented by an event function of MATLAB and triggered if the velocity is above a certain threshold. However, this value is set such that it can be neglected with respect to the peak velocity right after impact. Moreover, the value of the coefficient of restitution model is assumed to be fixed, however this is physically not the case and depends on the varying incoming velocity [12]. Especially in the combination of bistable structures with mechanical travel limits, where contact with the travel limit is already present in the stable equilibria. This is different in comparison with monostable oscillators, where the addition of the travel limit stiffness and damping characteristics occurs at high velocities in the unstable configuration. The double well characteristics of bistable structures and their corresponding unique trajectories contains different velocity profiles and consequentially relatively lower velocity profiles should be taken into account at the impact. Therefore, according to this theory the utilisation of different coefficient of restitution values will increase the accuracy of the bistable model.

Differences in bifurcation point observed from the model and experimental measurements start to occur, when the travel limits are placed at a location beyond the linear stiffness segment of the force-deflection curve. This can be explained by the difference between the simulation and experimentally measured mechanical behaviour, showing less stiff characteristics and locations of the stable equilibria in the experiment.

All in all, this dynamical model is able to represent the dynamical behaviour when the travel limits are placed in the linear segment of the force deflection curves. However, a better representation of the damping characteristics at the impact, less manufacturing tolerances and especially the clamping conditions will make this validation more accurate. Therefore it can be concluded that this model is a valid representation of the bistable energy harvester, and exhibits some differences due to minor manufacturing tolerances.

4.4.3 Voltage output

With respect to the research objective, the voltage output shown in figure 4.10 could not be used as a correct measure to determine the bifurcation point. Moreover, the quality of the generated power output over the $1\mathrm{M}\Omega$ resistance and the terminals of the PVDF foil resulted in dubious outcomes, since the peak output voltages showed no consistent periodic pattern. However, the transducer in this prototype were used to qualify the difference in the dynamics rather than used for efficient energy harvesting. From the simulated oscillator displacement, shown in figure 4.7(a) it could be observed that smaller travel limit locations resulted in lower output displacements due

to the motion limitation. The same observation could be seen in the simulated results of the RMS velocity profile in figure 4.7(b). The generated power output by the PVDF can be related to the induced velocity, since the difference in stress is rate dependent. Moreover, the parallel guidance flexure exhibits the largest stresses near the clamping conditions as it is configured in the stable equilibria of the bistable force deflection curve. Therefore, the reduction in amplitude decreases the not only the RMS voltage but also stresses and an significant decrease in power output can be expected. However, this limitation is not necessary unwanted, since the reduction in stresses increases the potential of piezo ceramic energy transducers to be used in bistable oscillators and might be in terms of efficiency a worthy competitor for state of the art energy harvesters found within literature [9].

4.5   Conclusion

In this work, a new design parameter is proposed to make bistable vibration energy harvesting a viable solution for capturing low-frequency vibrations. The design parameter was based on the limitation of the poof mass motion with hard travel limits. By changing the design parameter, the height of the potential energy barrier can be tuned in order to require lower input accelerations for oscillation in the desired trajectory of the potential energy characteristics. The effect of the design parameter was demonstrated with a bistable oscillator prototype, from which the mechanical analysis was performed through a finite element simulation and used in the numerical simulation of the dynamical analysis. The mechanical analysis were experimentally tested with a force-deflection measurement and the difference in dynamics upon changes of the design parameter were captured by a dynamical experiment on a custom made air bearing stage. A decrease in acceleration was observed from the experiment, where the proof mass amplitude was more constrained as the oscillator was subjected to an increasing acceleration sweep. It was demonstrated that the dynamical model was capable of capturing the performance of the dynamics, when the excitation were confined in the linear negative stiffness part of the force-deflection curve and started to differ at the transition from negative to positive stiffness. Moreover, the design parameter is able to tune the input acceleration, but reduces the amplitude in comparison with the original unconstrained configuration, resulting in a trade-off to be made. Furthermore, the PVDF energy transducer were able to show qualitatively the dynamical performance, however no conclusions could be made with respect to the generated power output. It is suggested that the travel limits also reduces the stresses in the parallel guidance flexure and therefore increase the possibility for efficient energy harvesting on low-frequency with the use of a piezo ceramic energy transducer.

5 5

Discussion, Conclusion and Recommendations

In this chapter, a reflection on the significance and the development of the project process is made, accompanied with activities containing successes and unsuccessful results. In the conclusions, the main observations regarding to the research question is described followed by the general conclusion found within this research. Finally, recommendations for fruitful future research topics are presented.

5.1 Significance

Bistable mechanisms shows great potential for energy harvesting from low frequency vibrations. They consist of large frequency bandwidths and therefore more reliable in case of mistune with the real world. In addition these systems have great responsive behaviour in low frequency environments, offering great possibilities for human input motions to be captured and used as a powering mechanism for, for example in human health care applications.

Although industries have reserved thoughts on bistable energy harvesters, because of their requirement for high accelerations to overcome the potential energy barrier.

This research shows the construction of a design parameter in bistable energy harvesters to cope with the high energy barrier in low frequency environments, without giving up the bistable characteristics of the original design. However, it shows a drop in power output since the harvester motion will be constrained and results in a trade-off between power output and amount of decrease in required acceleration to overcome this barrier. Therefore, this research contributes to be a step closer to the implementation of bistable energy harvesters for low frequency environments.

5.2 Overview of project activities

Figure 5.1 contains the overview of the total project. The total duration of the project was 16 months, started on the $11^t h$ of November 2019 and lasted until the $11^t h$ March 2021. During this project many skills from basic principles up to practical implementations were learned. The project started with a literature review on the different design parameters of resonant energy harvesters utilising end-stops. Elaboration of this research was performed by an experimental study on a resonator with curved end-stops. During this study, knowledge was scavenged on how to analyse relatively basic energy harvesters and contributed to the simulations skills used in the analysis of the main focus of the thesis, respectively the analysis of bistability for vibration energy harvester mechanisms.

In the course of the project, an effort was made to contribute to a different project, called *"Project Mask"*. A large part of the thesis was carried out during the global Covid-19 pandemic, incorporating a global concern on the supply of protective face masks. As a consequence of this, people started to construct their own uncertified facemasks and imposed a danger to the human health. Therefore the project objective was to construct a simple test facility for every household or institution to test immediately their own fabricated face mask without undergoing a test process by a institution. This project resulted in a collaboration paper published in the journal of ABSA international [8]. Moreover, the executed experiments, performed with te test facility were in collaboration with the RIVM (Dutch national institute for health and environment). It was very special that the test facility was opened by the current Minister President, Mark Rutte.

Figure 5.1: Overview of the project development. The blue coloured blocks represents the main focus throughout the thesis, followed by red blocks representing the numerical simulation activities, grey indicates the experimental and practical work and the resulting research papers are indicated in green.

5.3   Successful achievements

In this thesis process, many different achievements were made with successful and unsuccessful results. Although the unsuccessful results did not resulted in the desired outcomes it contributed to the knowledge used in the analysis of the successful results. The main successes are listed below:

5.3.1   The general project process

The greatest achievement of the thesis, is the construction of a personal proposed project instead of choosing the elaboration of a prior devised project. In the view of the author, it is the freedom and unconstrained thesis process, that allows somebody to expose himself and show his creativity and maximum performance.

The literature study on the identification of design parameters of end-stops in resonant energy harvesters, contributed to the final topic of bistable energy harvesters. It helped to detect one of the research gaps within literature and the construction of the proposal of the syntheses of bistability and end-stops. It was discovered that the principles of end-stops were not used in bistability, though the challenges of high potential energy barriers were published. The combination of these two separate principles, successfully helped the research on bistability to be a step closer to practical implementation in low frequency environments.

Moreover, during the whole learning process many extra skills were acquired to successfully fulfill this thesis program. The weekly update meetings of our own research group, contributed to be more confident on the topic of the project. And on top of that, the updates helped to improve the presentation skills and increased the discipline towards the project, because it was expected that everybody presented their weekly progress. Furthermore, it is anticipated that the skills of academic writing, project management, prototyping and the experience of unsuccessful results, is a good preparation towards the world of engineering.

5.3.2   Design process

The construction of the design process was observed to cover the largest part in the thesis process. It contained the actual establishment of the final prototype design, and mechanical as well as dynamical simulations. The design process started with the identification of the functions and their corresponding sub solutions, as soon as they were clear they were subjected to a selection process. The selection process were conducted using a Pugh selection diagram and the final design was constructed. This process worked out very well, since it greatly gives all the concepts equal opportunities and is less sensitive to subjective selection of the designer.

The simulations were the most successful achievements in this thesis. The process started with the simulation of a linear resonant harvester incorporating contact mechanics of the end-stops and finally these skills were used to construct a nonlinear bistable mechanical and dynamical simulation. These skills helped to be more confident for the analysis of nonlinear problems instead of only using experimental work.

5.3.3 Practical process

The first practical topic learned was that prototyping is not always easy to do, especially when you are dealing with flexures. Flexures offers great possibilities for vibration energy harvesters due to their flexibility, however they are also sensitive to parasitic influences such as for example thermal tension during the cutting process of the laser, causing the flexure to behave differently than expected. The second topic learned, is that the mechanical simulation is not exactly the same as the experimentally tested results. Different approaches have been used to successfully test the mechanical bistable behaviour, however all experiments showed differences near the locations of the stable equilibria. Since the negative stiffness slope shows the same characteristics for the experiment as the simulation it is assumed that the simulation is a correct representation of the mechanical behaviour. From the sensitivity analysis, reported in Appendix C, it could be observed that the pretension contains the most sensitive characteristics with respect to the locations of the stable equilibria, however it could be assured by means of spacers that the amount of pretension is guaranteed. Therefore, it is assumed that the definition of the clamping conditions in the simulation is not the same as in the experiment, and the flexures still contains more unconstrained degree-of freedoms resulting in lower stiffness of the suspension near the stable equilibria.

For the dynamical response of the energy harvester, it was assumed that the contribution to the difference between the intra and interwell trajectory is mainly caused by the amount of acceleration. Therefore, the system is initially tested on an electromagnetic shaker with a maximum amplitude generation of 13mm. From this experiment it could be observed that the system did not show the desired interwell oscillations, since the input vibration amplitude was less than the amplitude of the bistable system. In other words, the motion ratio was larger than 1 ($\lambda > 1$). As a consequence of this unsuccessful experiment, a custom made air bearing stage is used instead, capable of performing experiments with low frequency excitations. Because this stage has a maximum stroke of 550mm it was easy to perform an experiment with corresponding low motion ratios.

With this experimental setup, the system could be tested and resulted in explainable results with respect to the research questions.

5.4 Unsuccessful efforts

Prior to the desired results there were mostly unsuccessful efforts made that did not work out well. However he unsuccessful attempts contributed to new and improved attempts to achieve success.

5.4.1 Bistable contact mechanics model

The quality of the end-stops are the main cause of the energy harvester to show dynamical effects, which are not captured by the mechanical analysis, since they add an extra contribution to the dynamical response of the bistable energy harvester. Therefore, it was assumed that an end-stop contact mechanics model in combination with the bistable simulation in ANSYS mechanical APDL should result in a more accurate simulation of the bistable energy harvester utilising end-stops. A contact mechanic analysis were successfully carried out on a resonant harvester, reported in

Appendix G and the same knowledge were used in the bistable configuration. However, it was observed that the simulation time increased enormously and mostly did not converge to a desired result. Besides, it was very time consuming and many model iterations were used, resulting in no successful simulation.

5.4.2   Symmetrical bistability

The simplest configuration of a clamped beam is the use of symmetrical bistability, which means that the flexure's have equal dimensions on either side of the proof mass. This was the first configuration to experimentally investigate, however from simulation and experimental work it was observed that it acquired too much force to overcome the potential barrier, which could not be delivered by the experimental setups in the lab. Moreover, the motion limits constrains the amplitude to be smaller than in the unconstrained configuration, forcing the flexure to be configured as a "S" shape and introduces a rotation to the proof mass. This resulted in the collision of the flexure with the end-stop as it was placed more closer to the origin of the range of motion. Although these mechanical effects had a negative consequence on the performance of the energy harvester, there were many options to cope with the induced challenges. The first option was to increase the weight of the proof mass, which reduces the required force according to the second law of Newton ($F = ma$). However this was not desired, since it increases the overall volume and the impact velocity with the end-stops. The second option was stiffness compensation by means of a parallel guidance mechanism in combination with a single buckled beam. This configuration was more desired and therefore implemented, since it allowed the proof mass to have a straight motion, and the predictable stiffness of the parallel guidance mechanism could be designed to meet the provided acceleration for the experimental setup.

5.4.3   Energy transducer

In the energy harvester prototype of this work the energy transduction is done with the use of PVDF foil near the clamping of one of the two parallel guidance flexures. First of all, the PVDF was difficult to be cut into shape, since it directly showed short circuit conditions of the two piezo electric layers. To prevent short circuit, different approaches have been made, starting with the investigation of solvents such as acetone to solve one layer until the separation layer and then cut into shape. This approach was successful, however not very efficient since large area's were solved by the acetone. The second approach was the utilisation of a microscope and a scalpel to remove the edges and no coupling can occur between the top and bottom layers. Moreover, the energy collection of the PVDF is lower than of piezo ceramic energy transducers, however this type of energy transducer is not suitable for the prototype due to their brittle material characteristics in combination with high stresses in the flexures of the prototype. Because, the main topic of this research is energy harvesting, the energy generation is used to rather investigate the dynamics than the capability of efficiently energy harvesting. Therefore, the PVDF is used to show how the dynamical changes when different end-stop positions are used.

5.5   Conclusions

Vibration energy harvesting is an optimistic power source for future low power electronics such as wearable healthcare applications as for example diabetes monitors. The classical method for energy harvesting is to investigate the dominant frequency form the energy spectra of the application and used as a design parameter for the construction of the energy harvester. However, small differences in practice results in poor output performance. This is especially the case with human motion vibrations and increases the challenges to design a mechanism being able to capture this kinetic energy in an efficient way.

An overview of end-stops in resonant energy harvesters is given and proves to be able to enlarge the frequency bandwidth, resulting in more reliable behaviour in energy varying spectra. Five design parameters are identified and reviewed by their trade-offs in performance and reliability. However, challenges occur in case of miniaturization, since they greatly amplify their input vibration to larger excitations. Scaling down a harvester, such that the input vibration becomes larger than the output motion of the oscillator imposes a problem and makes the collision of the proof mass with the end-stops unavoidable.

Resent development in vibration energy harvesting shows that bistable energy harvesters are more robust against uncertainties and have high amplitude magnification in case of high input vibrations ($\lambda < 1$). However, these systems require relatively high input acceleration in low frequency environments to overcome the potential energy barrier and transform their motion trajectory from intrawell to interwell. In the investigated prototype of this thesis the design principle of motion limits were used to influence the bifurcation point and as a result the two questions from the problem statement could be answered:

Research question: *How is the bistable mechanism affected by the utilisation of end-stops?*
The simulation of the bistable energy harvester showed that limiting the proof mass motion by means of hard and rigid motion limits resulted in a reduction of the bifurcation point towards lower input accelerations in comparison to the unconstrained design. Moreover, the same behaviour is obtained by the dynamical experiments of the bistable energy harvester prototype. This design parameter makes it possible to disconnect the dependency of the stable equilibria positions on the pretension and altered with the locations of the end-stop. This makes it possible to design the stable equilibria positions within a predefined bistable system, without losing their stiffness characteristics upon changes of the stable equilibria positions. However, the decrease in required acceleration comes along with an decrease in amplitude, resulting in trade-offs to be made.

All in all, it can be concluded that end-stops in bistable structures are a reliable and rather simple design strategy to reduces the amount of potential energy in order to transforms its trajectory from intrawell. Moreover this manipulation does not increases the overall volume and complexity of the structure, since it is done in the original design space. Besides, the use of end-stops makes bistable systems more robust to input signals containing varying acceleration profiles, reducing the potential of inducing the same challenges as for the malfunction of resonators in an energy varying spectra. Moreover, bistable mechanisms are sensitive to manufacturing tolerances

5

such as misalignments or not perfect satisfying the clamping conditions. Therefore, the additional tuning parameter of the end-stops makes it possible to compensate for these tolerances. Think for example of a larger buckling flexure, this results in more negative stiffness and as a consequence require higher forces to be overcome the potential energy barrier. The end-stops could reduce the potential barrier and makes it possible to use the system instead of starting a new design procedure. Therefore, end-stops in bistable mechanisms provides multi-purpose solutions to the occurrence of challenges with vibration energy harvesters in low frequency environments.

5.6   Recommendations

The investigation of end-stops as motion limits in bistable energy harvesters indicates that lower acceleration profiles are obtained, when the motion limits are placed closer to the origin of the range of motion. However, at the expense of the output amplitude, resulting in an optimization problem. When the unconstrained configuration is excited with an acceleration sweep, it can be seen that it consist of intrawell oscillations, however in this trajectory of intrawell no snap-through behaviour could be obtained. It is interesting to perform a optimization study, to find an optimum location for the motion limits, consisting of the same amount of travel, however with the promising non linear phenomena of snap-through behaviour.

Secondly, extension of this work towards the electrical domain could be obtained with piezo ceramic energy transducers. The limitation of the proof mass motion, reduces the stress near the clamping conditions of the parallel flexure's. Therefore, energy harvesting with this configuration could provide a worthy competitor for state of the art works found in literature and brings us closer to the integration of these systems within the real world.

Thirdly, many works found within literature utilises impact based frequency up-converter principles to harvest energy from low frequency input motion. This work provides a good basis for frequency up conversion principles, since hard impact velocities can be obtained by the negative stiffness after snap-through occurs. In addition, the motion limits helps to design the required bifurcation point for the variations in the energy spectra. A possible configuration is an ortho-planar spring, consisting of a monolithic structure and is therefore less sensitives to wear and offers great potential for miniaturization. All in all, this recommendation provides a feasible mechanism design for the replacement of the conventional battery within low power electronics.

Fourthly, it is worthwhile to mention that an elaboration of the combination of the mechanical contact analysis with a bistable mechanism in ANSYS Mechanical APDL, might improve the system mechanical analysis and as a consequence also the dynamical analysis. Besides a more thorough experimental investigation on how the kinetic energy loss in these systems might contribute to a better understanding on how to extract a larger energy fraction of the captured kinetic energy.

Finally, some general remarks are given, which should be taken into account for being more efficient throughout the thesis program:

- Construct, prior to a definitive problem formulation, different prototypes to get acquainted

with how mechanisms work in practice and their corresponding manufacturing processes. This workflow gives a better understanding of how mechanism design work in reality, rather than only focussing on the optimal design you have in mind.

- When building bistable energy harvesters, focus on the quality of the clamping definitions. In this work, it is observed that the clamping conditions are significant design aspects and can result in different outcomes when they are designed poorly.

- Although the motion limits are made from aluminium, it is experienced that the plastic of the 3D printed frame and spacers are the main cause of low parameter values for the coefficient of restitution, representing the additional damping at impact. Therefore, in case of a impact based structure try to design the end-stops to be the most compliant component in the structure. Besides, 3D printing is excellent for quick prototyping, however do not neglect the project by the construction of the final design with a less defined material.

General project remarks:

- Begin simple, and expend the project to be more complicated. Inverse process result mostly in unfounded results and chaotic work processes.

- Do not pursue all the additional feedback, since it is easy to loose grip on the total project.

- Start writing at an early stage in the project, although it does not contribute to the final thesis report, it will help to be focused on the project.

Finally, two visual recommendations are given for interesting energy harvesting concepts:

- Ortho planar spring configuration:
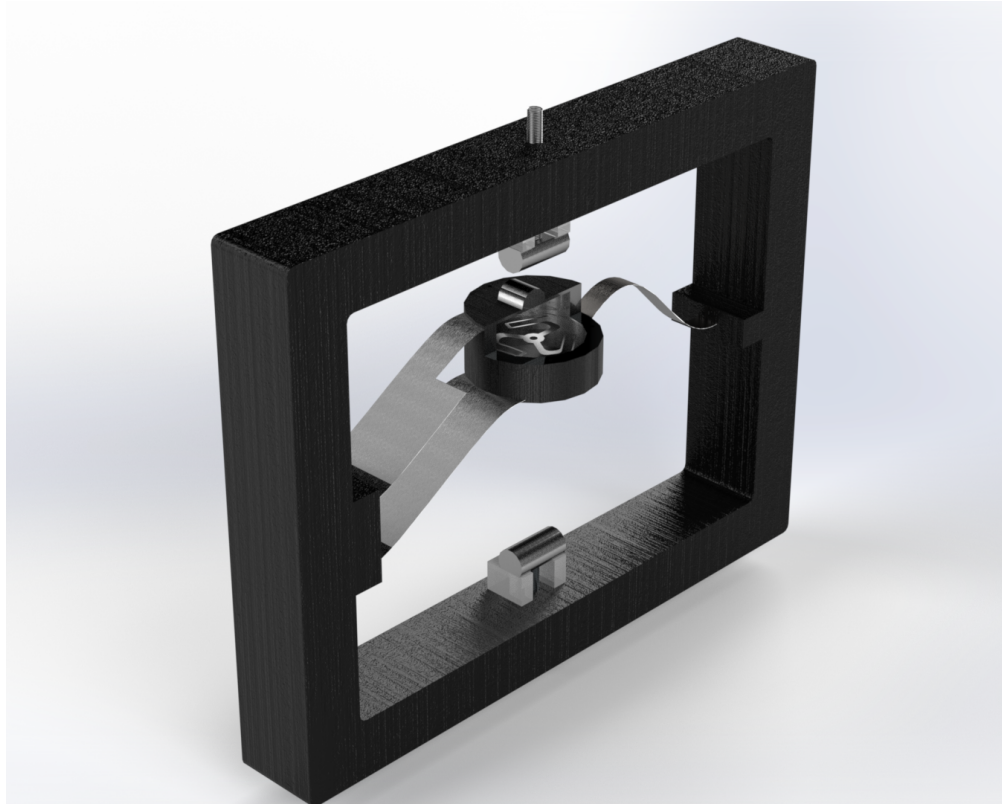
Figure 5.2: Ortho planar spring configuration with section cut showing the internal spring.

- The double stage bistable energy harvester. When bistable energy harvesters are subjected to higher frequency oscillations, the non-linear dynamics start to be more dominant, and the addition of the extra trajectory containing chaos can be expected. This design contains two bistable components and results in multi stable force-deflection characteristics. As soon as interwell oscillations alternate their motion with chaotic motion, the system require an extra vigour to force the system to destabilize their steady state interwell trajectory. In literature this is done with an electrical force induced by the electrical circuit, however no works were found to pursue this principle in the mechanical domain [25]. In this proposed design, the extra force can be obtained by the snap-through behaviour of the second flexure, when the impact with the curved end-stops occur.
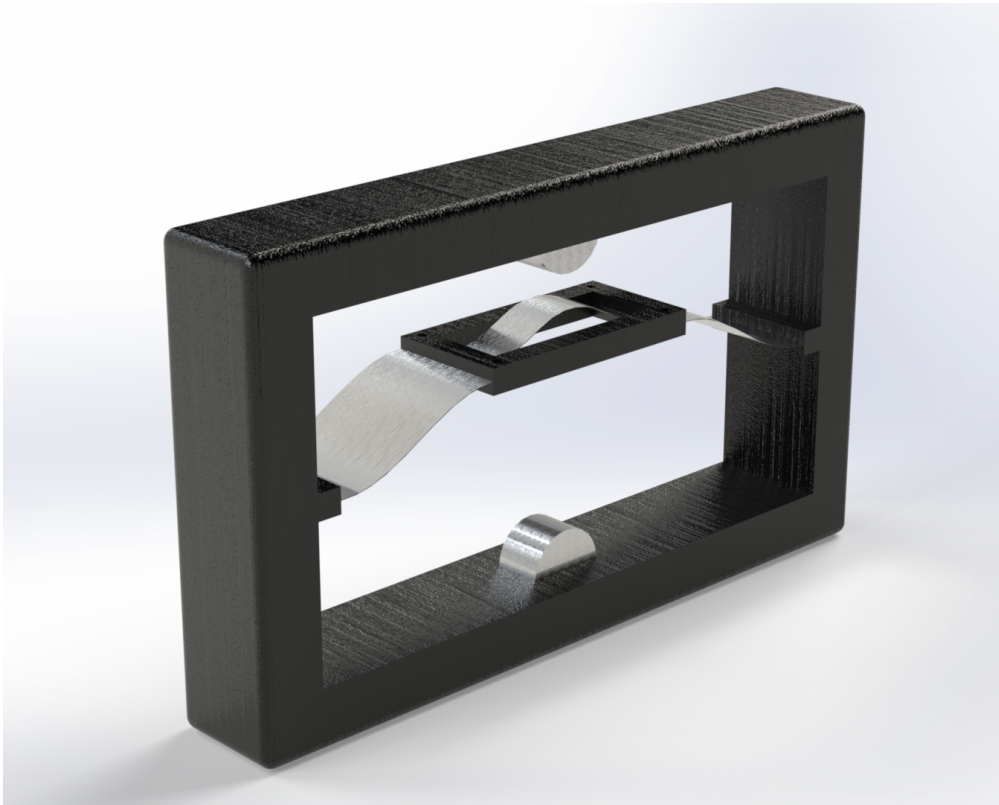
Figure 5.3: Double stage bistable energy harvester configuration

Acknowledgements

A

Design procedure

In this chapter the design process is described. First the solutions for the basic principles in the energy harvester are obtained, than a Morphological scheme is used to eliminate the infeasible solutions. Secondly, the results from the fist scheme is used to create a second Morphological scheme with possible design embodiments. From this second scheme six concepts were generated and subjected to a Pugh selection procedure to reveal the final design.

A.1   Basic principle analysis

In this report, it is found that bistability in human input environments offers great possibilities when they are excited in their interwell trajectory. However, the problem is the large energy barrier between the stable equilibria. It is investigated how end-stop influence the bifurcation point at which the system transforms its motion from intra to interwell motion. This section describes the design procedure for the investigated design, starting with a basic principle analysis. In this design five basic principles are observed consisting of: Bistability, End-stop configuration, End-stop stiffness characteristics, Type of impact and Energy transduction. For each principles, solutions are found and reviewed by their properties.

Figure A.1: Morforlogical chart of basic design principles

Bistability

From literature, it became clear that in general three different bistable configurations are used, namely magnetic repulsive, magnetic attractive and mechanical bistability. Although all these configurations have desired bistable characteristics for the energy harvesting in low-frequency envirnments, the magnetic field of the magnets is not desired in small scale electronics. The reason is

the occurrence of interference with the electrical circuit in case the shielding is not correctly executed. Moreover, scaling down magnets comes along with challenges, like manufacturability and reliability since they consist of brittle material characteristics.

End-stop configuration

The bistable double potential wells makes it straightforward to constrain the oscillator amplitude on two sides, therefore the double sided end-stop configuration is used instead of the single sided configuration. In case the end-stops are placed on one side the required force to overcome the potential barrier is only reduced for one side and the force for the other stable equilibria is equal compared with the unconstrained design.

End-stop stiffness characteristics

The objective in this research is to reduce the required force needed to overcome the potential barrier. To accomplish this objective, end-stops are used, which may consist of two major classes, hard and soft end-stops. Hard stops, have the property of rapid increasing stiffness at the location of impact, whereas soft stops have gradual increasing stiffness characteristics. State of the art works lack the ability to quantify what are hard or soft end-stop characteristics, therefore both characteristics are observed.

Type of impact

The impact with the end-stops is an important design aspect, since they contribute to the dissipated energy by the end-stops. Contact can be created in several ways, therefore the most common types are observed and reviewed. In practice three contact area's can occur, denoted by rectangular, line or point contact areas as shown in figure A.2. A rectangular contact area is created when two flat surfaces collide, in which the definition of the contact area is defined by the contact surface immediately after impact. The line contact can be created by a cylinder and a flat surface, or two equally orientated cylinders. Lastly point contact occurs, when two spheres or two perpendicular cylinders collide. Since, the kinetic energy loss is dissipated by the end-stop damper and partially converted into heat, friction is an important design principle which should be as small as possible to increase the efficiency of the captured kinetic energy. The amount of friction in the system due to impact depends on the impact area, and since a point contact starts with the smallest area it is the most desirable type of impact for our system.

Energy transduction

Bistable system has the ability of using all three energy transduction mechanisms, however not all are desirable. Electro-magnetism is not preferred in small electronic devices because of the same reasons with magnetic bistability, since they can interfere with the circuit and has challenges on small scales. Electrostatic transduction, depends on small movements of two electrodes with opposite polarity. Bistable systems has in interwell trajectories mostly large amplitudes which goes against the fundamentals of electrostatic transduction. However, in case of miniaturization of
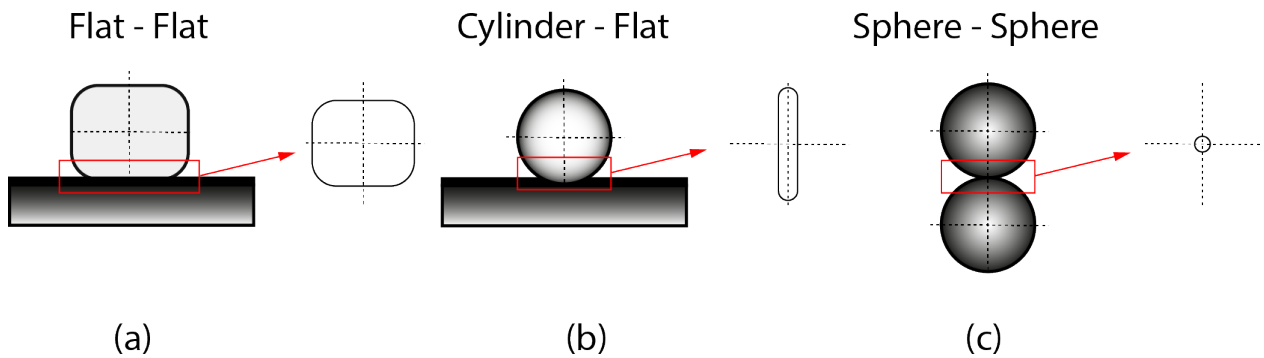
Figure A.2: Types of impact: a) Rectangle contact area, b) Line contact area, c) Point contact area
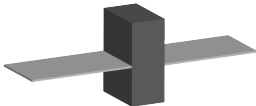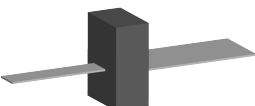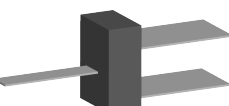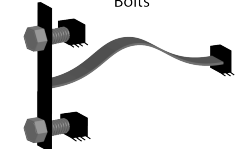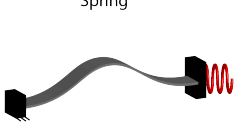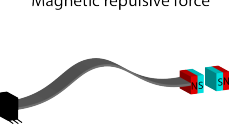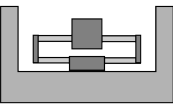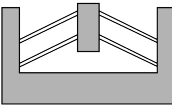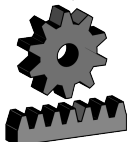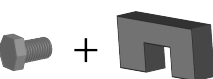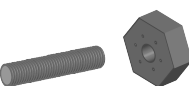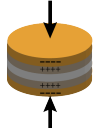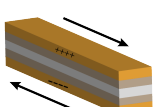
bistable structures the possibilities of energy harvesting with electrostatic energy transduction becomes a more obvious design choice. Since mechanical bistable structures lose significant amount of input energy to strain energy for its transition from intrawell to interwell, piezoelectric transduction is a great solution to retrieve a portion of the lost energy and therefore highly desirable in our system.

Figure A.3: Resulted Morphologic overview after solutions are eliminated

A.2   Concept syntheses

Using the solutions of the Morphologic scheme of the basic principle analysis, a second Morphologic scheme is created consisting of sub concept solutions. Several feasible concepts are generated and briefly described by their functionalities.
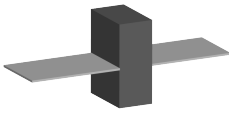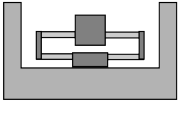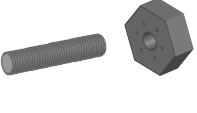
Figure A.4: Morphological overview with sub concept solutions for the design functions

This Morphological overview also consist infeasible concept solutions, starting with the induction of bistability by means of magnetic repulsive forces. Magnetic forces can be modelled and designed, such that they provide the exact force needed to overcome the critical buckling load, however as already mentioned in the previous section magnetic forces are mostly undesirable in small electronics and therefore not a feasible design element for the mechanical bistable energy harvester prototype.

The chosen energy conversion principle is piezo electricity, however the electricity can be generated with three configurations, namely: in case of compression, in flexural due to bending or in shear. The reason to choose for piezoelectricity is to regain a fraction of the energy, which is used for strain energy to overcome the potential energy barrier. Therefore, the most interesting configuration to generate energy from the mechanical bistable concept is the flexural configuration of piezoelectric transducer.

Concept 1

The first concept is based on symmetrical bistaiblity. The bistability in this concept is induced by a compressed spring. The simple physics and predictable behaviour makes it an interesting design element for accurate designing the preload. However, the compliance of the spring makes it possible to change under dynamical loading and change the bistable characteristics as well as different stable equilibria positions. The end-stop configuration is made of a compliant spring, which suspend the end-stop on either sides and cancels out the rotational degree-of-freedom of the end-stop. This end-stop design in combination with a lead screw makes it possible to move with straight motion and with high accuracy to the desired location on the force-deflection curve. The energy transduction in this configuration is done with the use of a flexural dependent piezoelectric transducer, located on one of the flexures of the bistable configuration.
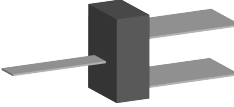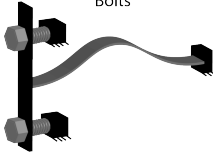
Mechanical bistability	Preload	End-stop design	End-stop movement	Piezo electric transduction
Symmetrical bistability	Spring	Compliant spring 1	Lead screw	Flexural

Pros: High accuracy of end-stop movement
Cons: Rotation of the proof mass, no perfect definition of the stable equilibria (spring is no perfect fixure)
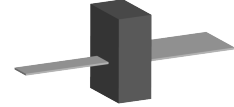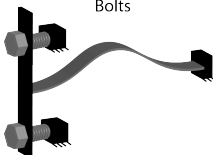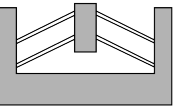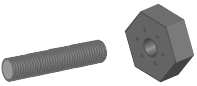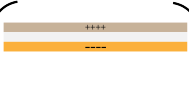
Concept 2

The second concept is based on a parallel guidance mechanism in series with a post buckled beam. This configuration does not allow the proof mass to rotate and is desirable in case of frequency-up converter configurations, since their motion is a straight motion and orientated in the direction of the forcing. This allows perfect coupling and transfer from the inertial energy of the proof mass onto the second mechanism. Besides, the parallel guidance mechanism can be used as a stiffness compensation element in this concept. The perfect predictable behaviour of positive stiffness of the parallel guidance flexure can be a design element to influence the negative stiffness of the buckling beam. The preload is provided by a axial load displacement, which is kept constant with a bolt on connection on the main frame. A spacer can accurately ensure the amount of preload as the system is assembled in the unloaded configuration. The system is loaded by removing the spacer between the bolted connections and tightened down to fill up the displacement for the amount of preload. The end-stop in this concept consist of a conventional spring, with physically know linear stiffness. However, the compliance of the end-stop does not guarantee the location of the stable equilibria in case of high impact velocities occur. Moreover, this solution for the end-stop should be combined with a linear translation mechanism to change the location of the end-stops. The linear translation mechanism consist of a rack and pinion and is able to position the end-stop with high accuracy. The energy transduction is done near the clamping conditions of the parallel guidance mechanism, because the application area is larger and collect therefore the largest amount of energy.

Mechanical bistability	Preload	End-stop design	End-stop movement	Piezo electric transduction
Parallel guidance	Bolts	Conventional spring	Rack and pinion	Flexural

Pros: No rotation of the proof mass, stiffness compensation,
Cons: No perfect definition of the stable equilibria when end-stops are used (spring does not perfectly limits the motion), increase in required component

Concept 3

The third concept is based on bistability induced by the buckling of two asymmetrical flexures in series. The asymmetrical design offers a great design element, since variations in width and length can influence the buckling modes and can be used to design the desired stiffness characteristics. The preload is provided by a bolted connection. The motion limit in this concept is constructed using an end-stop suspension consisting of bistable characteristics. This design is a possible embodiment of a soft end-stop, where indentation of the end-stop is likely to occur. Although this configuration consist of bistable characteristics, it is not desired that the end-stop will deflect to the other stable equilibria. Therefore, this configuration is only used to limit the proof mass motion with positive stiffness. However, if not designed properly or in case of high impact velocities the end-stop could deflect to the second equilibria and stops to function as a travel limitation of the proof mass. Furthermore, the design of the end-stops can be manufactured monolithically, this reduces wear and offers great potentials for miniaturization. In this design the end-stops can be tuned in stiffness and stable equilibria by means of the space between the walls. In this concept the space between the walls are influenced with a lead screw, this provides high accuracy to the locations of the walls and as a consequence the stiffness of the bistable end-stop. The energy transduction is done at the place of clamping on the widest parallel flexure to capture the largest energy due to high strain areas.
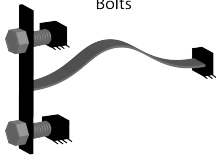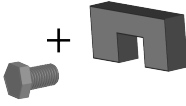
Mechanical bistability	Preload	End-stop design	End-stop movement	Piezo electric transduction
Asymmetrical bistability	Bolts	Compliant spring 2	Lead screw	Flexural

Pros: Manufacturability, less wear
Cons: No perfect definition of the stable equilibria (due to the compliance of the end-stops), rotation of the proofmass

Concept 4

The fourth concept is based on the symmetrical bistable structure and the bistability is induced by bolted connection with the frame. The end-stop is a solid block and designed to have higher stiffness characteristics than the bistable structure, this ensures that the end-stops limits the proof mass motion. The shape of the proof mass and the end-stops are cylindrical and orientated perpendicular, such that the contact area is constructed to be a point contact and reduces the dissipated energy by the end-stop damper in case of a collision. In this concept the end-stops are moved by means of spacers between the end-stops and the frame. This might be rather simple, but is very labour intensive in comparison to the other solutions, since the spacers should be added individually. The energy transduction is done near one of the clamping conditions, because this concept consist of equal flexure dimensions on either sides of the proof mass.
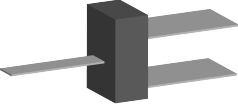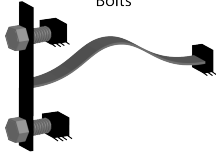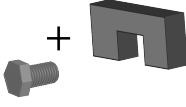
Mechanical bistability	Preload	End-stop design	End-stop movement	Piezo electric transduction
Symmetrical bistability	Bolts	Cylindrical shaped solid block	Spacers	Flexural

Pros: Simple design, perfect location of the motion limit, manufacturability
Cons: Rotation of the proof mass, inefficient end-stop movement

Concept 5

The fifth concept is based on the same functions as concept 4, however this time the bistability is induced by the positive stiffness of a parallel guidance mechanism in combination with the negative stiffness from the buckling flexure. This configuration allows straight motion of the proof mass and because of the predictable behaviour of the parallel guidance mechanism a design element for stiffness compensation. The energy transduction is done near the clamping condition on one of the parallel guidance flexure.
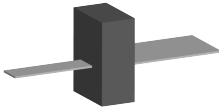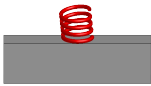
Mechanical bistability	Preload	End-stop design	End-stop movement	Piezo electric transduction
Parallel guidance	Bolts	Cylindrical shaped solid block	Spacers	Flexural

Pros: No rotation of the proof mass, simple, perfect location of the motion limit, manufacturability
Cons: Inefficient end-stop movement

Concept 6

The last concept is based on the asymmetrical bistability induced by a compressive spring force at the end of the beam. The end-stop design is the same as explained in concept 2, a spring in combination with a rack and pinion to set the correct motion limit. The energy transduction in this concept is done near the clamping condition of the widest flexure.

Mechanical bistability	Preload	End-stop design	End-stop movement	Piezo electric transduction
Asymmetrical bistability	Spring	Conventional spring	Rack and pinion	Flexural

Pros: High accuracy of end-stop movement
Cons: No perfect definition of the stable equilibria when end-stops are used (spring does not perfectly limit the motion and spring is no perfect fixture for stability), increase in components

A.3   Concept selection

After the concept generation process, the Pugh method is used to choose which concept is the most suited for our research. The Pugh method is based upon criteria for our design requirements and labelled with a number between 1 and 5. When a criteria has a higher weight factor it is assessed to be more significant. The concept grading is done with the following criteria:

- Accuracy (5): The system should be limited on a specified location, to ensure the reduction in potential energy barrier.

- Durability (5): The durability of the system should be high, since the impact exercises large forces onto the system.

- Manufacturability (3): The system should be rather simple to be manufactured, since high forces might causes the system to fail. Therefore, in case of failure, all the components should easily be replaced.

- Miniaturization (1): Scaling opportunity for small scale low power electronics.

- Simplicity (4): The system should be simple, for the ease of testing.

From figure A.5 it comes clear that concept 5 is the most desirable concept for our investigation. In terms of accuracy, the solid end-stop is preferable over the compliant end-stops. The solid characteristics of the end-stop ensures the motion limit to be placed with high accuracy at a designed location. The compliant end-stops cannot guarantee this location due to their compliance, which will be more dominant in case of high impact velocities. For the same reason, the bolted configuration is chosen for the preload over the compliant spring. Although the preload could be designed with high accuracy of the linear stiffness characteristics of the spring it is not desirable due to

Criteria:	Weights:	Concept 1	Concept 2	Concept 3	Concept 4	Concept 5	Concept 6
Accuracy:	5	2	3	3	5	5	1
Durability:	5	3	2	3	4	5	2
Manufacturability:	3	3	1	3	5	5	1
Miniturization:	1	4	1	4	2	2	1
Simplicity:	4	2	1	4	5	5	1
Total:		46	31	59	82	87	29

Figure A.5: Concept selection diagram, with weighted criteria

their compliance. Moreover, the stable equilibria positions and the stiffness characteristics of the bistable structure will be influenced in case of tolerances in the preload. The manufacturability is an important aspect, since it should be constructed for investigation and no high quality production, therefore the manufacturing processes should be rather simple and in case of failure easily be rebuilt with off the shelves products. The rack and pinion systems, scores therefore very low, since this is a complex system in case of a rebuilt. For miniaturization, the lead screw configurations scores the best. It is possible to scale down a rack and pinion, however it has its limitations in terms of reliability and manufacturability. As already said in the brief introduction of the concept generation phase, the spacers are labour intensive and therefore not able to be used in scaled configurations. However, in terms of simplicity for our system it is the easiest way of changing the end-stop position. The rack and pinion and lead screw are more sophisticated systems which are too difficult to be replaced in case of failure.

There is one missing design solution to be reviewed in the selection process of the final design, and that is the configuration of bistability. The reason for this is that each mechanical bistable configuration has its own stiffness characteristics. It was assumed that the design element for stiffness compensation of the parallel guidance flexure could be of use for a design, suitable to be tested with the test equipment of the lab. Figure A.6 shows schematically the differences in force-deflection curve of each individual bistable mechanism.
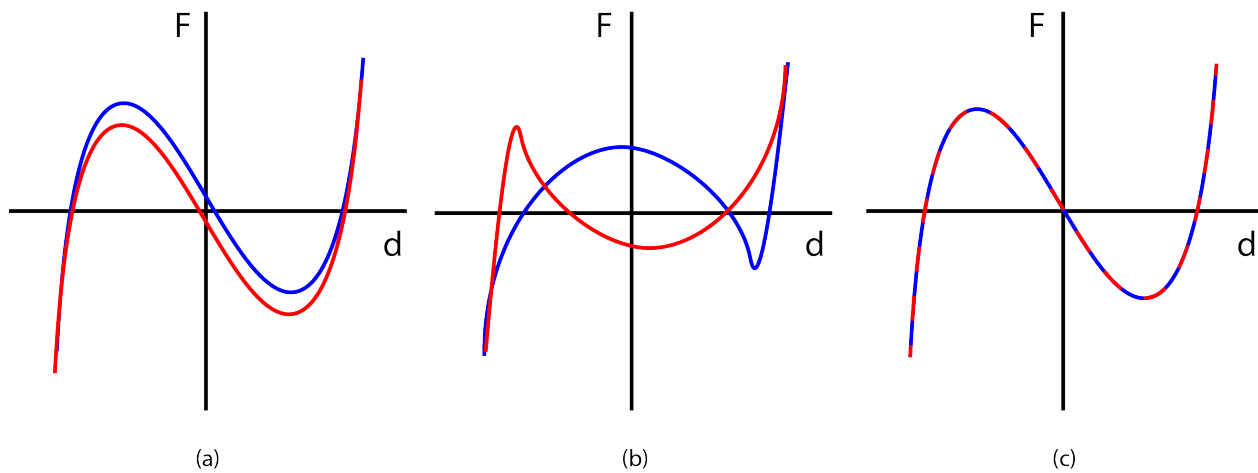
Figure A.6: Force deflection curves of three different bistable configurations: a) Symmetrical bistability, b) Asymmetrical bistability, c) Parallel guidance & Buckled beam bistability.

From this figure it can be observed that the designs of symmetric and asymmetric bistable configurations consist of a hysteresis path. In general, this is not the classical form of hysteresis due to stick slip or damping phenomena in the system, however due to the differences in deflection points resulting in other load paths. This is not the case in the Parallel guidance mechanism, the explanation for this is that the proof mass rotation degree of freedom is eliminated and straight motion of the proof mass is forced. Besides, the asymmetrical design, does not have the origin of the range of motion located on the zero force axis. Because of these observations it is decided beforehand to use the parallel guidance mechanism. Moreover, this design is more desired for frequency up converters.

Embodiment of concepts
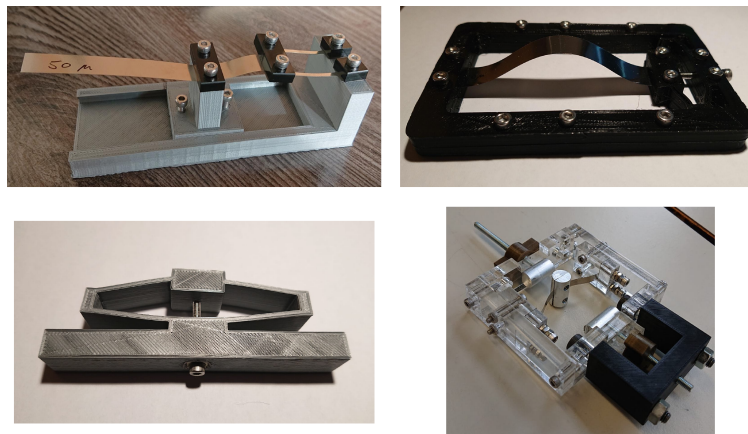
Figure A.7: Embodiment of some of the design solutions

# B

The energy harvester design

When the final design configuration was determined, the real investigation of bistable oscillators could be performed. This Appendix describes the fabrication process of the bistable energy harvester prototype.

The harvester design in this work consist of a parallel guidance mechanism in series with a post buckled beam. A schematic overview of this configuration can be seen in figure B.1 . Since a parallel guidance mechanism consist of a well-defined stiffness characteristics, it can be constructed such that the negative stiffness part of the buckled beam can be reduced almost up to a level of zero stiffness. However, from literature it was observed that in comparison with the monostable mechanisms, the snap-through behaviour of the negative stiffness in bistable mechanisms is responsible for the increase in power output. However, from the work reported in this thesis it is known that negative stiffness is responsible for the height of the potential energy barrier, and an increase will result in the requirement for large input acceleration to overcome the potential energy barrier. However, this increase in potential energy is constrained and depends on the limitations of the experimental setup in the lab. Therefore, the tuning of the bistable stiffness with the parallel guidance mechanism is used to compensate for the stiffness and allow the bistable energy harvester to be tested with experimental setups in the lab.
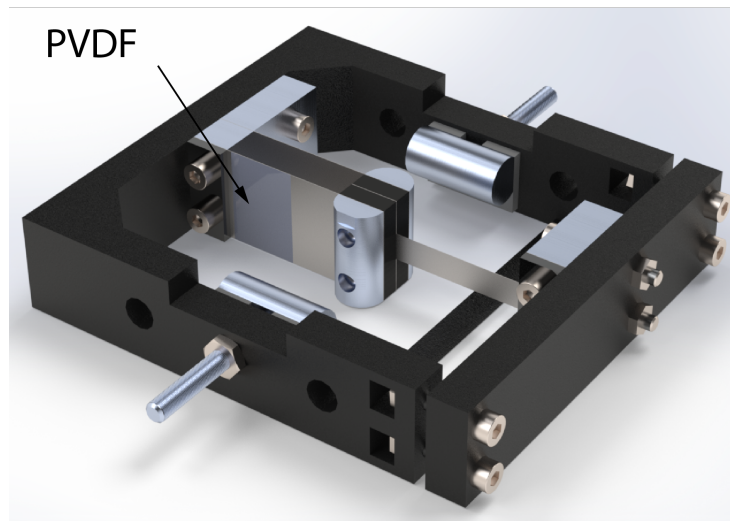
Figure B.1: Schematic view of the energy harvester design

B.1 Fabrication

Figure B.3 shows an exploded view of all the components, which are used in the design of the bistable energy harvester. The flexures are made from 0.1mm thick spring steel and cut into shape with the use of a micro laser cutting machine. The end-stops and proof mass are made out of 10mm aluminum rod and milled into shape. The orientation of the proof mass is perpendicular orientated to the end-stops, this ensures that the contact area is configured as a point at impact and limits the amount of dissipated energy induced by friction. The clamping components are cut out of a 8mm

tank plate and cut in to shape with a milling machine. Furthermore, the frame was constructed out of 100% infill 3D printed frame to give the system its maximum rigidity and reduces flexibility during dynamical excitations.

During the assembly of the flexures and the proof mass, it was experienced that the backside of the proof mass was not entirely flat. This resulted in small misalignment of the parallel guidance and buckling flexure as it was assembled. Therefore, a mall was used in which the proof mass and its flexures were orientated correctly before the screws in the proof mass were tightened firmly. A schematic interpretation of this procedure is given in figure B.2.
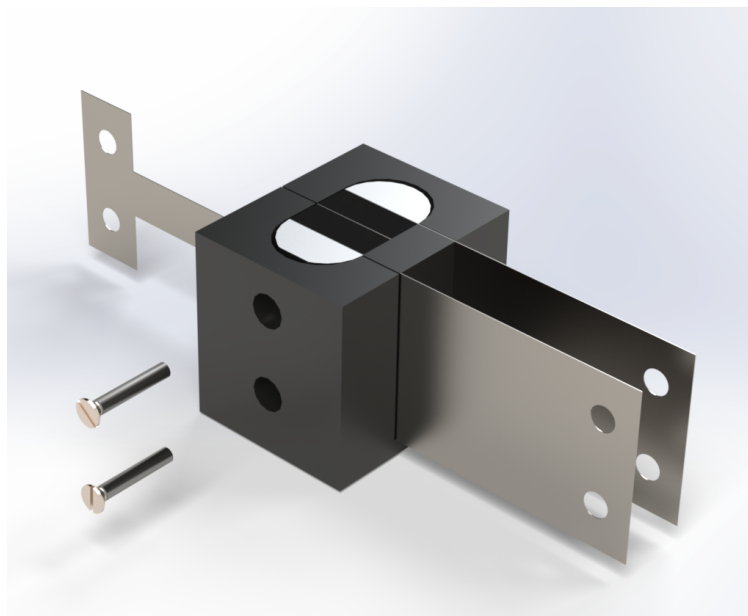

Figure B.2: Proof-mass assembly tool, for correct alignment of the parallel guidance mechanism as well as the buckled beam.

The reason for the aluminum material properties of the clamping conditions is to give the clamping a much higher stiffness than the bistable mechanism. This is paramount, since the degree-of-freedoms at both ends in the model is simulated to be constrained with infinite stiffness. Therefore it is assumed that the material properties of aluminum will mimic the same behaviour and will provide the structure with perfect clamping conditions.

The 100% infill 3D printed PLA frame is constructed out of two components, a U shaped frame and a rectangular block. Extra rigidity of the frame is provided by a reinforcement bar located near the ends of the U shaped frame. The separate rectangular block allows the bistable mechanism to be configured initially in the unloaded configuration, where after the bistability could be induced by the attachment of the rectangular block on the u shaped frame.

The integration of the bistable suspension in the frame starts with the alignment of the parallel guidance flexure and the buckling flexure. In case the alignment is ensured, the clamping compo-

nents were added to the ends of the bistable structure, however not fully tightened down. Than the clamping component of the parallel guidance flexure were added onto the U shaped frame and the clamping components of the buckling flexure on the rectangular block. In this configuration, the system is unloaded and the amount of preload could be set by means of a spacer between the frame and the rectangular block. Then the screws of the clamping components were fully tightened down with enough force to ensure that the connection is firmly. This procedure should carefully be taken into account when building bistable energy harvesters, since overtightening might exert an extra moment onto the system, giving rise to unexpected behaviour. In case the clamping components were defined and the system is ensured to be configured in the unloaded configuration, the spacer could be removed and the bistability could be induced by the bolted configuration of the two 3D printed components. Changes in the design parameter, embodied by the mechanical end-stops were done with spacers between the backside of the end-stops and the frame. Different locations of the end-stops were achieved by unscrewing the nut of the end-stop and the new location can be set by the addition or by removing the amount of spacers.
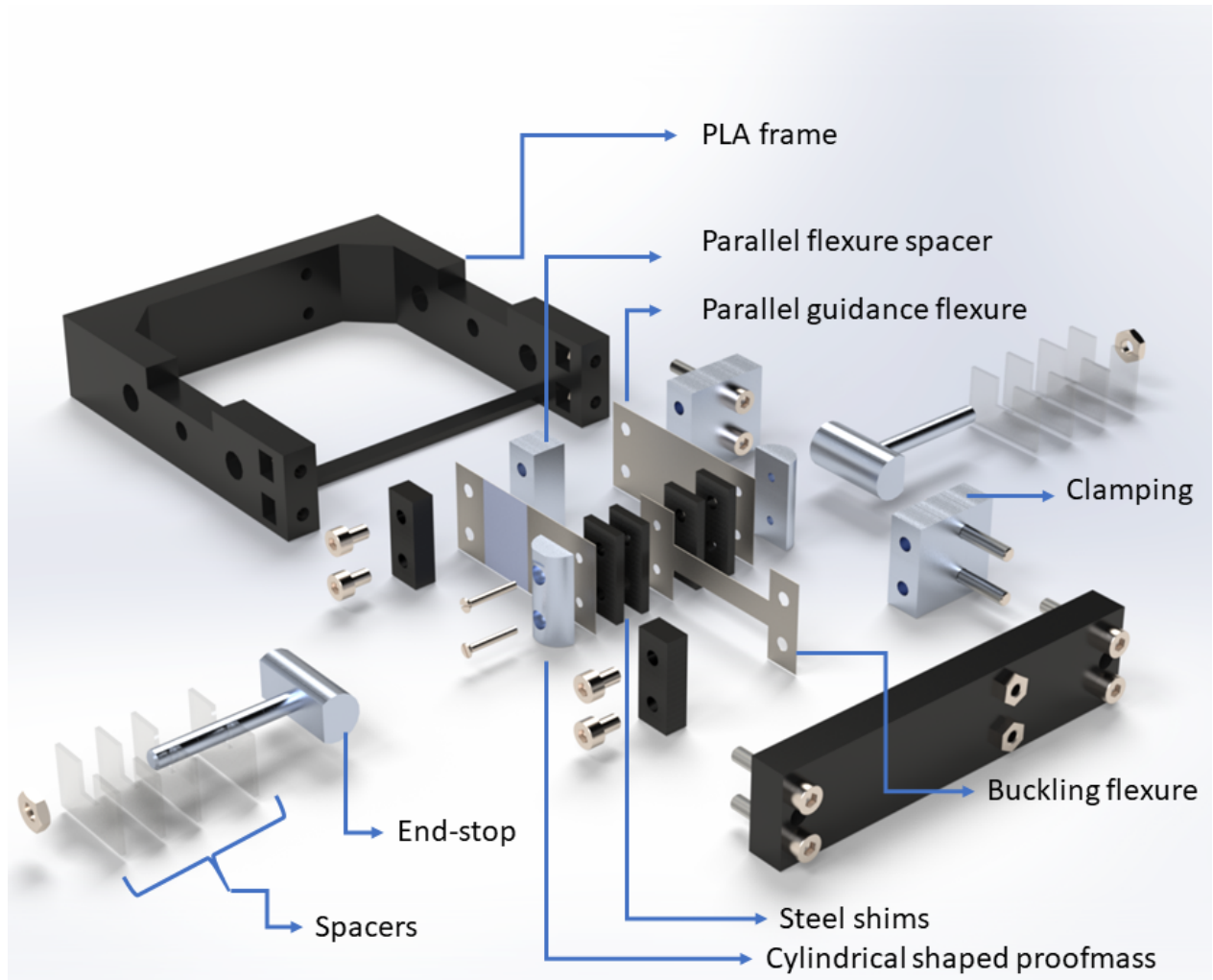
Figure B.3: Schematic exploded view of the bistable oscillator

C

Mechanical analysis

In this chapter, the mechanical analysis of the design is explained in detail. Starting with mechanical modelling in ANSYS mechanical APDL and eventually validated with an experimental measurement of the force-deflection characteristics.

C.1   Mechanical analysis

ANSYS mechanical APDL is used to simulate the mechanical behaviour of the bistable oscilla-
tor. In this section, it is explained how the geometry of the simulation was built, followed by the
buckling analysis and the force-deflection analysis. The contributions of the parallel guidance stiff-
ness and the buckling flexure are derived analytically and a sensitivity analysis is performed to
investigate the weak spots within the bistable design design.

C.1.1   Geometry

Before the construction of the geometry, the element type and material properties are assigned to
each components of the structure. The element types used in this model is a BEAM 188 element,
based upon Timoshenko beam theory, which takes into account shear deformation effects. Table
C.1 shows the parameter values for the material properties used in this model.

Flexures:			Proof mass:		
Parameter	Symbol	Value	Parameter	Symbol	Value
Elastic modules	E_f	190e9 GPa	Elastic modules	E_s	69e9 GPa
Poisson ratio	v_f	0.34	Poisson ratio	v_s	0.34
Density	ρ_f	7.89e3 $\frac{kg}{m^3}$	Density	ρ_s	2.70e3 $\frac{kg}{m^3}$

Table C.1: Material properties for the components used in the ANSYS model

The first part of this model was to create the geometry of the bistable mechanism. Please note
that the dimensions of the flexures are not mentioned in this section and the reader is referred to
appendix F for detailed information of the dimensions of the individual components. The geometry
was built using a structure of consisting of keypoints, which are connected with line segments. The
geometry can be seen in figure C.1, in which the key-points are labelled to identify the components
of the bistable mechanism. Keypoint sets 2, 7 and 4, 8 represents the parallel guidance flexure and
1, 5, 6 the buckling flexure, wile the rigid part of the proof mass was constructed with keypoints
2, 3, 4. After the body of the structure were defined by line segments, a mesh was applied to
give the system a 3D interpretation. Since this model consist of intensive nonlinear characteristics
due to buckling it is highly assumable to have numerical errors, therefore small imperfections
are made to the geometry and mesh to prevent the system of having no converged results. The
geometrical imperfection was made to the parallel guidance flexure, which has its ends located on
the same position. However it was experienced that the model was converging faster to a solution
in case a small imperfection of 1 micron was added to the location of the keypoint 7. Moreover
an asymmetrical mesh was applied to the flexures and the proof mass as can be seen in figure C.2.
When the geometry was constructed, each individual component was defined with their material
properties. Furthermore, it is well known that a line is defined by two points, however the line
segments of the buckling flexure and the proof mass consist of three keypoints. The reason can be
explained by the utilisation of keypoint 1 for the measurement point and keypoint 5 for the parasitic
force, to help the numerical solver to converge to its post buckled state. Each extra keypoint will
be explained in more detail in the buckling analysis and the force-deflection analysis respectively.
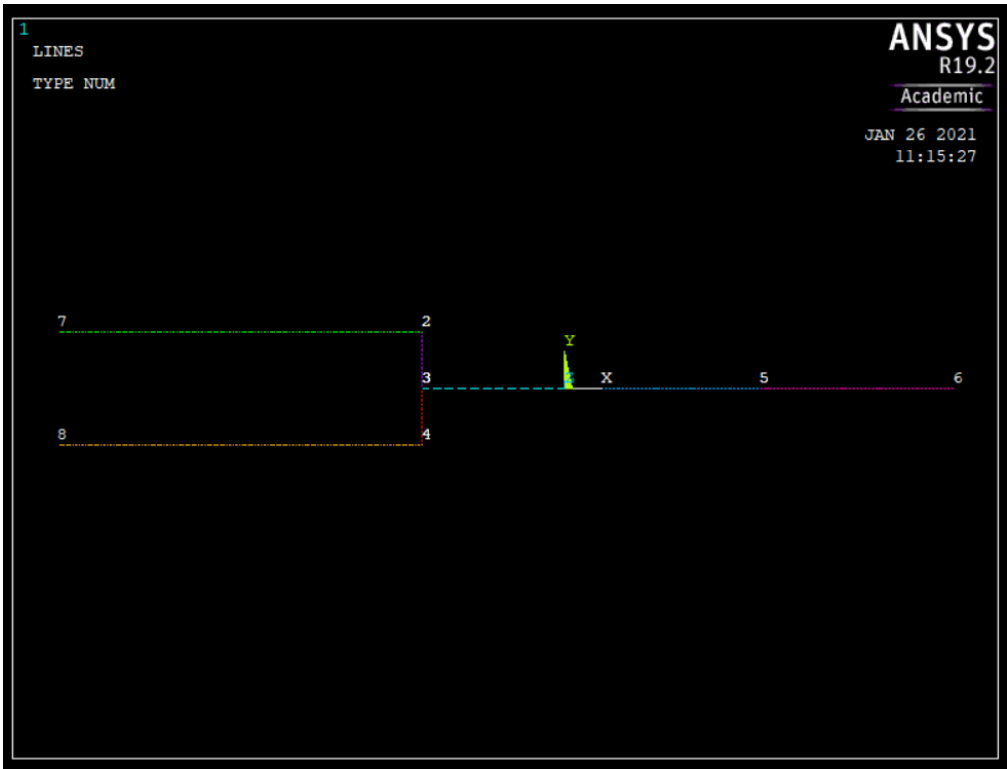
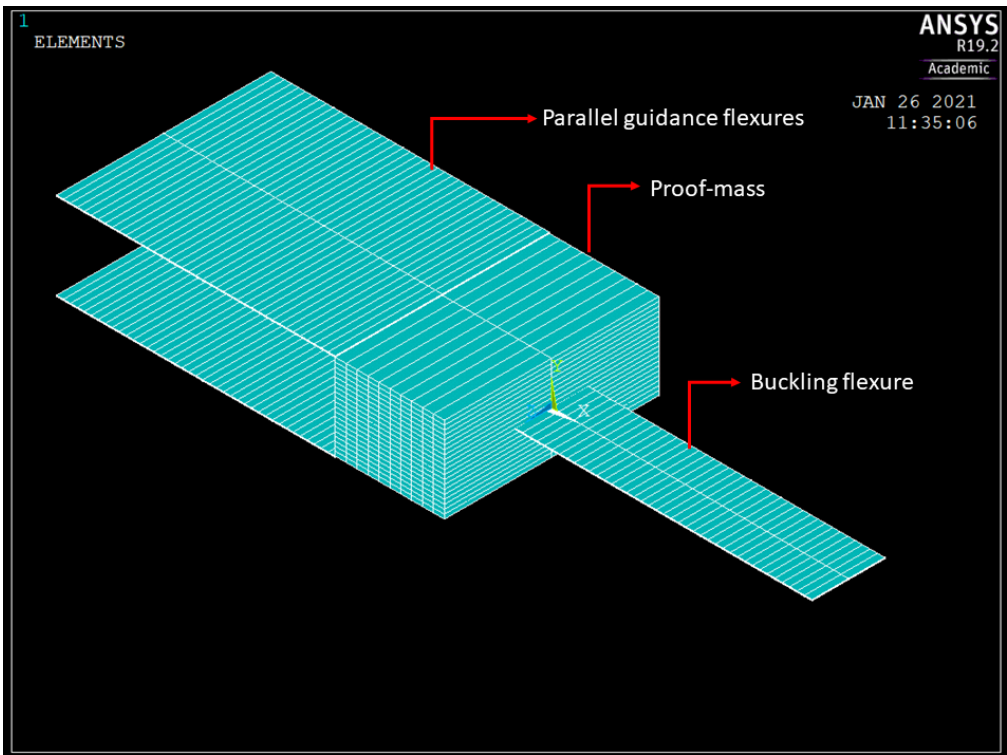**Figure C.1: Geometric overview of the bistable oscillator in ANSYS**

Figure C.2: Meshed geometric overview of the bistable oscillator in ANSYS
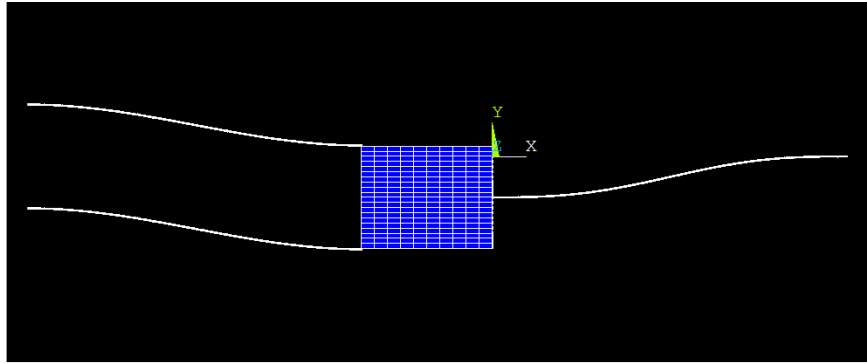
C.2   Buckling analysis

Buckling analysis is a very intensive nonlinear process for numerical solvers, therefore the software of ANSYS is used. Before inducing buckling, the boundary conditions should be added onto the bistable system. It is physically known that each ends of our structure are clamped, which means that all translational and rotational degree-of-freedoms (dofs) will be constrained. The same is done in the bistable model, where all dofs at the ends of the bistable system are constrained. However to allow the system to buckle, the axial degree of freedom of the buckling flexure is relieved in order to apply preload by means of a displacement. To help the system inducing buckling, an extra keypoint was added in the geometry in the middle of the buckling flexure. At this location a small parasitic load was applied to help the solver to allow the flexure to buckle. The buckling was forced by placing a uniform unity load force on the free axial dof on the end of the buckling flexure. The boundary conditions are shown in figure C.3
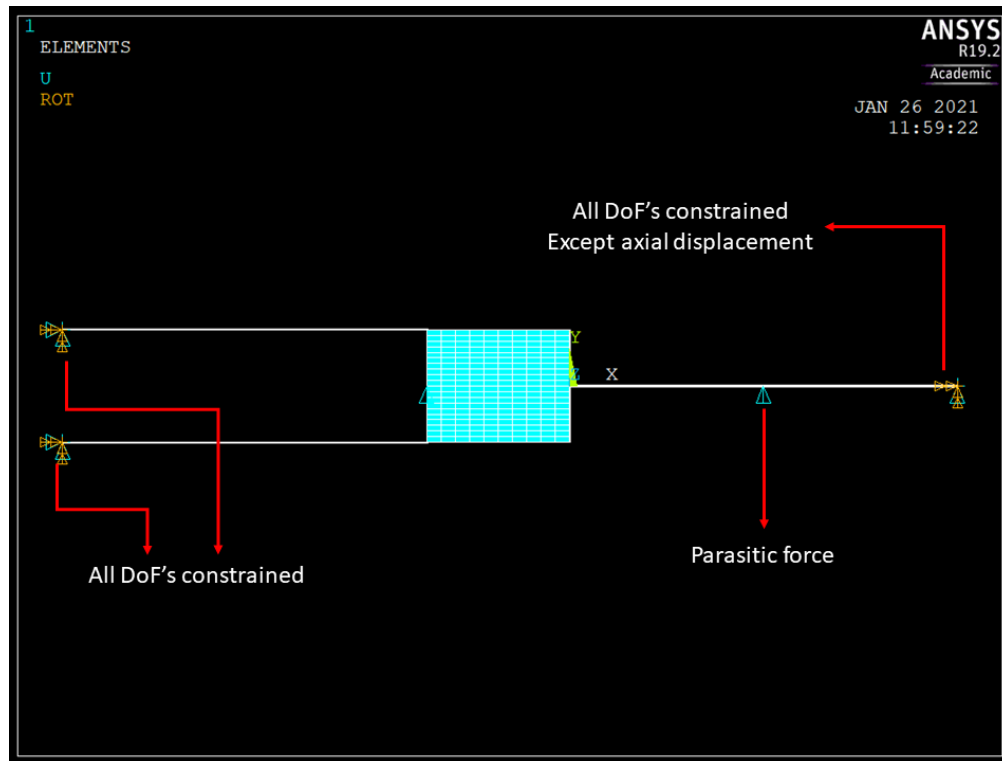

Figure C.3: Boundary conditions for the mechanical simulation model in ANSYS

Figure C.4 shows three buckling modes of bistable system. The first mode is defined as the state in which the system require the lowest amount of energy to remain in this state after the load surpasses the first buckling mode. The position of the proof mass in this configuration is defined as the stable equilibria position, shown in figure C.4(a). The second mode, is the point at which the system snaps-through the middle and deflects to the second stable equilibria as shown in figure C.4(b). However this configuration is the location on top of the potential energy barrier and therefore considered as the unstable configuration of the bistable mechanism. The third mode is shown in figure C.4(c), it consist of a "S" shaped form of the buckling flexure. However, this configuration

is only visible as the system is excited with high frequencies. This configuration is not visible in proposed bistable design, which is indented for low-frequency excitations and therefore only mode 1 and 2 are taken into account for the mode configurations of the bistable energy harvester design during excitation.

(a)
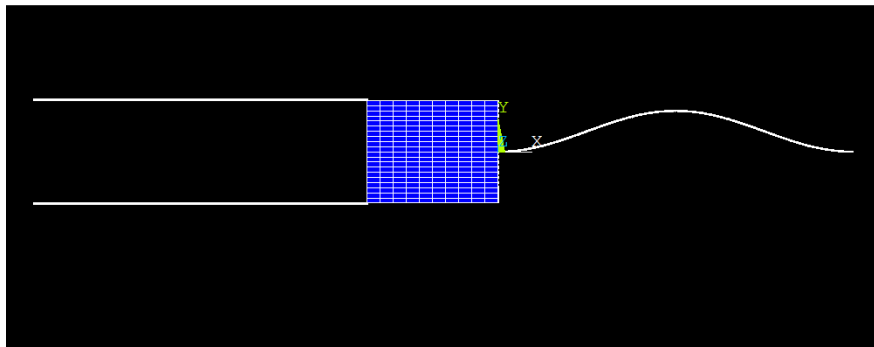
(b)
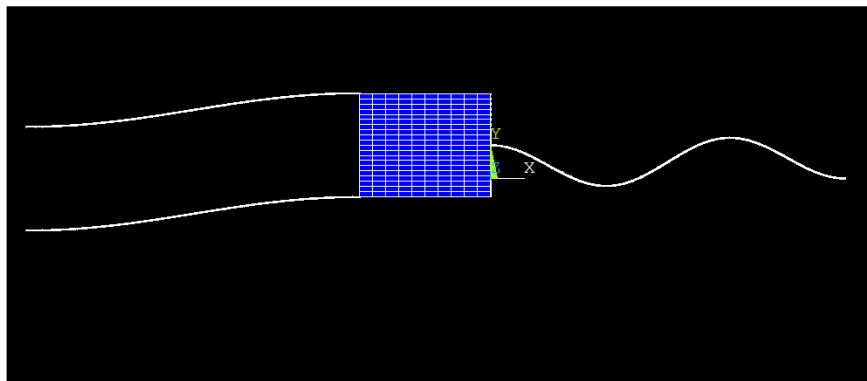
(c)

Figure C.4: Resulting buckling modes of the buckling analysis in ANSYS, a) Buckling mode 1 , b) Buckling mode 2 , c) Buckling mode 3

C.3   Force deflection analysis

When the buckling analysis was performed, the analysis proceeded with the analysis of the force-deflection characteristics. In the geometry section, it was explained that the geometry consist of an extra point in the middle of the proof mass. This point is called *the actuation point* and is used as the measurement point for reaction forces to measure the force which is needed to move the system between the stable equilibrium points. In addition, the potential energy characteristics are simulated to gain knowledge on the height of the potential energy barrier.

In the geometry part, it was said that the dimensions of the flexure's can be obtained in Appendix F. However to obtain the correct dimensions, different requirements should be satisfied. This model was used to design the negative linear stiffness of the buckling beam to be compensated with the positive stiffness and fulfill the requirement needed for the test equipment available in the lab. Moreover, the range of micro laser cutting machine was limited and imposed a limitation on the length of the flexures. Therefore, the geometry was subjected to the following requirements:

- Acceleration unconstrained system $< 2g$

- Flexure length/width $< 28mm$

The objective of this research is, to investigate what the effects of hard and rigid mechanical end-stops are, when they are used to limit the bistable oscillator motion under the condition of dynamical loading. The dynamical experiment is performed on a custom made air bearing stage, which is able to test low-frequency energy harvesters. One of the major drawback of this stage consist of an inbuilt safety switch for overheating, which is activated when the baseplate oscillates with a very rapid motion. Therefore it is determined that the desired interwell motion of the unconstrained configuration should occur below an acceleration of ($2g$). This acceleration was designed according to the second law of Newton ($F = m \cdot a$), where the weight of the proof mass defines the amount of acceleration needed for actuation. The force needed for actuation was observed from the force-deflection simulation and according to this value a proof mass consisting of $15.2g$ was constructed to fulfil this requirement.

Although the parallel guidance flexure was used to be a design element for the bistability, it were set to a predefined dimension and the dimensions of the buckling beam were changed to compensate in stiffness. However, the length of the buckling flexure was fixed and this resulted in only one control parameter for the stiffness of the bistable structure. After some iterations the final design dimensions were constructed to fulfill the requirements for the experimental setup in the lab and manufacturing possibility.

From this analysis it was observed that the geometry of the parallel guidance flexures and buckling flexures influences the height of required forces, to overcome the potential barrier. However, these parameters didn't influence the locations of the stable equilibria. The main contribution for these locations came from the preload parameter. When the desired force was established, the same simulation was used to find the desired preload. For this analysis the requirement was to find the

largest area in which the linear negative stiffness part is more significant available than the non-linear negative stiffness parts, which are located near the stable equilibria positions. The reason for this requirement is, that it is assumed that when the end-stops are placed on the linear negative stiffness part of the force-deflection curve, the contribution of intrawell induced by the nonlinearities near the stable equilibria are less observable and the system immediately will oscillate from rest to the desired interwell oscillation. After some iterations, the pretension was established to be 2.7mm.

(a)   (b)
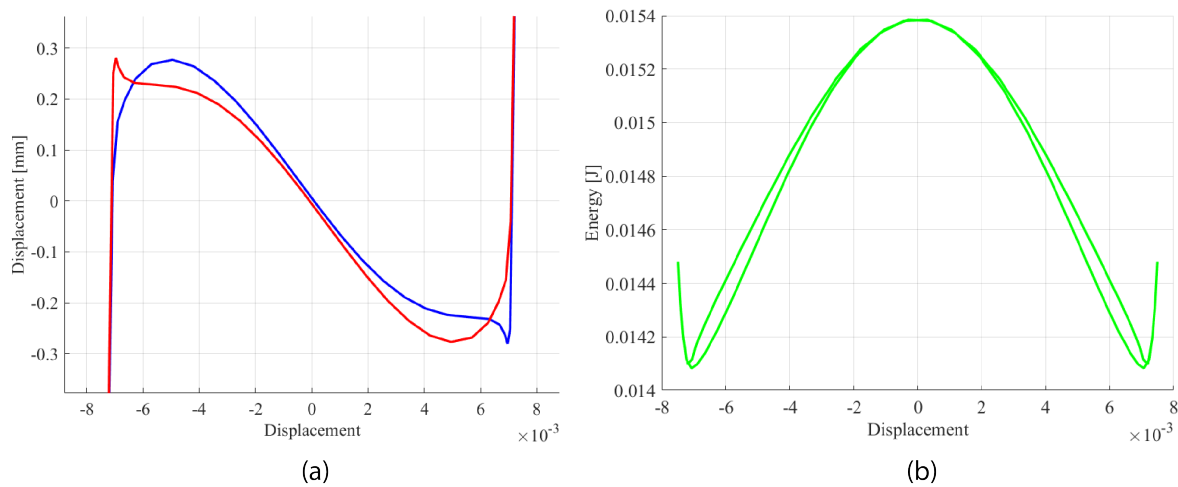
**Figure C.5: Simulation results, a) Force deflection characteristics, b) Potential energy characteristics**

The simulated force-deflection graph can be seen in figure C.5(a). From this figure it becomes obvious that the solver experiences an extreme nonlinear phenomena near one of the stable equilibria positions. Moreover, this figure verifies the claim, made in Appendix A, where it was said that a parallel guidance flexure in combination with a buckling flexure has no difference in load path and consist of the same deflection point (figure A.6). This is observed in the linear negative stiffness part of the force-deflection curve, however small differences can be observed and explained through the occurrence of a numerical error. Furthermore the potential energy characteristics of the bistable configuration are shown in figure C.5(b), where the stable equilibria positions are segregated by a large potential energy barrier consisting of a value of $1.3mJ$.

C.3.1   Mechanical analysis verification

Validation of this analysis was done using a quasistatic force deflection experiment of the bistable energy harvester (1). In this experiment a PI 505 linear motion stage (2) is used in combination with a Futek LSB200 force sensor.

In the simulation the actuation point was located in the middle of the geometry of the proof mass. However, in reality this is an infeasible actuation location for the experimental measurement due to the obstruction of the frame. Therefore, the proof mass was extended with a bracket, to mimic the

same actuation point. Moreover, the experiment was performed vertically and an additional mass of $50gr$ was added on top of the proof mass extension bracket to ensure contact between the force sensor and proof mass. This allows lateral movements to occur, which are imposed by the lateral movements of the manufacturing tolerances of the prototype, without introducing extra moments or forces onto the system. The total overview of this experimental setup can be observed in figure C.6.
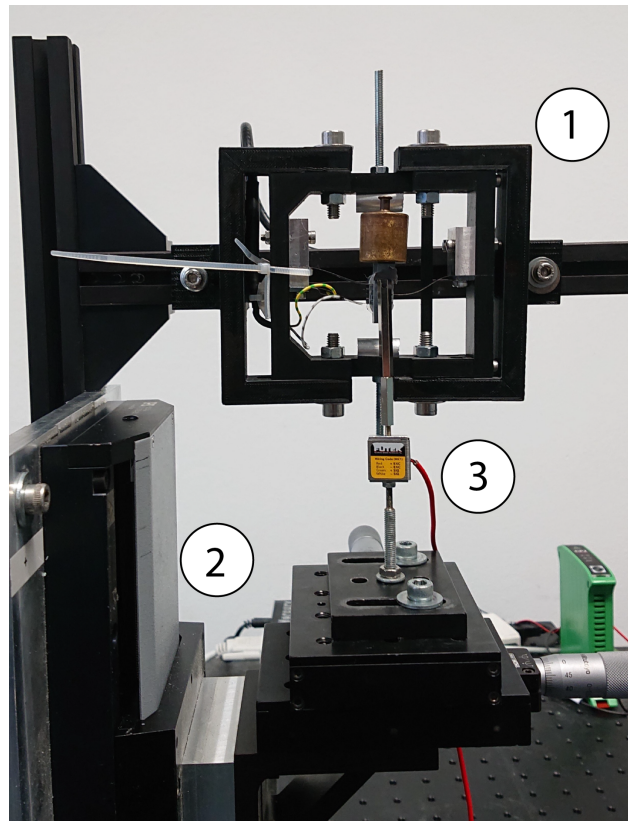
Figure C.6: Force-deflection setup with indicated components: 1) Energy harvester mechanism; 2) Linear stage; 3) Force sensor.

The measured force deflection curve can be observed in figure C.7. In which different locations of required forces, as well as locations of the stable equilibria can be observed with respect to the simulated results. This can be related to small manufacturing tolerances of the bistable oscillator prototype with respect to the simulation. To validate this claim a sensitivity analysis is performed to investigate the parameter for this behaviour and used as an indication of showing the weak spots within the bistable energy harvester design.
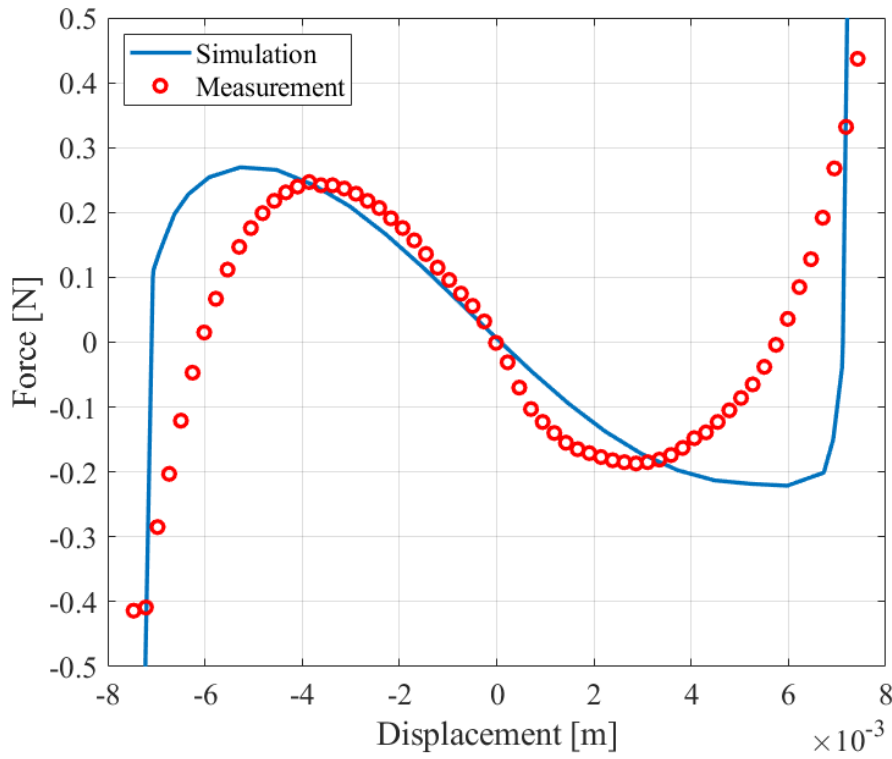
Figure C.7: Simulated and measured force deflection curve

C.4 Sensitivity analysis

For the sensitivity analysis the effect of changes within the following parameters were observed:

- Length parallel guidance flexure

- Width parallel guidance flexure

- Length buckling beam

- Width buckling beam

- Pretension

In order to find the parameter, which might cause the system to behave differently with respect to the simulation it is assumed that the prototype dimensions could have a maximum error of 15%. The results for each individual parameter can be seen in figure C.8.

This analysis verifies the statement of the effect of changes in geometry and pretension. The geometry defines the height of the required force to overcome the potential barrier and the pretension is responsible for the locations of the stable equilibria. Besides, the sensitivity analysis shows expected results. Take for example the length of the buckled flexure C.8(c), it is expected that a longer

buckled flexure reduces the amount of negative stiffness. Therefore, in case of an equally orientated parallel guidance flexure in combination with a larger buckled beam reduces the negative stiffness slope between the stable equilibria. The same pattern can be observed in the other figures.

In the verification section, it can be seen that the stable equilibria is not located on the same location as in the simulation. This could be caused by a mismatch of the amount of preload. In other words it is likely that the system has less pretension. However, measurements show that the system has at least 2.7mm pretension or higher, which is not as expected.

On the contrary, this analysis reveals good results on how the system behaves under slight differences in parameter values of the flexure geometry. Measurements of the width showed, that this value was a very consistent value and assumed to be perfect in comparison with the values in the simulation.

The length of the flexures are the main cause of the difference in required force, it was observed that the proof mass has a small rotation, resulting in no consistent values of the length of the parallel guidance flexure and buckling flexure. Referring back to this analysis, it can be seen that small differences in length resulted in different required force. The parameter, which shows the most significant change in output, is the parallel flexure, shown in figure C.8(a). The reason for this sensitive character of the parallel guidance flexures can easily be explained by the mechanics of the stiffness contribution of both flexures. A parallel guidance flexure is constructed by two flexures, which can be simplified by the mechanics of two linear springs. The compliance of parallel springs can be added up, in that case, the contribution of the difference in length is twice as much significant in comparison with the buckled flexure.
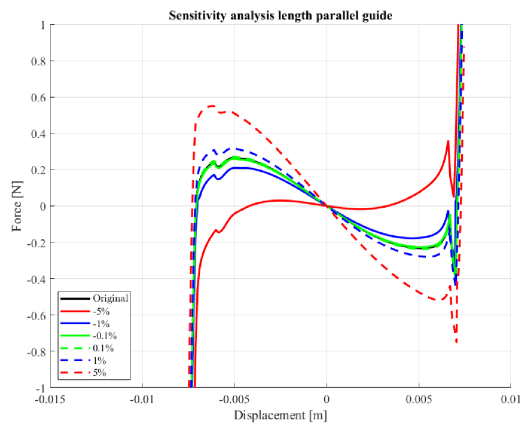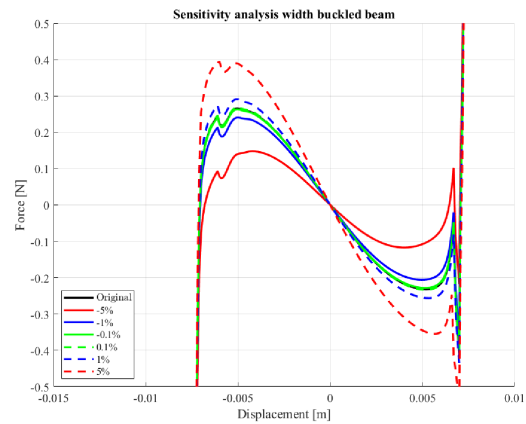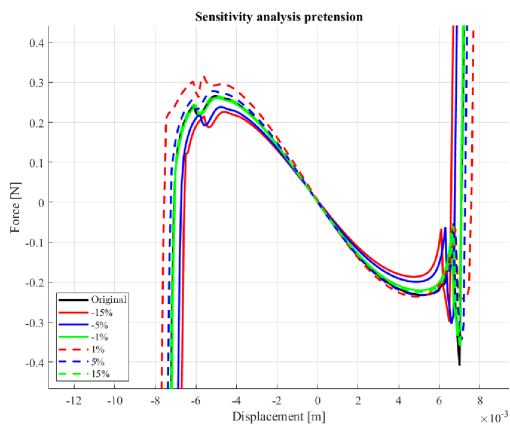
(a)
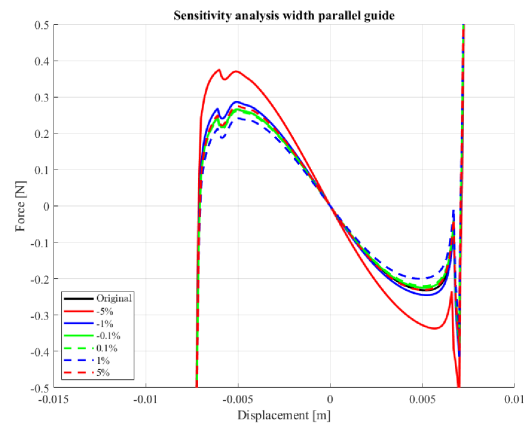
(b)
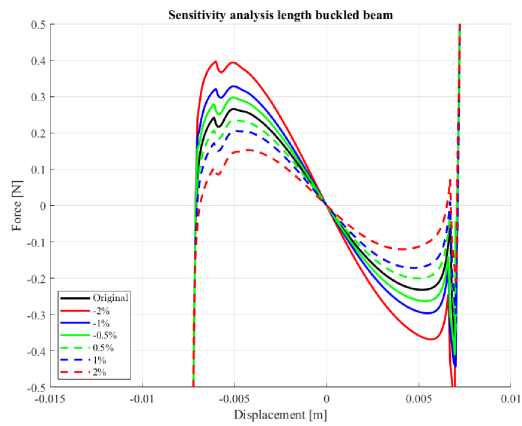
(c)

(d)

(e)

Figure C.8: Sensitivity analyse. a) length parallel guidance flexure's , b) width parallel guidance flexure's, c) length buckling beam, d) width buckling flexure , e) pre-tension

C.4.1   Analytical framework

In this section, the participation of force induced by the buckling beam are derived using the analytical framework of the parallel guidance mechanism. A parallel guidance mechanism is a well-defined mechanism, of which the stiffness easily can be derived as a consequence of the linear characteristics and therefore also its contribution to the force-deflection curve. However, the contribution of the negative stiffness part in this bistable configuration is more difficult due to their nonlinear characteristics of buckling. Since the theory of bistability induced by a parallel guidance mechanism and a buckling beam consist of the addition of the forces of individual components, it can be used to compensate for the stiffness. Moreover, the contribution of the negative stiffness can be derived by subtracting the analytical calculated stiffness of the parallel guidance flexure from the total stiffness found with the use of the force-deflection simulation of the total system. First the derivation of the stiffness of the parallel guidance flexure will be explained.
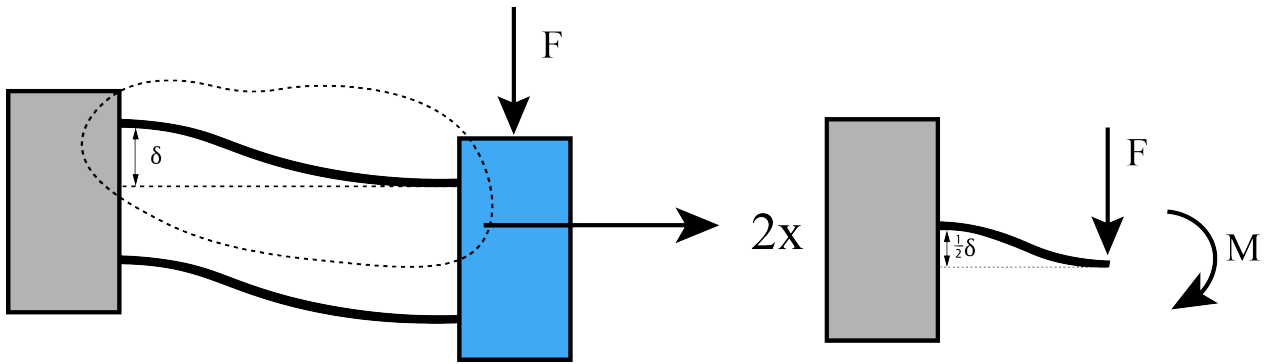
Figure C.9: Schematic overview of the decompensation of a parallel flexure in two flexures

Figure C.9 schematically shows how one flexure of the parallel flexure can be modelled using the superposition principle of the so called "vergeet me nietjes" formula for cantilever beams. The deflection of one single cantilever beam can be calculated using formula (C.1).

$$\delta = -\frac{FL^3}{3EI} + \frac{ML^2}{2EI} \tag{C.1}$$

However, this configuration accounts for only half of the total displacement ($\frac{1}{2}\delta$), so the resulted formula for the total stiffness of one of the parallel flexure can be calculated using formula (C.2).

$$C_{y,i} = \frac{12EI}{L^3} \tag{C.2}$$

As already said in the sensitivity analysis part, a parallel flexure mechanism can physically be described by two springs in parallel, or replaced by one spring consisting of a stiffness equal to the addition of both individual stiffness values of each flexure. So the resulting stiffness can be calculated using formula (C.3).

$$C_y = 2\frac{12EI}{L^3} = \frac{2Ebt^3}{L^3} \tag{C.3}$$
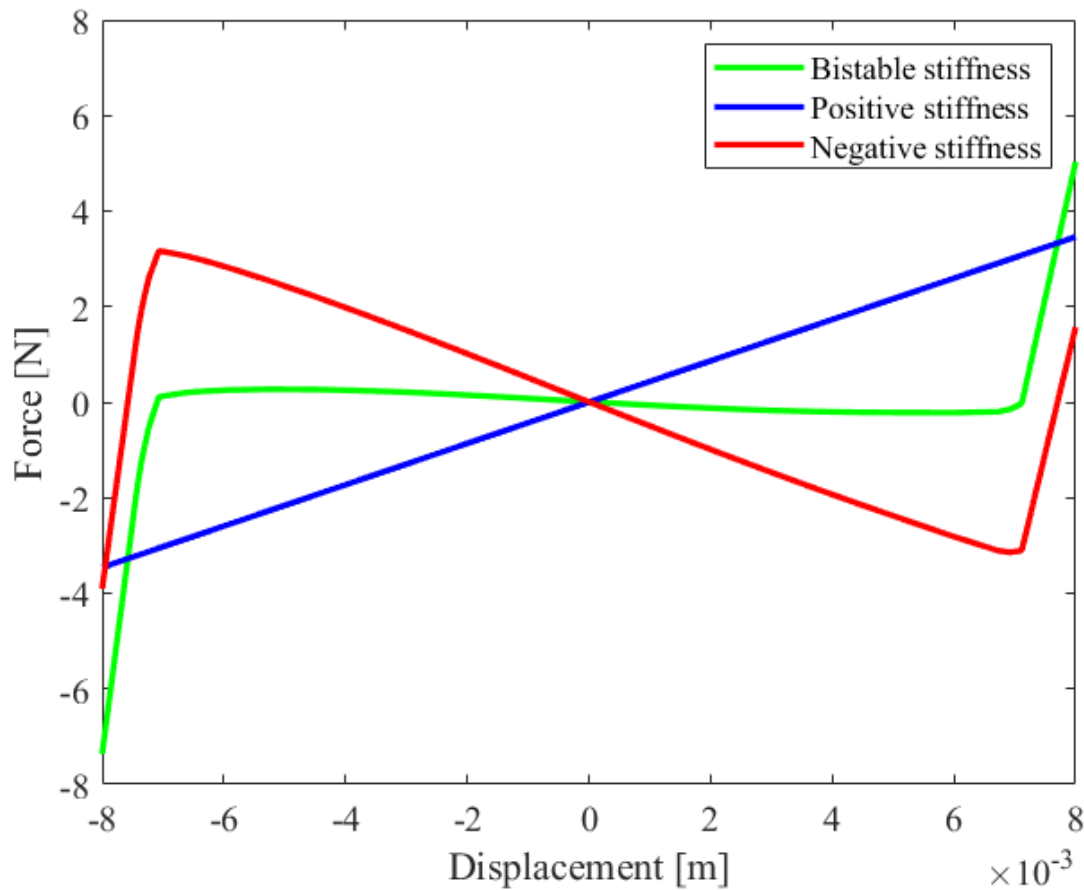
Figure C.10: Contribution of the amount of positive and negative stiffness in the bistable mechanism

The force contribution of each stiffness element in proposed bistable system system can be observed in figure C.10, in which the force of the positive stiffness of the parallel guidance mechanism is subtracted from the simulated bistable force deflection, to reveal the force of the buckling beam.

Since the system is bistable, the negative stiffness part should have a larger contribution than the positive stiffness of the parallel guidance flexure. This can be verified with this plot, where the force off the negative stiffness is significantly reduced by means of the positive stiffness of the parallel guidance mechanism. Moreover, the part of the linear negative stiffness can be calculated. In this design, the contribution of the positive stiffness is calculated to be 432*nm* and the negative stiffness 504*nm*, resulting in more negative stiffness and explains the bistable characteristics..

From this analysis it can be observed, that vibration energy harvesting of small electronics with the use of buckled beams require high forces to oscillate in the desired interwell oscillations. More-over, the utilisation of this buckled beam as a bistable energy harvester was not able to be tested with the experimental setups available in the lab. Therefore it was a well-considered decision to use the bistable configuration in combination with a parallel guidance mechanism.

C

D

Dynamical analysis

This chapter describes the dynamic analysis of the bistable oscillator. First the model is explained in detail, followed by experimental verifications with the use of the prototype described in chapter "The energy harvester design". At the end, an extra section is dedicated to experimental work which were not conduced to groundbreaking observations, however still of importance for this investigation.

D.1   Dynamical analysis

This chapter, elaborates on the main findings of the previous section *Mechanical analysis*. The objective is to find the positive effects of the motion limits in bistable mechanism configuration. The dynamical analysis starts with an explanation on how the dynamical model is created, then the experimental setup is explained on which the energy harvester design is tested. And finally, the validation of the model with the experimental observations is done with a critical discussion based upon the observed differences.

D.2   The dynamical model

D.2.1   Bistable dynamical model:

The dynamical model is created using a lumped-parameter mass-spring-damper system, consisting of an individual mass, stiffness and a damping parameter((D.1)). This modelling principle is mostly used in a linear resonance harvester, because of their fixed values for the parameters. The only fixed value in our system is the mass, and therefore our system can be dedicated to the class of non-linear energy harvesters. This means that the damping as well as the stiffness of the system changes locally.

$$M\ddot{X} + C\dot{x} + Kx = F(x) \tag{D.1}$$

The stiffness of our system is extracted from the mechanical analysis and used as a input parameter in the dynamical simulation. The damping in our system is observed using a logarithmic decrement method. Which uses the method of *Plucking* to reveal the damping characteristics of the system. The principle of plucking means, that the proof mass is moved with a certain distance from the stable equilibria and released to show how the systems oscillations damp out, schematically shown in figure D.1(a). This principle is analogue to the ball on the mountain principle, defining its stable equilibria position when it rolls down and finds the minimum of potential energy. The oscillations are tracked and used as a measure to investigate the damping with formula (D.2). In which $x(t)$ is the amplitude at time t and $x(t+nT)$ the amplitude after n oscillations. Finally the damping ratio can be calculated using formula (D.3).

$$\delta = \frac{1}{n}\ln\frac{x(t)}{x(t+nT)} \tag{D.2}$$

$$\zeta = \frac{1}{\sqrt{1+(\frac{2\pi}{\delta})}} \tag{D.3}$$

Figure D.1(b) shows the results from the experimental measurement. Though, it is assumed that the damping characteristics are non-linear, the results shows linear viscous characteristics and therefore used as a single valued parameter. The experimentally found damping coefficient was found to be on average 0.023. In practice implementation of a transducer adds also an extra damping coefficient when it is connected to a load resistance. In this report this additional damping is negligible,

since the PVDF has great flexibility and does not restrain the flexure's motion, resulting in only mechanical damping.

(a)   (b)
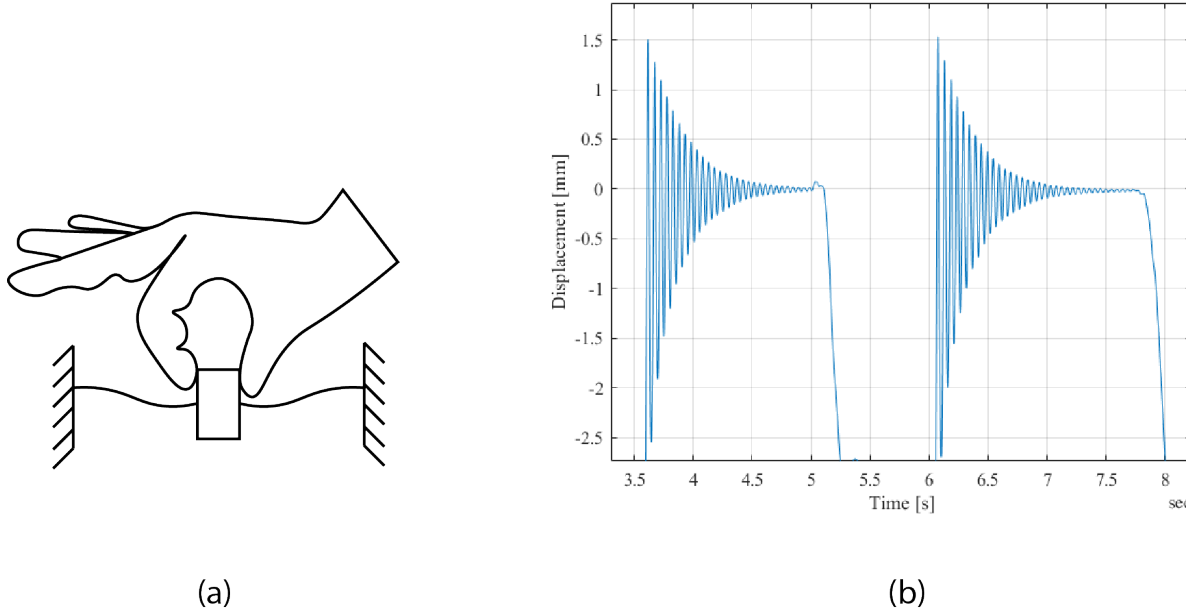
Figure D.1: Logarithmic decrement experiment, a) schematic interpretation of the plucking based experiment, b) experimental result

By knowing the damping coefficient, formula D.4 is used to identify the damping constant within our system. The stiffness in this equation is assumed to be the stiffness in the stable equilibria and found using the relation of formula D.5. The frequency was estimated using the frequency at which the oscillations of the logarithmic decrement measurement damp out.

$$C = 2M\zeta\sqrt{\frac{K}{M}} \tag{D.4}$$

$$\omega_0 = \sqrt{\frac{K}{M}} \tag{D.5}$$

D.2.2   End-stop model

Implementation of the end-stops in the bistable oscillator configuration adds nonlinear characteristics to the system. Therefore equation (D.1) is expanded with an extra force to (D.6), and the force is called F^{stop}. This force defines the damping and stiffness characteristics of the end-stops at the impact and can be described by the expression of (D.7).

$$m\ddot{x} + c\dot{x} + k(x)x + F^{stop} = F(x) \tag{D.6}$$

$$F^{stop}(x) = \begin{cases} K_s(x - \Delta_1) + C_s\dot{x}, & \text{if } x \geq \Delta_1 \\ 0, & \text{if } \Delta_2 \leq x \leq \Delta_1 \\ K_s(x + \Delta_1) + C_s\dot{x}, & \text{if } x \leq \Delta_2 \end{cases} \tag{D.7}$$

In figure D.3 a schematic overview is given, indicating the extra components of the expanded EOM. When the systems motion is oscillating without interacting with the end-stops it can only be described with equation (D.1). Exceeding a level of excitation, such the input excitation is larger than the generator length, results in collisions with the end-stops and induces nonlinearities. In the EOMS ((D.7)) additional stiffness and damping terms are added, which are caused by the collision.
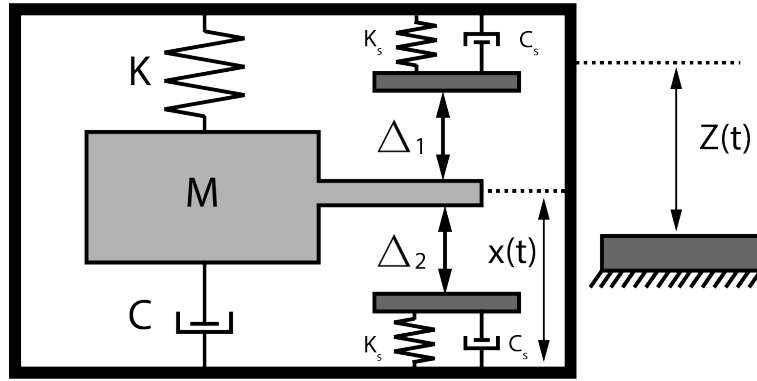
Figure D.2: Schematic overview of the oscillator with indicated modelling parameters

The stiffness of the end-stops are estimated using a Hertz contact point analyses [4]. Which is based on the collision of to perpendicular orientated aluminum cylinders. Since both objects consist of cylindrical shaped areas a point contact is created. The end-stop stiffness is calculated using formula (D.8), in which R' is defined as effective radii of the two cylindrical components and E' is the effective elastic modulus calculated using formulas (D.9) and (D.10).

$$K_s = E'\sqrt{2R'\eta} \tag{D.8}$$

$$\frac{1}{R'} = \frac{1}{R'_x} + \frac{1}{R'_y} \tag{D.9}$$

$$\frac{1}{E'} = \frac{1 - v_1^2}{2E_1} + \frac{1 - v_2^2}{2E_2} \tag{D.10}$$

In which:

- E' = Effective elastic modulus

- K_s = End-stop stiffness

- R' = Effective radii

- v = Poisson ratio

- η = indentation

The envelope of the contact stiffness can be seen in figure D.3. The envelope consist of a nonlinear stiffness characteristics and are difficult to be measured, therefore the following process is utilised in order to give a good estimation for our contact stiffness. The model is created using all the known parameters, except for the end-stop damping which will be explained next. The system is solved for the initial condition (0,0), which means that the system starts at the unstable position and travels towards the end-stop without an extra forcing term. Since the location of the end-stop is known, the amount of travel beyond this value is indicated as indention of the end-stop. This value is changed several times, until the indentation of the end-stop matches with the indentation corresponding to the hertz contact analysis.
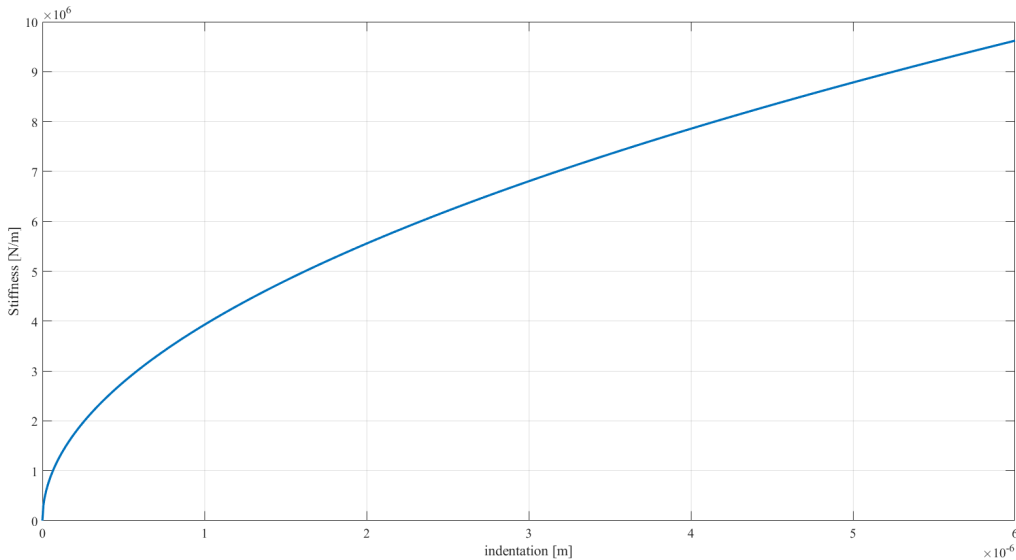
Figure D.3: Hertz contact stiffness analysis

The end-stop damping within our system was estimated using the coefficient of restitution. Which is defined as the difference in kinetic energy before and after the collision, and simplified using the proof mass velocity (D.11). This principle can simply be explained by the jump phenomena of a elastic ball on a rigid flat floor. When the ball is released, the gravitational force gives the system a certain velocity at which it impacts with the ground. When the impact occurs, the ball is pushed inwards due to the stiff characteristics of the floor, resulting in heat generation of the elastic indentation of the ball. This generation of heat, is defined as the energy loss, and reduces the velocity at which the ball jumps back. This parameter depends on the initial velocity and eventually will damp out until it rest on the floor and all the energy is dissipated by the end-stop damper. This jump phenomena of the ball is analogue to our impact of the proof mass suspended by a bistable suspension and the end-stops. Experimental observations were used to measure this value and described in the dynamical experiments section.

$$CoR = -\frac{V_2}{V_1} \tag{D.11}$$

The calculation of the system is done with a numerical ODE45 solver in MATLAB and the coefficient of restitution is implemented using EVENT functions. The reason for the use of EVENTS is that the ODE solver in MATLAB is not accurate when discontinuities are used and the EVENT function stops the solver when it is triggered, restarting the whole calculation for new initial conditions. The triggering of in this model is done, when the end-stop location is reached and consisting of a small velocity ($<0.0001 \frac{m}{s}$). In case the EVENT function is triggered, the ODE solver restarts with the end-stop location at which it is triggered and the incoming velocity multiplied with the coefficient of restitution.

In literature it was found, that bistable systems are incentive to variations in frequency, due to their broad frequency bandwidth. And since our objective is to reduce the amount of force to overcome the potential barrier, it is interesting to investigate how our system performs under an acceleration sweep. This introduces the parameter of interest for the bistable system, which is denoted as the bifurcation point and is defined as the acceleration at which the system transforms it trajectory from intrawell to interwell oscillations.

D.3   Dynamical experiments

The design was experimentally tested on a custom made air bearing stage. This air bearing stage consist of a maximum amplitude of $250mm$ and therefore, well suited for bistable energy harvesters, since they require an input motion larger than their range of motion to show its interwell characteristics. A picture of the air bearing stage can be seen in figure D.4.
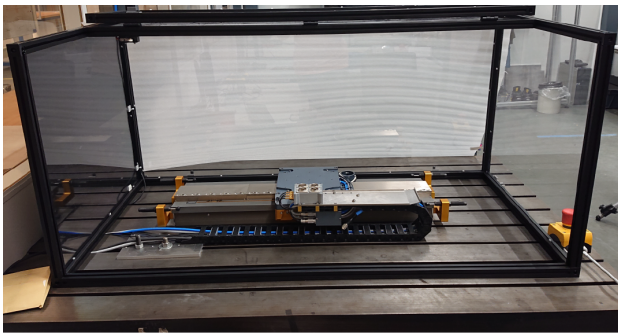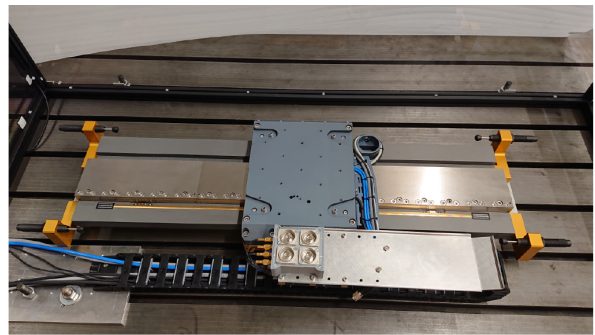

(a)   (b)

Figure D.4: The experimental test setup, consisting of an custom made air bearing stage

On this air bearing stage three different experiments are performed. Throughout the whole experiments the frequency is fixed to be $3Hz$, since the bistable oscillator is assumed to be intensive to differences in frequency for low frequency excitation input.

The first experiment, is the investigation of the coefficient of restitution characteristics on the incoming velocity. Where the bounding behaviour of the bistable oscillator proof mass was excited for 5 seconds for different acceleration signals, starting from 0.5g up till 2.0g. This experiment was done for four different end-stop locations to measure the behaviour of the coefficient of restitution. During the measurement a ramp function were used to increase the motion of the stage towards the desired signal, since it is physically not possible to start immediately on the desired motion signal. This ramp function uses the first second to build up to the specified acceleration signal and oscillates for four seconds at the desired signal to ensure steady state oscillation. The last 20% of the time series were used for the extraction of information of the coefficient of restitution. The coefficient of restitution were observed from gradient of the measured displacement signal of the proof mass relative to the base excitation and. An example of this input signal is shown in figure D.5 . This signal represents the input signal for the air bearing stage and uses a gain factor in the controller to specify the correct trajectory for the air bearing stage. The maximum output voltage of the NI DAC 9263 output module is 10V, and the output should be as close as possible to this value to reduce the influence of noise within the input signal.
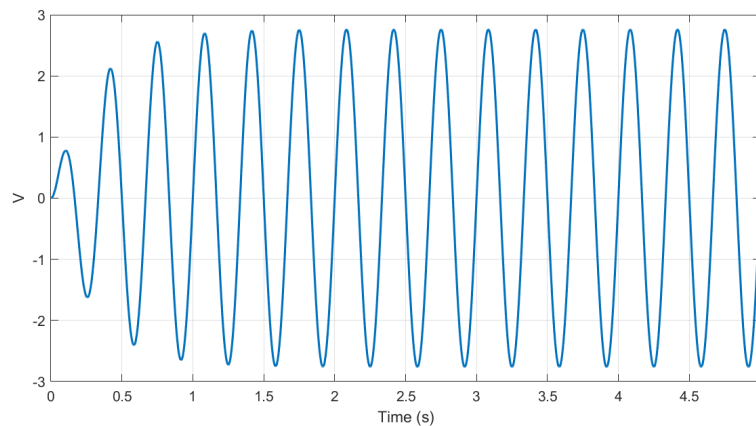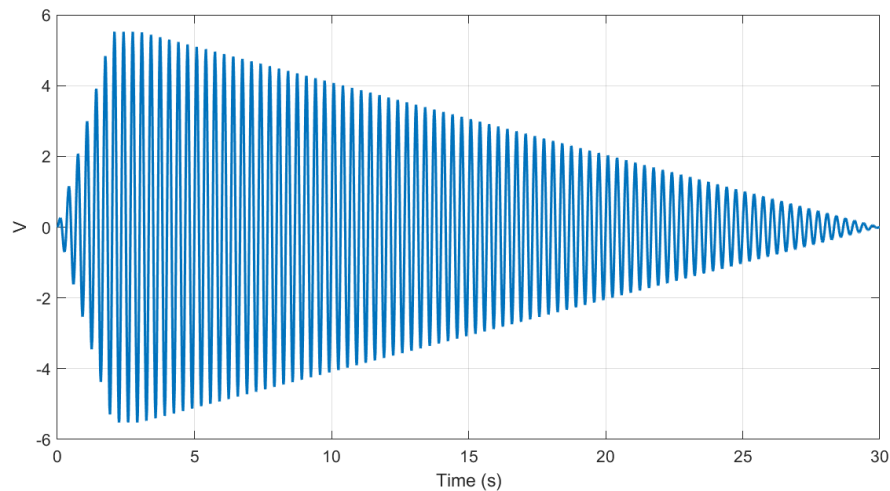

Figure D.5: This voltage signal represents the input signal for the air bearing stage, to perform the coefficient of restitution experiment under different acceleration conditions.

The second experiment consist of an acceleration up sweep, since the purpose of our dynamical analysis is to find the bifurcation point at which the system transforms its motion, for different end stop locations. This means, that the system begins with 0g acceleration and sweeps with an linear increasing motion towards a signal of 2g. This experiment is desired, since it directly shows how the bifurcation point changes when different end-stops are used. The input signal for the stage can be seen in figure D.6.

The third signal is basically the same as the previous sweep, however instead of using an increasing signal for the acceleration in this experiment a decreasing signal is used. The signal can be seen in figure D.7. Since the stage is unable to start from a specific acceleration, a up sweep is used for 2 seconds. Moreover to ensure steady state oscillation for the begin of the down sweep at 2%, the oscillator is forced to oscillate several seconds on that specific input acceleration signal. Where after the linear decreasing acceleration sweep can start to begin.
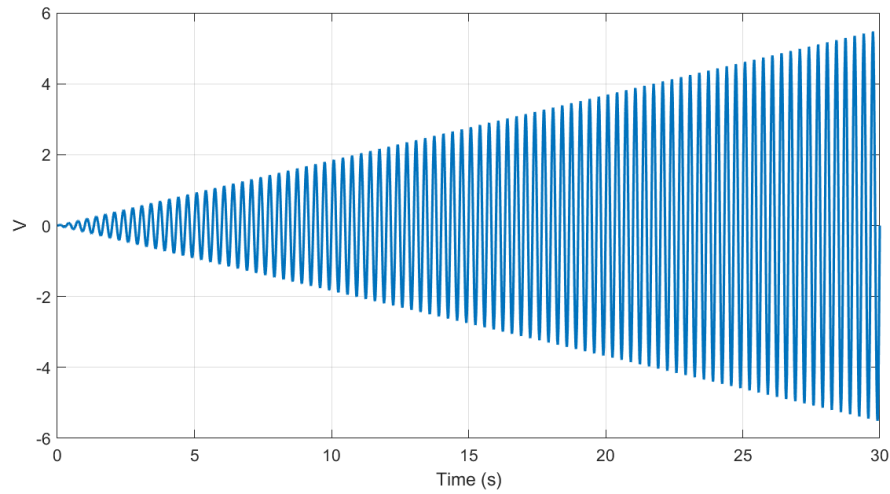
Figure D.6: This voltage signal represents the input signal for the air bearing stage, representing the acceleration up sweep


Figure D.7: This voltage signal represents the input signal for the air bearing stage, representing the acceleration down sweep

D.4   Dynamical validation

The validation of the dynamical model is done with the use of an end-stop displacement within the linear negative stiffness part. The reason for this choice, is the difference in stable equilibria of the experiment with respect to the simulation. Otherwise, it will very assumable or likely that model does not agree with the simulated dynamical results. The validation is done for both initial conditions and the results are shown in figure D.8. This overview shows for both initial conditions an accurate result compared with the experiment. In the zoomed plot above the validation plot, differences can be observed. Although in the displacement plot it can be observed that the simulation comes at rest after the impact, the re-bounce phenomenon keeps going on smaller scale and can be observed from the velocity plot. This behaviour is caused by the end-stop model using

the coefficient of restitution, which ideally begins at on at zero velocity. In reality this is beyond measurable and affects the simulation, however does this does not influence the performance of the simulation significantly. Besides, the envelope profile of the velocity signal matches quite good, however has a minor error of maximum 8%. The influence of intrawell is also more observable in the experiment than in the model, however not significantly visible to be taken into account as an error of the simulation.
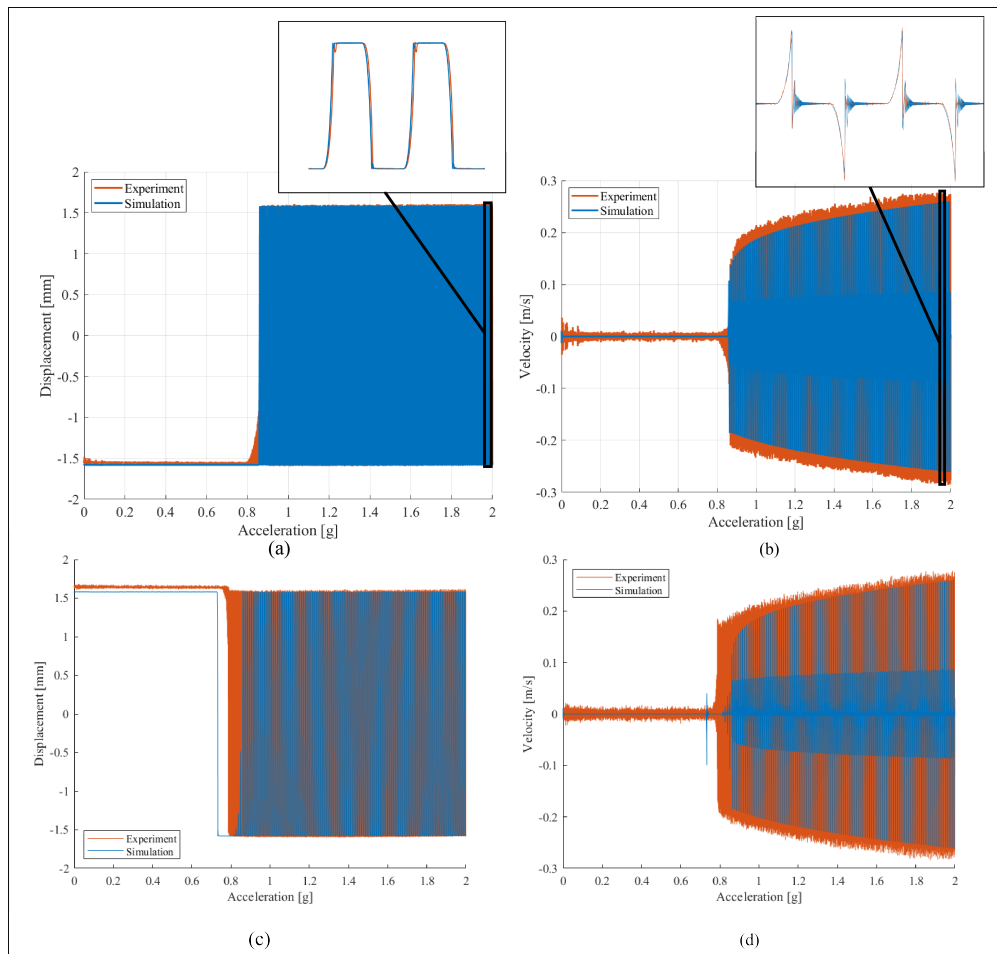
Figure D.8: Simulated and experimentally tested results. a & b Displacement and velocity results of experiments starting from the stable equilibrium position located in the negative region of the force deflection curve. c & d displacement and velocity results from the positive located stable equilibrium position

The coefficient of restitution model can be seen in figure D.9. In this experiment two sub experiments were performed, displacement measured in intrawell motion and interwell motion. The reason for utilising the displacement data is the accuracy of the laser sensor, however this could also be observed from the voltage data in case of a reliable energy traducer. The coefficient of restitution models in literature consist of exponentially decaying curves, resulting in high coefficient of restitutions in the low velocity region. This can be measured with intrawell motion or either with small distances of the motion limits. Since it is somewhat cumbersome to measure small end-stop displacement the intrawell motion is measured. The displacement is measured with reliable laser sensors, being able to accurately display the gradient of the displacement vector representing the velocity profile.
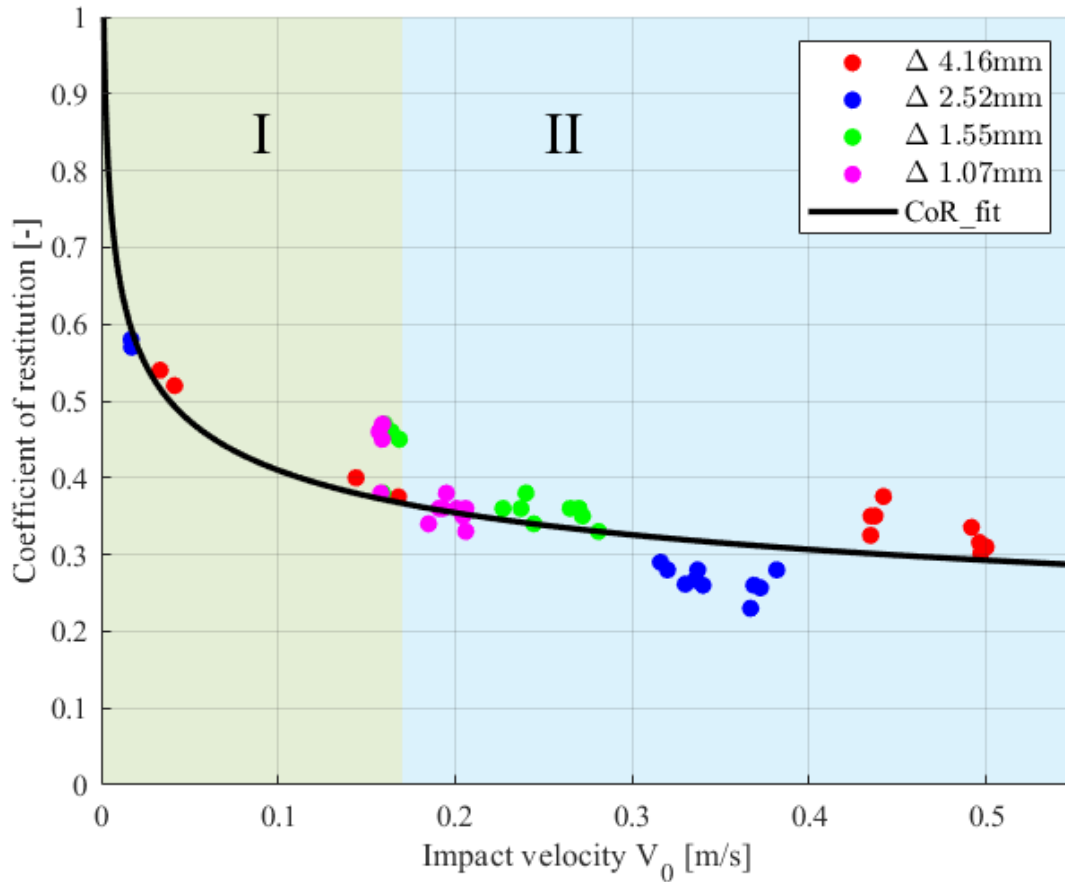
Figure D.9: Coefficient of restitution measurement, used to identify an accurate estimation. Area I, defines the experimental observations from intra well motion, Area II defines the experimental observations from interwell motion

The model for the coefficient of restitution behaviour is assumed to behave with the same characteristics as is found within literature, therefore the model is fitted with an exponential decaying curve in MATLAB. However, this is a modelling choice, since the heat generation is negligible with small incoming velocity and therefore it is assumed to have a fully elastic collision model.

However, this point is difficult to be measured. It is observed that the that the velocity after the impact is small in comparison with the incoming velocity at impact, and therefore it is assumed that the region containing high coefficient of restitution does not affect the dynamical simulation significantly. However, the section view of figure D.8 (b) shows for the dynamical simulation more visual velocity after impact than the experiment. For the coefficient of restitution experiment four different end-stop displacements are used and four data points in each area were measured to check if the CoR values have a repeatable behaviour. For a more reliable model for the coefficient of restitution, more data points should be used in the smaller velocity area to show the response in a more elastic regime. The coefficient of restitution model is a coefficient between 0 and 1, showing respectively fully plastic or elastic characteristics, however no plastic deformation can be observed on the end-stops. The reason for this is, that the end-stop damping is mainly caused by the plastic parts of the spacers and the frame, because this is more compliant than the aluminum end-stops and proof mass. Moreover, when the frame and the spacers are built from the same material, a coefficient of restitution of around 0.9 can be expected. Therefore the participation of intrawell depends on the damping characteristics of the part in the assembly containing the largest amount of compliance. Figure D.10 shows the difference between a simulation containing the CoR model and a CoR of 0.9. In this figure it can be seen that indeed that participation of intrawell is larger when the CoR values are higher. Although this CoR value shows an expected pattern, it is decided that the unfounded exponential decaying curve and the composite structure of the end-stops with the main frame is not sufficient to prove the correctness of this model. Moreover, the coefficient of restitution values calculated from this model in the dynamical simulation showed a large concentration around a value of values between 0.3 and 0.4. Therefore it is chosen to use a well estimated fixed guess for the comparison of the dynamical model with the experimental measurement.

(a)   (b)
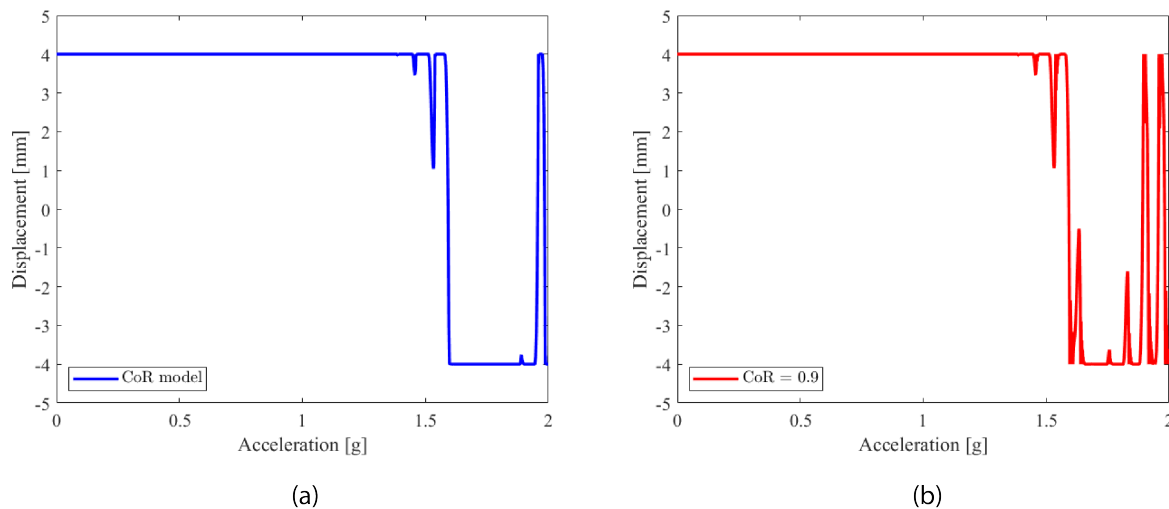
Figure D.10: Acceleration sweep for different CoR models. a) The CoR model used in this report D.9, b) Expected dynamical response of a CoR value belonging to collision of two aluminum objects.

D.4.1   No revolutionary results

Besides the previous described experiments containing the desired results, several other experiments are performed to investigate their dynamical contribution. It is shown, that acceleration sweeps can be used to identify the bifurcation point, however it is known from literature that nonlinear resonator harvesters act differently when they are instantaneously excited at their resonance frequency. Examples are end-stop configurations and duffing oscillators, these designs depends on the energy build up. In this experiment, it is shown that bistable oscillators with motion limits does not converge towards the same results as in nonlinear resonance harvesters found within literature. Though, an energy build up can be seen. In figure D.11 the results are shown.

(a)   (b)
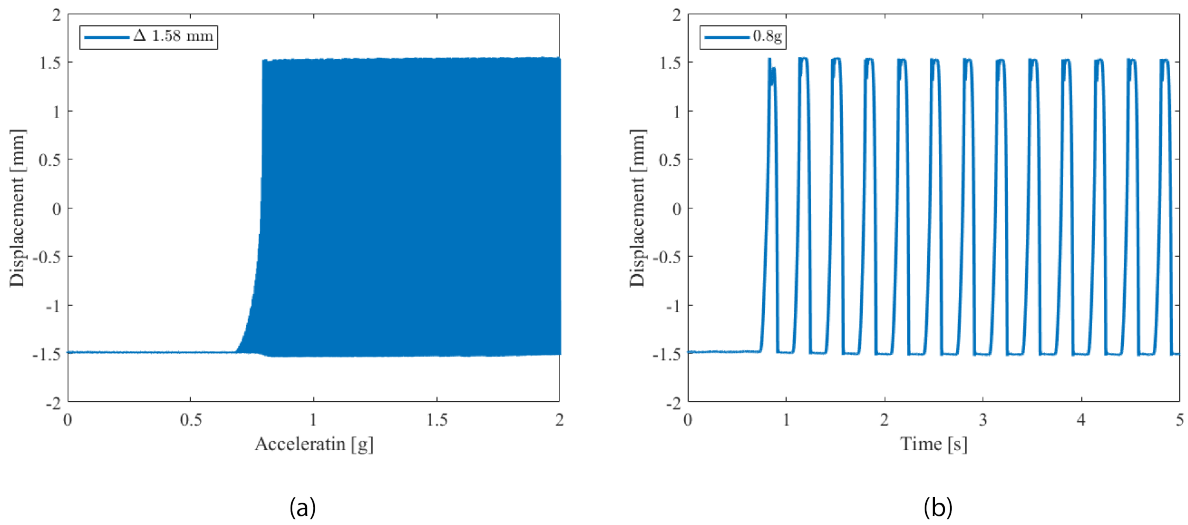
Figure D.11: a) Acceleration sweep b) Instantaneous excitation at a specific acceleration.

A continuation of this investigation in order to show the contribution of energy build up in such systems is done with the use of an down sweep. For non-linear resonance harvesters, such as duffing oscillators shows less desired results when it is subjected to a decreasing frequency sweep instead of an increasing frequency sweep. Figure D.12 shows the performance of our design subjected to a up sweep (a) and a down sweep (b). From this figure it can be seen that the envelope of the displacement during the acceleration up and down sweep differs, this is due to the fact that an increasing acceleration signal starts at rest. However, this is not possible for a decreasing signal, which is constructed to start at rest, and is increased towards the desired acceleration. Before the air bearing stage begins the acceleration down sweep, the system is excited to a steady acceleration signal for several seconds to ensure that the start condition contains its steady state characteristics. Since the envelope profile is more complicated than the acceleration up sweep, the measured acceleration profile is shown in the same graph of the displacement.

D.4.2   Unsuccessful dynamical experiments

An asymmetrical experiment is performed to investigate how the system reacts to asymmetry. In this section the end-stops are placed at different locations with respect to the centre of the range of
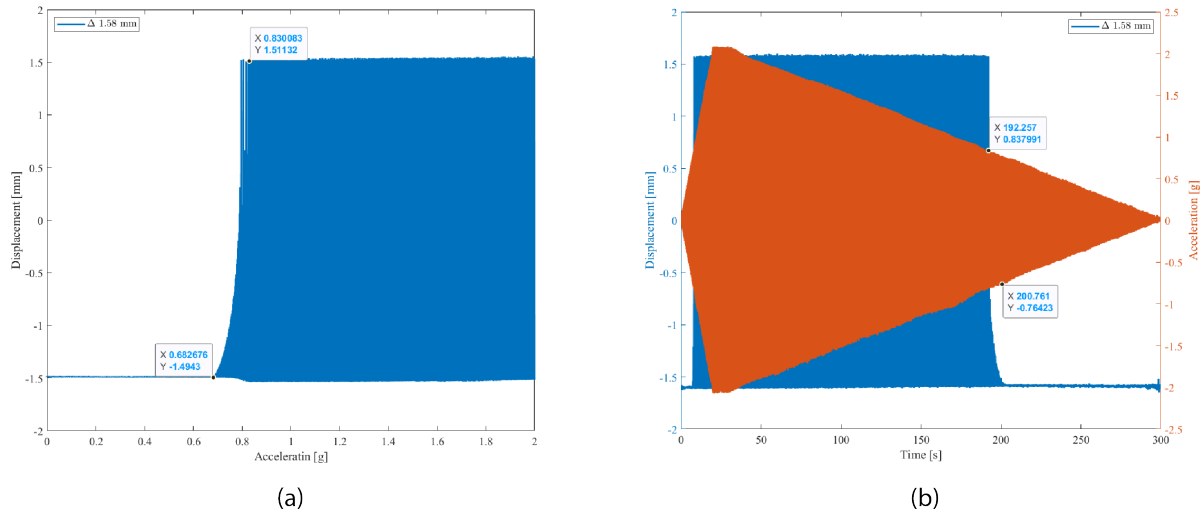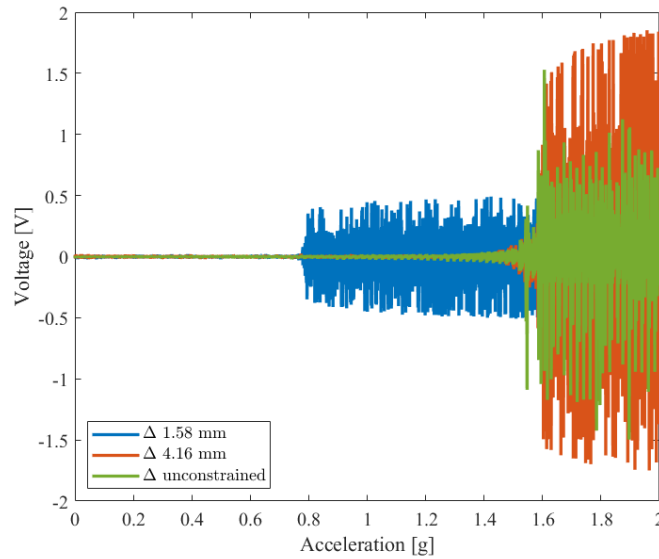
Figure D.12: Acceleration sweep experiment a) Up sweep, b) Down sweep

motion, $\Delta_1 \neq \Delta_2$. The results of the dynamical performance excited with an acceleration up sweep can be seen in figure D.13.
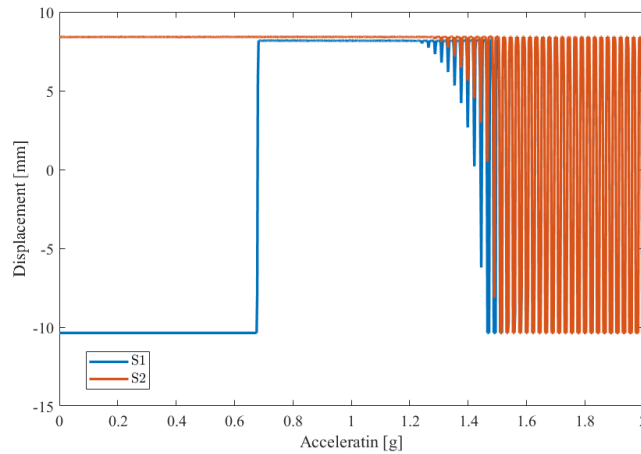
Figure D.13: Accleration sweep for asymmetrical configuration of the end-stops, in which *S1* is the initial condition in the negative area of the force deflection curve, *S2* initial condition in the positive area

This experiment is denoted to be unsuccessful, since the laser sensor failed to give accurate measurement data. The end-stops in this experiment were located at: $\Delta_1 \approx 4.2mm$ & $\Delta_2 \approx 1.5mm$. However, it still can be concluded that differences in initial conditions does not affect the dynamical response and it still depends on the bifurcation point corresponding to the end-stop located at the largest distance from the centre of the range of motion.

Figure D.14: Generated voltage for three different stopper displacements during an acceleration sweep

During every experiment, the voltage is measured which is generated by the PVDF foil on top of the parallel guidance flexure. Figure D.14 shows the voltage output. From this figure it can be seen that low voltages are measured and influence of noise is clearly visible. Therefore, the generated voltage cannot be used as a measure to accurately define the bifurcation point. Moreover the power output is too low to compare the generated power output with state of the art works from literature. However, it can be used to qualitatively indicate the participation of the intra well, since it can capture more accurately the vibrations than the laser sensor since it is located on the flexure's, which are more compliance than the proof mass.

E

Experiment protocols

E

Before the experiments were executed an experiment protocol were made to prevent wasted time as much as possible. Moreover, safety measures were taken into account since the air bearing stage is sophisticated lab equipment and definitely not foolproof.

E.1 Protocol 1: Force deflection experiment

It is known from the sensitivity analysis that our design is very sensitive to parasitic influences, therefore this protocol is used to influence the sensitive spots in our measurements to ensure that the experiment is performed well.
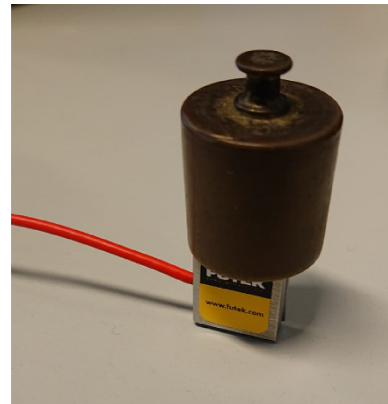
Step 1: Calibration of the force sensor

The first step is to calibrate the force sensor. It is known that the force sensor has a maximum payload capacity of $250gr$, therefore the calibration should be done with weights below this amount of weight. Figure E.1 shows how the following procedure is performed:

- 1.) Fill in the predefine force slope (0.3828) (This procedure is omitted)

- 2.) Make sure that the force sensor is positioned on a stable underground, such that less perturbation can occur.

- 3.) Observe the unloaded force output, then subtract this offset from the unloaded measured force.

- 4). Place the 20 gr accurate weight block on top of the sensor and observe the measured force.

- 5). In case of a large deviation $\geq 2\%$, adjust the force slope with small increments. In case of a desired measured value, repeat this process with different weights until satisfying results can be observed.


(a)   (b)

Figure E.1: a) Used weights to calibrate the sensor (20,50,100gr), b) Calibration configuration

Step 2: The measurement

The second step is the measurement of the force-deflection characteristics of the bistable oscillator. To reduce the amount of unwanted motion to act on our system, the PI stage is installed under a 90° angle as can be seen in figure E.2. The contact between the proof mass and force sensor is a steel rod pushing on an extension attached to the proof-mass. When the system is installed the following procedure is pursued to accurately measure the force deflection characteristics of the bistable design:

- 1.) Move the linear stage towards the proofmass and to make sure it makes contact and add the additional mass extension of the proof mass.

- 2.) Move the stage with small increments manually towards the other stable equilibria to prevent larger displacement than the allowed displacement described by the system.

- 3.) Move the stage back to the original starting position and reduce the motion a small faction such that it does not make no contact anymore.

- 4.) Set the displacement of the linear motion stage to match the maximum travel between the two stable equilibria, and start the measurement.
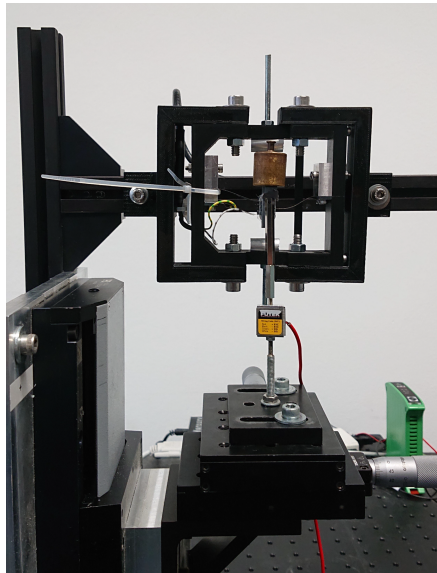
Figure E.2: Force deflection setup

Although this experiment has low potential of being hazardous, the following safety measures are taken into account for the environment as well as the measurement equipment:

- Programmed overload value for the sensor to be below 1 Newton, which is a safety factor of 2.5.

- The edges of the flexure's are sharp and to prevent the system to collapse the maximum travel is identified before each measurement.

E.2   Protocol 2: Dynamical experiment

The custom air bearing stage is sophistic lab equipment and cannot be used without proper instruction. This protocol describes briefly all the steps, which were taken into account to successfully execute the dynamical experiments.

Step 1: Preparation

- 1.) Provide the air bearing stage with 4 bar pressurized air.

- 2.) Activate the Power switch of the air bearing stage

- 3.) Start the Kollmorgan software and connect the stage with the controller. And make sure that the controller is in *service mode*!

- 4.) Open the safety box around the stage and attach the prototype to the stage.

- 5.) Close the safety box and make sure that the box is fully closed and the safety switch is activated.

- 6.) Change the controller settings from *Service mode* to *Analog input*

- 7.) Attach NI DaQ 9263 output and 9215 input module between the computer and the stage and connect all the measured signals.

- 8.) Start the linear motors of the air bearing stage by pushing the green button on the control panel of the stage

- 9.) Enable the motors within the interface of the controller software.

- 10.) Sent the desired input signal with the 9263 dac output module to the stage, and make sure to have a good signal to noise ratio!

- 11.) Observe the measured input signals for reliable results.

For each of the measurement containing different prototype configurations, the steps from 4 until 11 is repeated. The procedure after the measurement is achieved by following steps 6, 7, 5, and 4 in opposite direction. Furthermore, detailed information regarding to the construction process and work instructions of the air bearing stage can be found in the work of Molenaar et al. [38].

Step 2: Safety roadmap

The air bearing stage is a desired setup to measure the behaviour of low-frequency energy harvesters. However, low-frequency comes along with large input motion of the stage introducing hazardous working conditions in situations when safety measures are not taken into account. Therefore the safety measures for this experiment are:

- 1.) Make sure that during the experiment the safety box is closed

- 2.) Cover the area in the direction of the laser beam of the laser sensor, to prevent eye damage of the people passing by.

- 3.) Fasten all objects on the baseplate of the air bearing stage, to prevent components to come loose during experiment.

- 4.) Make sure that the cables do not obstruct the motion of the air bearing stage.

- 3.) Always observe the motion of the air bearing stage, excessive travel might damage the stage as well as the prototype and imposes a danger to the surroundings.

- 4.) In case of excessive travel, push the emergency button to power off the air bearing stage immediately.

- 5.) Do not place loose steel objects near the stage, since the motors are magnetically attractive and might damage when their motion path is obstructed.
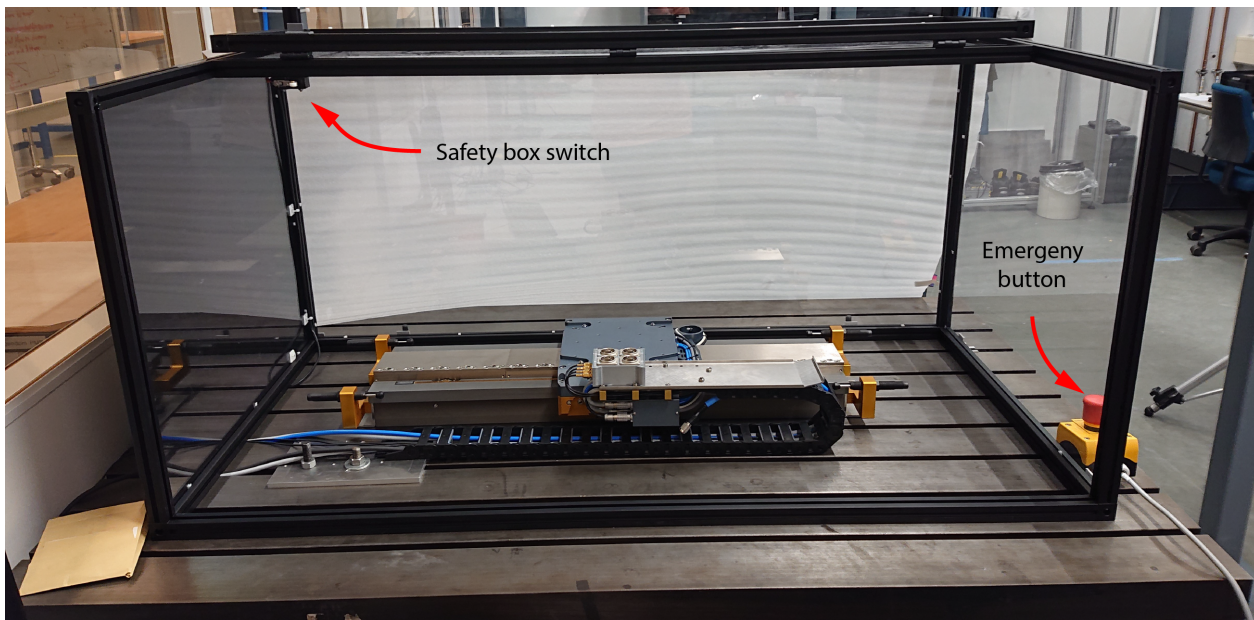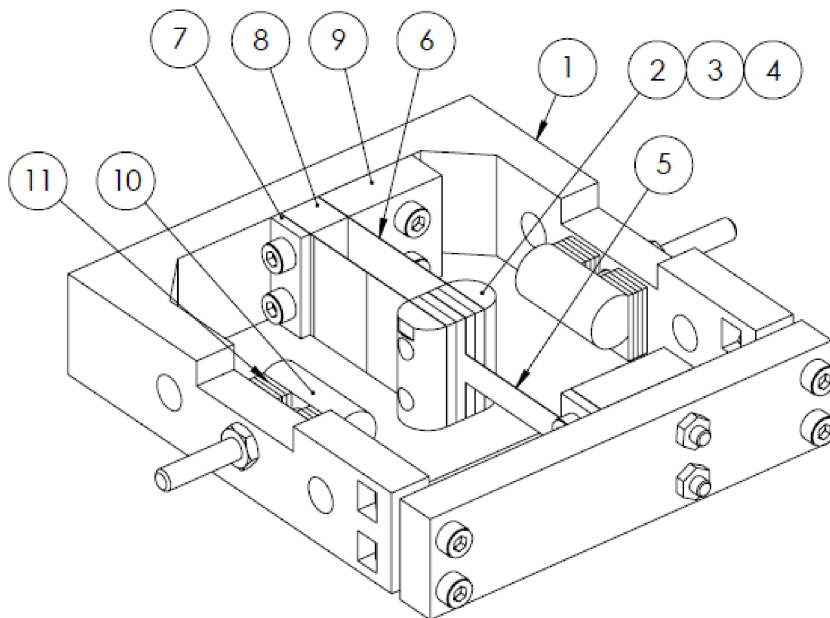

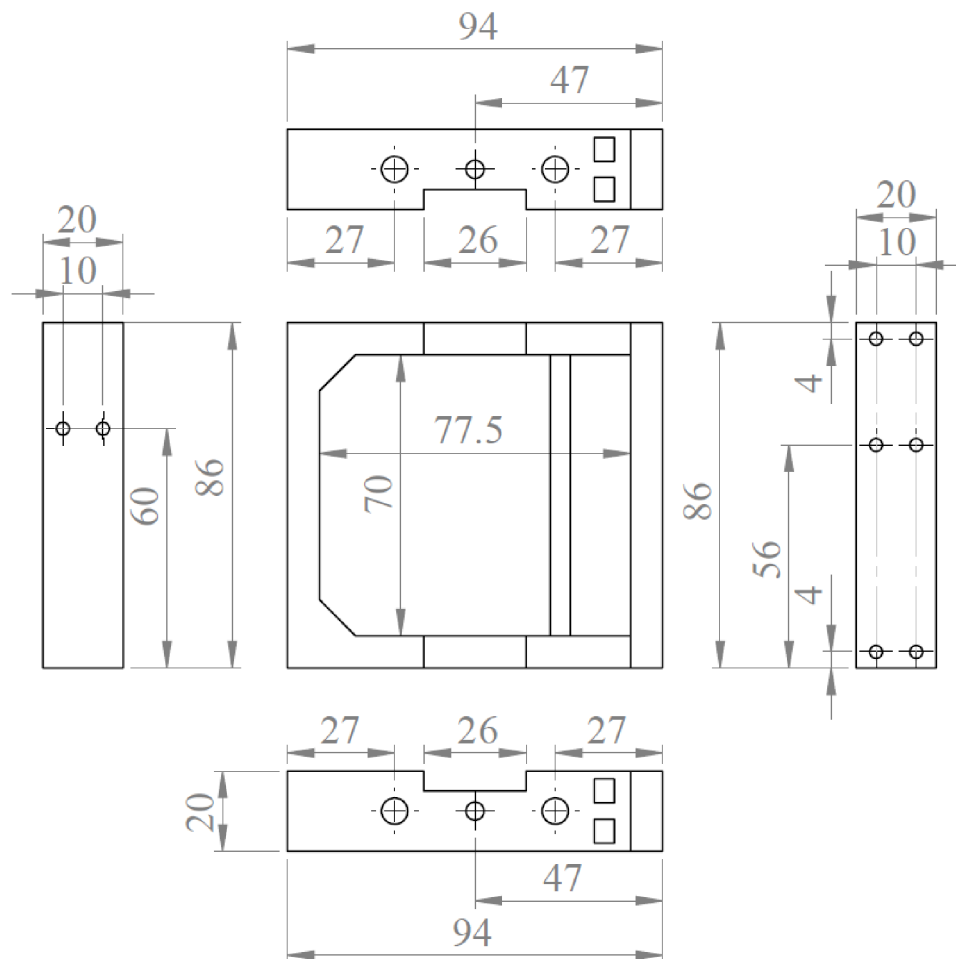**Figure E.3: Overview of the safety components of the test setup**

E

F

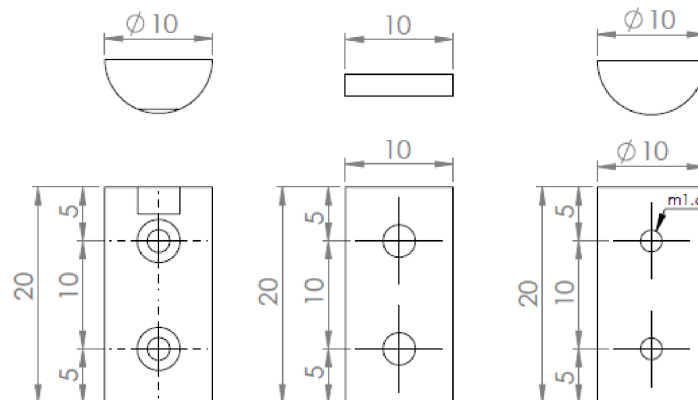# Technical drawings of the bistable oscillator

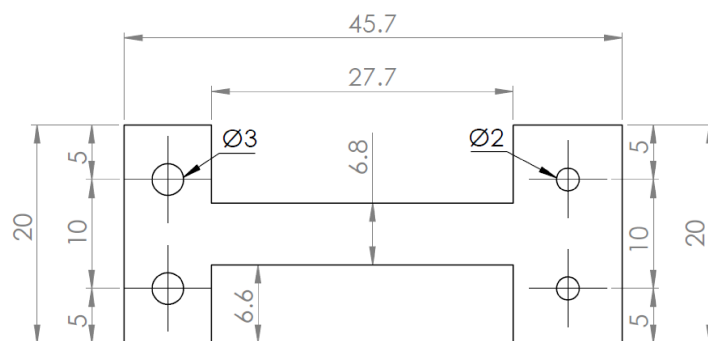| Item nr:	Qty:	Description
1	1	3D printed Frame
2	1	Proof mass front
3	4	Steel shims
4	1	Proof mass back
5	1	Buckle flexure
6	2	Parallel guidance flexure
7	2	Clamping top
8	1	Spacer parallel flexure
9	2	Clamping bottom
10	2	End-stops
11	-	Spacers

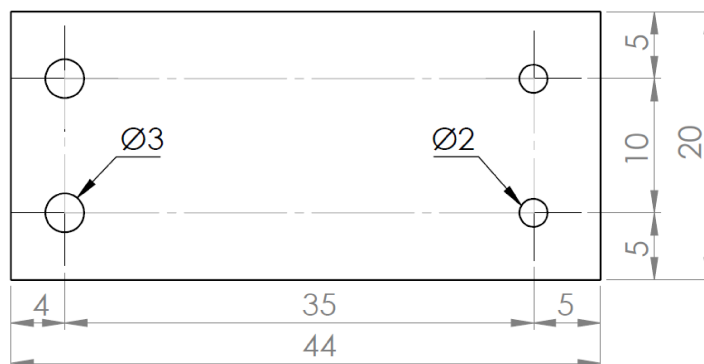## 1. 3D printed Frame

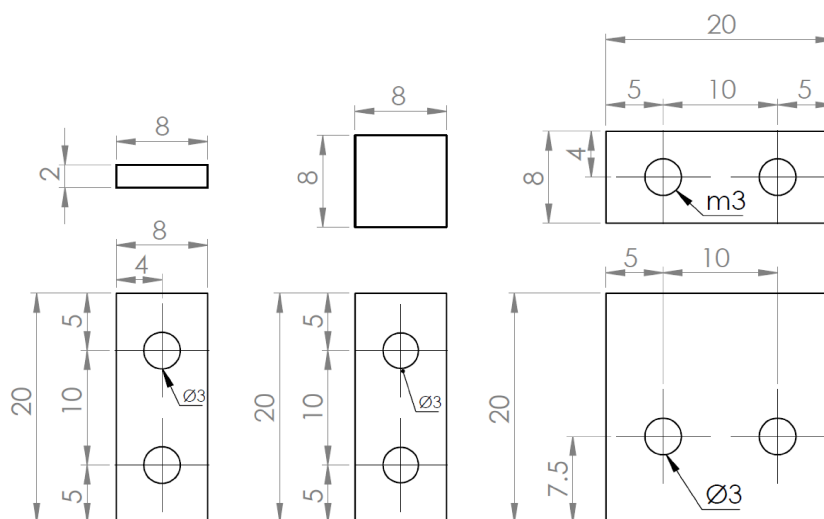## 2,3,4. Proof mass assembly

5. Buckle flexure

6. Parallel guidance flexure

7,8,9. Clamping components

10. End-stop
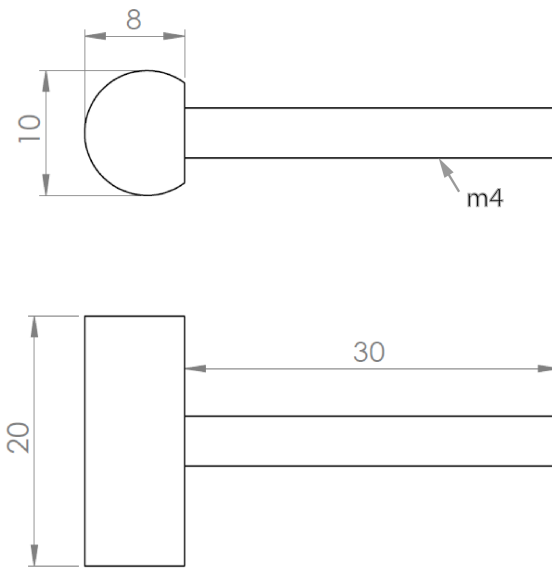
11. End-stop spacers

G
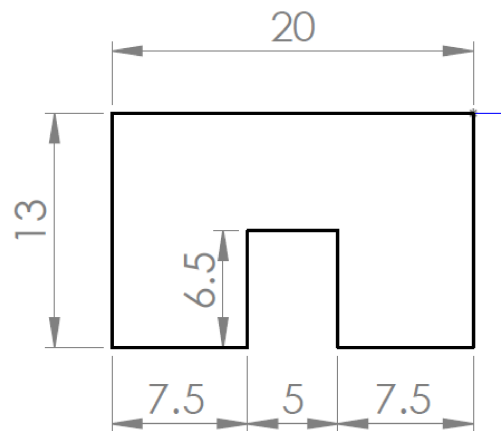
Contact mechanics model

In this chapter the contact mechanics model is described, but due to failure in commination with the bistable model not used in the thesis. Although these results were not used in the thesis itself, it helped to get acquainted with the mechanical and dynamical simulation. Besides the experiments were also a great learning process on how the experimental setups in the lab worked.

G

G.1   Curved end-stops

From literature review, it became clear that the shape of the end-stop has an important effect on the output performance of the energy harvester. Systems with rigid end-stops are mostly described and modelled as piecewise linear systems. However the stiffness of an end-stop could be a troublesome parameter to be found. In this research, the contact with the end-stop is modelled in order to investigate how the contact problem could be modelled using a finite element (FEM) software, after which it is verified with experimental work.

G.1.1   Background

End-stops have in general a multi-purpose design solution for problems, which will be introduced when linear resonant harvesters are used to capture ambient kinetic vibration energy. This design principle is one of the commonly used energy harvesting principles found within literature and often constructed from a spring steel cantilever in combination with a tip mass. It can be expected that resonant harvesters constructed from spring steel cantilevers are excited with excessive travel, when they are used in environments with energy varying spectra. In case of excessive travel, stresses beyond the yield stress can be expected and plastic deformation of the cantilever result in malfunctioning of the system. End-stop are used to limit the amplitude of the oscillator and therefore prevent the system from excessive loads. Besides upon impact, larger operational bandwidths can be expected and improves the reliability within a varying energy spectra as is compared with the bandwidth of a resonance peak of the linear resonator. The impact of the cantilever with the end-stops actuates many frequencies within the cantilever material resulting in non-linear behaviour and a broadening effect of the frequency bandwidth can be expected at the cost of the peak performance. The impact has the characteristics of rapid increasing their stiffness, however from the literature review it is observed that a gradually increase in stiffness might be more beneficial and larger nonlinear phenomena could occur. In this research the principle of curved end-stops are investigated. This is done with numerical simulations and experimental mechanical observations. The goal is to investigate the gradually increasing stiffness at impact with a contact mechanics model in ANSYS mechanical APDL

G.1.2   Prototype

The prototype can be seen in figure G.1 , consisting of a base, curved end-stops and a cantilever. The cantilever has a length of 92mm and a width of 10mm. The end-stops and base are made from 100% infill 3D printed PLA and the flexure is constructed with 0.5mm spring steel and cut into shape with a micro laser cutting machine. The geometry of the end-stops can be seen in figure G.2, and the parameters used as input for the mechanical simulation are listed in table G.1.

G.1.3   Mechanical analysis

The mechanical analysis of the system is numerically solved using ANSYS mechanical APDL. The first step was performed by creating the geometry in ANSYS, which can be seen in figure G.3. The
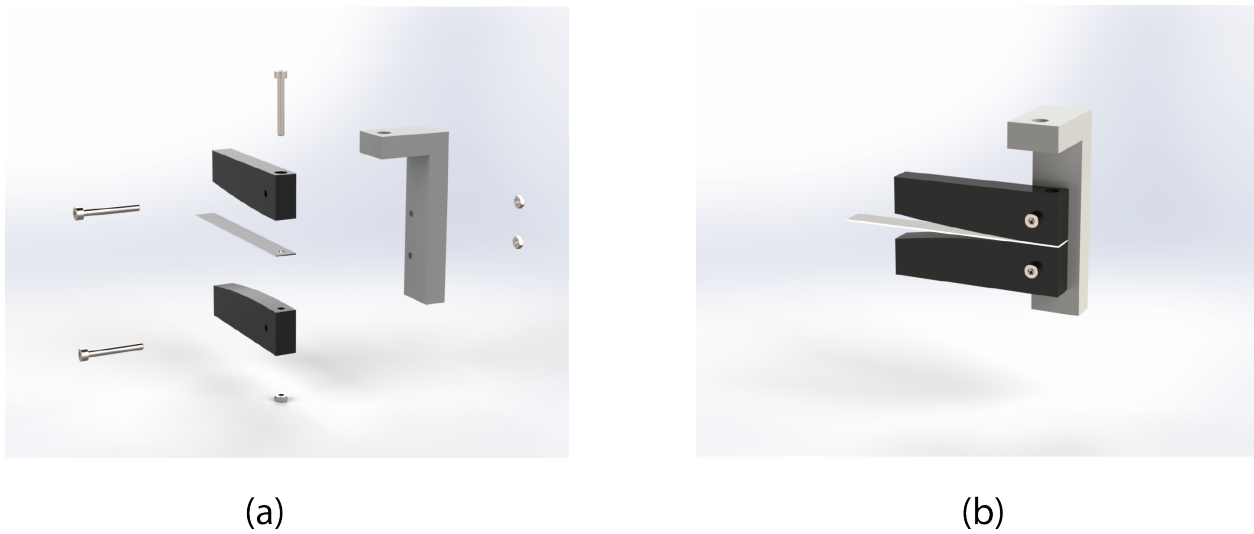
Figure G.1: Resonant energy harvester design with curved end-stops. a.) Exploded view of all the design components, b.) Assembled resonant energy harvester design.
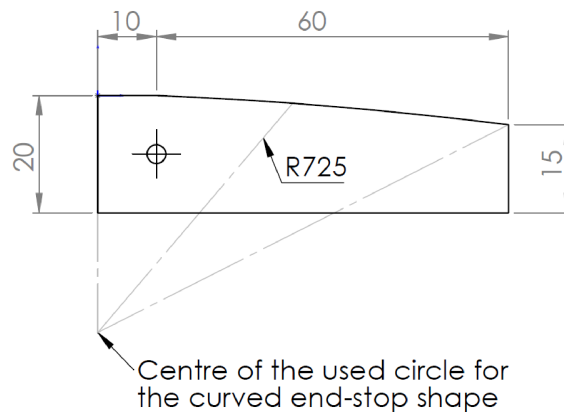

Figure G.2: Dimensions of the end-stops of the resonant energy harvester design.

Flexures:			End-stops:		
Parameter	Symbol	Value	Parameter	Symbol	Value
Elastic modules	E_f	190e9 GPa	Elastic modules	E_s	3.4e9 GPa
Poisson ratio	v_f	0.34	Poisson ratio	v_s	0.39
Density	ρ_f	7.89e3 $\frac{kg}{m^3}$	Density	ρ_s	1.25e3 $\frac{kg}{m^3}$

Table G.1: Material properties for the components used in the ANSYS model

system is designed to be symmetrical, therefore only one half of the total system geometry is used in the simulation. Moreover, the geometry is constructed in 2D for the cause of simplicity.

A contact analysis is performed, since the cantilever impacts with the end-stops. The contact is
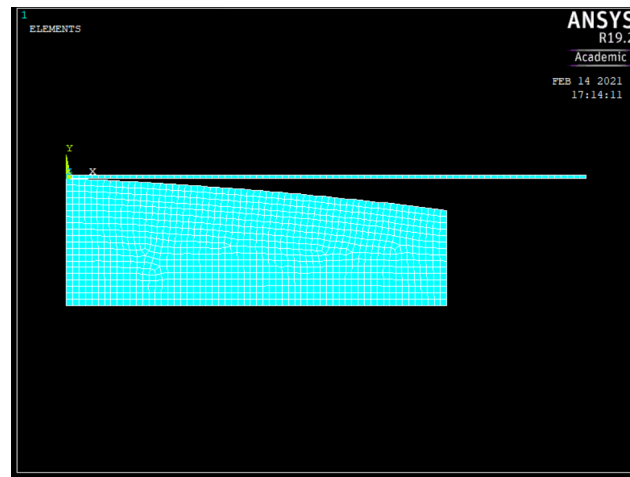
Figure G.3: Geometrical prototype representation by ANSYS mechancial apdl

generated by the bottom surface of the cantilever and the end-stop. In ANSYS the contact area are assigned to the contact lines, shown in figure G.4. In this figure the bottom surface of the cantilever is indicated with *"Moving contact area"* end-stop surface with *Target contact area*. Figure G.4(b) indicates the corresponding contact set, which will be used for the contact mechanics analysis model. In order to calculate the force-deflection characteristics of the system, boundary conditions are applied. Figure G.4(c) shows the locations of all the boundary conditions, in which all the degree-of-freedom of the cantilever root and the end-stops are fixed and an actuation point is applied near the end of the cantilever.

The mechanical validation is done with the use of a quasistatic force-deflection experiment. In this experiment a PI linear stage (M505) is used in combination with a Futek LSB200 force sensor. The experimental quasistatic force deflection setup can be seen in figure G.5. The contact between the force sensor and the cantilever is configured by the use of a needle, which is glued onto the end of the cantilever in order to ensure contact. The resulted numerical and experimental outcomes can be seen in figure G.6. From these results it can be observed that the envelope of both curves are in good agreement, however the point at which the system transforms its stiffness is positioned at a different location. The explanation is rather simple. The starting point of the simulation is in the middle of the design, however this point should be found with the use of visual observations in the experiment. Therefore, it could not be guaranteed, that the starting point is at the same location as is used in the simulation and resulted in a displacement shift in the experiment. Moreover it was observed that the curved end-stops did not converged to the expected results, since curved end-stops did not constrain the cantilever beam but followed the mode shape until cantilever amplitude was limited by the end of the beam. This limit could also be described by a hard end-stop located on the same position at the end of the end-stops, but without the curvature in the middle. Because of this observation and the verification of the simulation no further investigation were pursued in the dynamical domain, since the curved end-stops were constructed such that they opposes no limitation to the cantilever amplitude until the end of the end-stop.
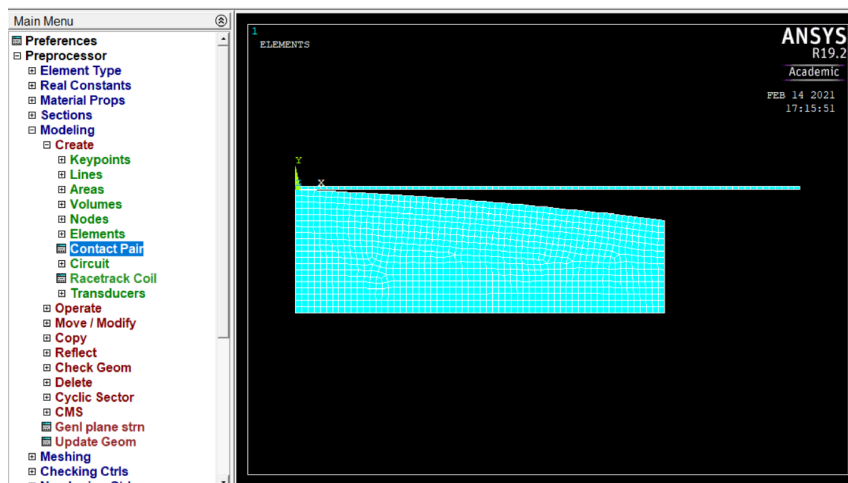
(a)
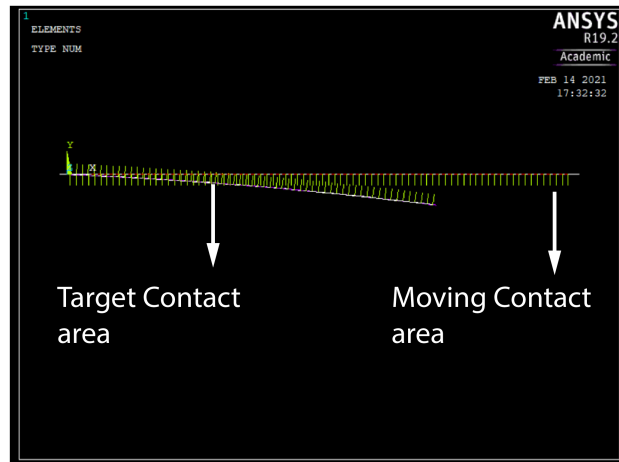
(b)
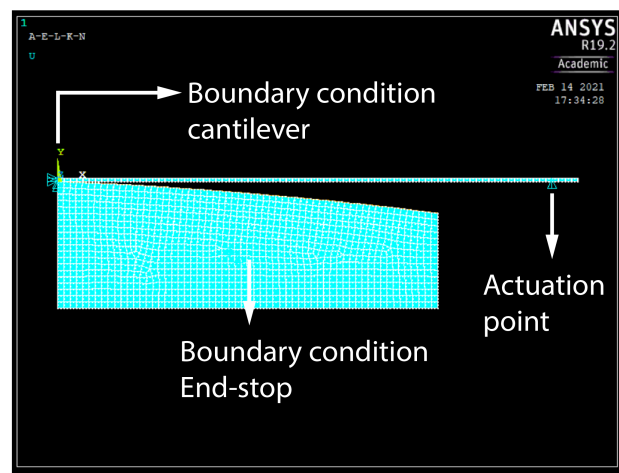
(c)

Figure G.4: Boundary conditions of the mechanical contact analysis in ANSYS. a) GUI command for the generation of a contact pair, b) Generated contact, c) Overall boundary conditions.
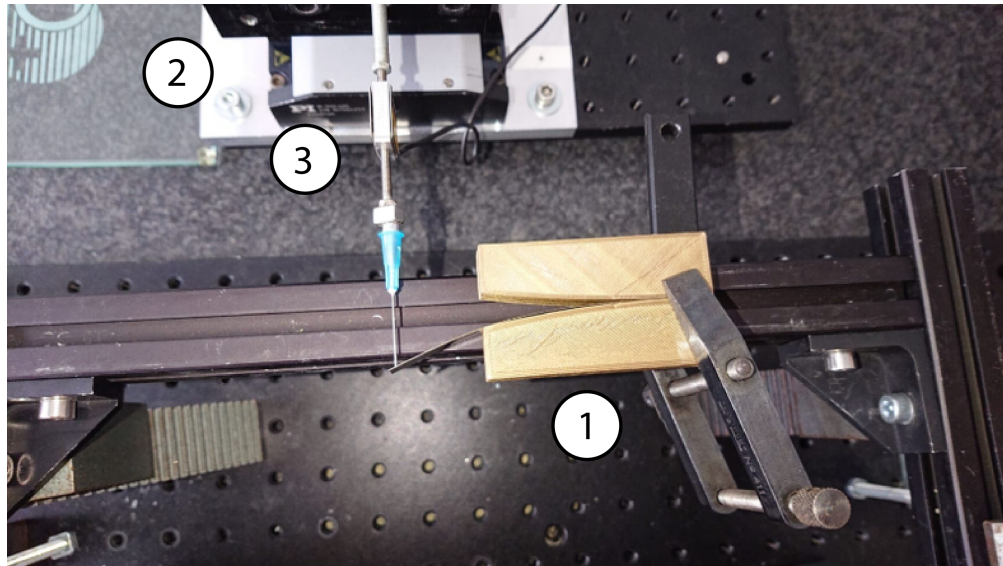
Figure G.5: Quasi-static force deflection setup. 1.) Resonant harvester prototype, 2.) PI linear stage (M505), 3.) Force sensor.
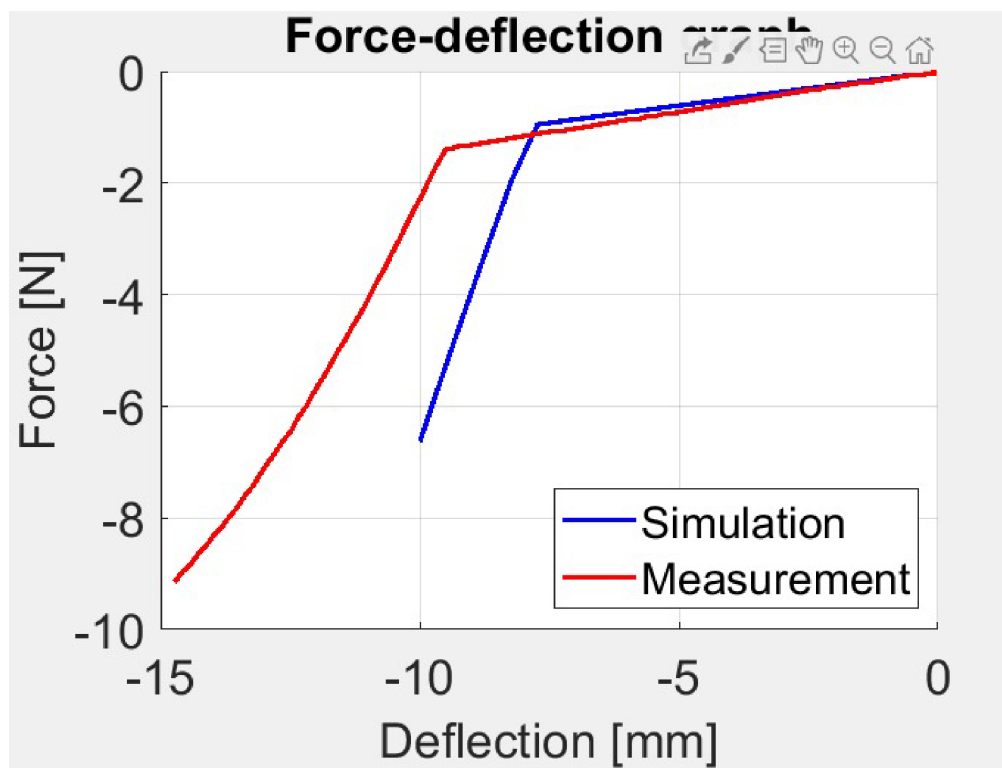

Figure G.6: Simulated and experimental results.

Bibliography

[DRC] DRC dam impact guide.

[Tur] Turbine Light Illuminates Highways With Wind.

[3] (2020). Mechanical watch. Wikipedia.

[4] , v. B. (2015). Advanced Engineering Design, Lifetime Performance and Reliability. Engineering-abc, Delft, sixth edition.

[5] Amor, N. B. and Kanoun, O. (2007). Investigation to the Use of Vibration Energy for Supply of Hearing Aids. In 2007 IEEE Instrumentation Measurement Technology Conference IMTC 2007, pages 1–6.

[6] Ashraf, K., Md Khir, M. H., Dennis, J. O., and Baharudin, Z. (2013). A wideband, frequency up-converting bounded vibration energy harvester for a low-frequency environment. Smart Materials and Structures, 22(2):025018.

[7] Bhavikatti, S. S. (2005). Problems and Solutions in Engineering Mechanics. New Age International.

[8] Blad, T., Nijssen, J., Broeren, F., Boogaard, B., Lampaert, S., van den Toorn, S., and van den Dobbelsteen, J. (2020). A Rapidly Deployable Test Suite for Respiratory Protective Devices in the COVID-19 Pandemic. Applied Biosafety, 25(3):161–168.

[9] Blad, T. W. A. and Tolou, N. (2019). On the efficiency of energy harvesters: A classification of dynamics in miniaturized generators under low-frequency excitation. Journal of Intelligent Material Systems and Structures, 30(16).

[10] Blystad, L.-C. J. and Halvorsen, E. (2011a). An energy harvester driven by colored noise. Smart Materials and Structures, 20(2):025011.

[11] Blystad, L.-C. J. and Halvorsen, E. (2011b). A piezoelectric energy harvester with a mechanical end stop on one side. Microsystem Technologies, 17(4):505–511.

[12] Blystad, L.-C. J., Halvorsen, E., and Husa, S. (2010). Piezoelectric MEMS energy harvesting systems driven by harmonic and random vibrations. IEEE Transactions on Ultrasonics, Ferroelectrics, and Frequency Control, 57(4):908–919.

[13] Brans, J. A., Blad, T. W. A., and Tolou, N. (2019). A Review of Design Principles for Improved Mechanical Reliability of Cantilever Piezoelectric Vibration Energy Harvesters. In 2019 7th International Conference on Control, Mechatronics and Automation (ICCMA), pages 408–415.

[14] Cottone, F., Gammaitoni, L., Vocca, H., Ferrari, M., and Ferrari, V. (2012). Piezoelectric buckled beams for random vibration energy harvesting. Smart Materials and Structures, 21(3):035021.

[15] Dhakar, L., Liu, H., Tay, F., and Lee, C. (2013). A new energy harvester design for high power output at low frequencies. Sensors and Actuators A: Physical, 199:344–352.

[16] D'Mello, Y., Skoric, J., Xu, S., Roche, P. J. R., Lortie, M., Gagnon, S., and Plant, D. V. (2019). Real-Time Cardiac Beat Detection and Heart Rate Monitoring from Combined Seismocardiography and Gyrocardiography. Sensors (Basel, Switzerland), 19(16).

[17] Edwards, B., Xie, M., Aw, K. C., Hu, A. P., and Gao, W. (2013). An impact based frequency up-conversion mechanism for low frequency vibration energy harvesting. In 2013 Transducers Eurosensors XXVII: The 17th International Conference on Solid-State Sensors, Actuators and Microsystems (TRANSDUCERS EUROSENSORS XXVII), pages 1344–1347.

[18] Fan, K., Cai, M., Liu, H., and Zhang, Y. (2019). Capturing energy from ultra-low frequency vibrations and human motion through a monostable electromagnetic energy harvester. Energy, 169:356–368.

[19] Gafurov, D. and Snekkenes, E. (2009). Gait Recognition Using Wearable Motion Recording Sensors. EURASIP Journal on Advances in Signal Processing, 2009.

[20] Geisler, M., Boisseau, S., Perez, M., Gasnier, P., Willemin, J., Ait-Ali, I., and Perraud, S. (2017a). Human-motion energy harvester for autonomous body area sensors. Smart Materials and Structures, 26(3):035028.

[21] Geisler, M., Boisseau, S., Perez, M., Gasnier, P., Willemin, J., Ait-Ali, I., and Perraud, S. (2017b). Human-motion energy harvester for autonomous body area sensors. Smart Materials and Structures, 26(3):035028.

[22] Goldsmith, W. (2001). Impact. Courier Corporation.

[23] Gu, L. and Livermore, C. (2011). Impact-driven, frequency up-converting coupled vibration energy harvesting device for low frequency operation. Smart Materials and Structures, 20(4):045004.

[24] Halim, M. A. and Park, J. Y. (2014). Theoretical modeling and analysis of mechanical impact driven and frequency up-converted piezoelectric energy harvester for low-frequency and wide-bandwidth operation. Sensors and Actuators A: Physical, 208:56–65.

[25] Harne, R. L. and Wang, K. W. (2013). A review of the recent research on vibration energy harvesting via bistable systems. Smart Materials and Structures, 22(2):023001.

[26] Haroun, A., Yamada, I., and Warisawa, S. (2015). Study of electromagnetic vibration energy harvesting with free/impact motion for low frequency operation. Journal of Sound and Vibration, 349:389–402.

[27] Jiang, W.-A. and Chen, L.-Q. (2014). Snap-through piezoelectric energy harvesting. Journal of Sound and Vibration, 333(18):4314–4325.

[28] Kluger, J. M., Sapsis, T. P., and Slocum, A. H. (2015). Robust energy harvesting from walking vibrations by means of nonlinear cantilever beams. Journal of Sound and Vibration, 341:174–194.

[29] Lei, L., Kuang, Y., Shen, X., Yang, K., Qiao, J., and Zhong, Z. (2016). Optimal Reliability in Energy Harvesting Industrial Wireless Sensor Networks. IEEE Transactions on Wireless Communications, pages 1–1.

[30] Li, W. G., He, S., and Yu, S. (2010). Improving Power Density of a Cantilever Piezoelectric Power Harvester Through a Curved L-Shaped Proof Mass. IEEE Transactions on Industrial Electronics, 57(3):868–876.

[31] Liu, H., Lee, C., Kobayashi, T., Tay, C. J., and Quan, C. (2012a). Investigation of a MEMS piezoelectric energy harvester system with a frequency-widened-bandwidth mechanism introduced by mechanical stoppers. Smart Materials and Structures, 21(3):035005.

[32] Liu, H., Lee, C., Kobayashi, T., Tay, C. J., and Quan, C. (2012b). Piezoelectric MEMS-Based wideband energy harvesting systems using a frequency-up-conversion cantilever stopper. Sensors and Actuators A: Physical, 186:242–248.

[33] Liu, W., Liu, C., Li, X., Zhu, Q., and Hu, G. (2018). Comparative study about the cantilever generators with different curve fixtures. Journal of Intelligent Material Systems and Structures, 29(9):1884–1899.

[34] Mak, K. H., McWilliam, S., Popov, A. A., and Fox, C. H. (2011). Performance of a cantilever piezoelectric energy harvester impacting a bump stop. Journal of Sound and Vibration, 330(25):6184–6202.

[35] Mann, B. and Sims, N. (2009). Energy harvesting from the nonlinear oscillations of magnetic levitation. Journal of Sound and Vibration, 319(1-2):515–530.

[36] Masana, R. and Daqaq, M. F. (2011). Relative performance of a vibratory energy harvester in mono- and bi-stable potentials. Journal of Sound and Vibration, 330(24):6036–6052.

[37] Mathie, M. J., Coster, A. C. F., Lovell, N. H., and Celler, B. G. (2004). Accelerometry: Providing an integrated, practical method for long-term, ambulatory monitoring of human movement. Physiological Measurement, 25(2):R1–R20.

[38] Molenaar, S. (2021). Examination of large amplitude vibrations of a nonlinear oscillator for energy harvesting.

[39] Narimani, A., Golnaraghi, M. E., and Jazar, G. N. (2004). Frequency Response of a Piecewise Linear Vibration Isolator. Journal of Vibration and Control, 10(12):1775–1794.

[40] Roundy, S., Wright, P. K., and Rabaey, J. (2003). A study of low level vibrations as a power source for wireless sensor nodes. Computer Communications, 26(11):1131–1144.

[41] Soliman, M. S. M., Abdel-Rahman, E. M., El-Saadany, E. F., and Mansour, R. R. (2008). A wideband vibration-based energy harvester. Journal of Micromechanics and Microengineering, 18(11):115021.

[42] Soliman, M. S. M., Abdel-Rahman, E. M., El-Saadany, E. F., and Mansour, R. R. (2009). A Design Procedure for Wideband Micropower Generators. Journal of Microelectromechanical Systems, 18(6):1288–1299.

[43] Terrier, P., Ladetto, Q., Merminod, B., and Schutz, Y. (2000). High-precision satellite positioning system as a new tool to study the biomechanics of human locomotion. Journal of Biomechanics, 33(12):1717–1722.

[44] Tornincasa, S., Repetto, M., Bonisoli, E., and Di Monaco, F. (2012). Energy harvester for vehicle tires: Nonlinear dynamics and experimental outcomes. Journal of Intelligent Material Systems and Structures, 23(1):3–13.

[45] Von Bergen, N. H. (2016). Advancements in technology for patients with congenital heart disease: Implantable rhythm devices. Progress in Pediatric Cardiology, 42:23–29.

[46] Wang, Z., Elfrink, R., Rovers, M., Matova, S., van Schaijk, R., and Renaud, M. (2014). Shock Reliability of Vacuum-Packaged Piezoelectric Vibration Harvester for Automotive Application. Journal of Microelectromechanical Systems, 23(3):539–548.

[47] Woodward, M. I. and Cunningham, J. L. (1993). Skeletal Accelerations Measured during Different Exercises. Proceedings of the Institution of Mechanical Engineers, Part H: Journal of Engineering in Medicine, 207(2):79–85.

[48] Xiong, Y., Song, F., and Leng, X. (2019). A piezoelectric cantilever-beam energy harvester (PCEH) with a rectangular hole in the metal substrate. Microsystem Technologies.

[49] Yuan, Z., Liu, W., Zhang, S., Zhu, Q., and Hu, G. (2019). Bandwidth broadening through stiffness merging using the nonlinear cantilever generator. Mechanical Systems and Signal Processing, 132:1–17.

[50] Zhao, D., Wang, X., Cheng, Y., Liu, S., Wu, Y., Chai, L., Liu, Y., and Cheng, Q. (2018). Analysis of single-degree-of-freedom piezoelectric energy harvester with stopper by incremental harmonic balance method. Materials Research Express, 5(5):055502.

[51] Zhou, K., Dai, H. L., Abdelkefi, A., Zhou, H. Y., and Ni, Q. (2019). Impacts of stopper type and material on the broadband characteristics and performance of energy harvesters. AIP Advances, 9(3):035228.

[52] Zhu, D., Harris, N., and Beeby, S. (2012). Performance of Linear Vibration Energy Harvesters under Broadband Vibrations with Multiple Frequency Peaks. Procedia Engineering, 47:5–8.

[53] Zhu, D., Tudor, M. J., and Beeby, S. P. (2009). Strategies for increasing the operating frequency range of vibration energy harvesters: A review. Measurement Science and Technology, 21(2):022001.

[54] Zhu, Y. and Zu, J. W. (2013). Enhanced buckled-beam piezoelectric energy harvesting using midpoint magnetic force. Applied Physics Letters, 103(4):041905.

G